UNIVERSIDADE DE ÉVORA

ESCOLA DE CIÊNCIAS E TECNOLOGIA

DEPARTAMENTO DE FÍSICA

ADVANTAGES AND DRAWBACKS OF A LINEAR FOCUSING SYSTEM WITH LOW MELTING POINT MOLTEN SALTS

Telma Sofia Risso Lopes

Orientação: Doutor Thomas Fasquelle

Doutor Hugo Manuel Gonçalves da Silva

Mestrado em Engenharia da Energia Solar

Dissertação

Évora, 2019

UNIVERSIDADE DE ÉVORA

ESCOLA DE CIÊNCIAS E TECNOLOGIA

DEPARTAMENTO DE FÍSICA

ADVANTAGES AND DRAWBACKS OF A LINEAR FOCUSING SYSTEM WITH LOW MELTING POINT MOLTEN SALTS

Telma Sofia Risso Lopes

Orientação: Doutor Thomas Fasquelle

Doutor Hugo Manuel Gonçalves da Silva

Mestrado em Engenharia da Energia Solar

Dissertação

Évora, 2019

Constituição do Júri de provas públicas:

Presidente: Diogo Canhão de Sousa Canavarro

Investigador Auxiliar Convidado - Cátedra Energias Renováveis

Arguente: Paulo Manuel Ferrão Canhoto

Professor Auxiliar - Departamento de Física

Orientador: Thomas Fasquelle

Membro Colaborador - Universidade de Évora

Agradecimentos

Em primeiro lugar gostaria de agradecer aos meus orientadores, Thomas Fasquelle e Hugo Gonçalves da Silva, não só por terem aceite orientar-me neste trabalho mas também pela forma como o fizeram. Foram incansáveis e sem eles nada disto teria sido possível. Como tal quero agradecer-lhes por todos os ensinamentos que me transmitiram ao longo destes meses, assim como todo o incentivo, apoio e paciência que tiveram para comigo.

Quero também deixar um agradecimento especial à minha família, namorado e amigos por estarem sempre presentes e me apoiarem ao longo de todo o meu percurso académico.

Ao meu colega Francisco M. Lopes pela sua contribuição neste trabalho com o tratamento e fornecimento dos dados meteorológicos essenciais para proceder às simulações.

Por fim, a todos os meus colegas da EMSP tanto pelas diversas ajudas que me foram dando assim como pelo bom ambiente de trabalho que me proporcionaram que torna tudo muito mais fácil. Obrigada a todos.

The more our knowledge increases, the more evident is our ignorance.

(John F. Kennedy)

Abstract

Parabolic trough power plants have been the most commercially implemented solar thermal electricity plants in the world. As such, several studies have been carried out over the last years in order to improve the efficiency/reduce the costs of this type of plants. From here it came the possibility of using the salts, that are currently used in this type of plants as storage fluid only, as heat transfer fluid (HTF). Its use as HTF seems to be a viable solution, however its implementation requires careful analysis. The project that gave rise to this dissertation aims to study this feasibility. During this work, the advantages and disadvantages of the salts in relation to the thermal oils (HTF currently used in this type of installations) will be presented and demonstrated, and SAM simulations will be performed to analyse the performance of a platform with the different fluids. Finally, the changes caused in the LCOE as well as in the power block design and efficiency will be determined.

Key Words: Solar Energy; Concentration; Thermal Storage; Molten Salts; High Temperature.

Resumo

VANTAGENS E DESVANTAGENS DOS SAIS FUNDIDOS DE BAIXO PONTO DE FUSÃO NUM SISTEMA DE FOCO LINEAR

As centrais lineares de coletores cilíndrico-parabólicos são atualmente a tecnologia de geração solar termoelétrica mais utilizada em todo o mundo. Como tal, vários estudos têm vindo a ser realizados ao longo dos últimos anos com o intuito de melhorar a eficiência/reduzir os custos deste tipo de plantas. Daqui surgiu a possibilidade de utilizar os sais fundidos, já utilizados neste tipo de plantas apenas como fluido de armazenamento, também como fluido de transferência de calor (HTF). A sua utilização como HTF parece ser uma solução viável, no entanto a sua implementação requer uma análise cuidada. O projeto que deu origem a esta dissertação tem como objetivo estudar essa viabilidade. Ao longo deste trabalho serão apresentadas e demonstradas as vantagens e desvantagens dos sais em relação aos óleos térmicos (HTF utilizado atualmente neste tipo de instalações), realizadas simulações em SAM para analisar a performance de uma plataforma com os distintos fluidos e por fim determinadas as alterações provocadas no LCOE assim como no desempenho e eficiência do bloco de potência.

Palavras-chave: Energia Solar; Concentração; Armazenamento térmico; Sais Fundidos; Alta Temperatura.

Table of contents

List of figures

List of tables

Nomenclature

Acronyms	
$CAPEX$	Capital Expenditure
CSP	Concentrated Solar Power
DT	Drainage Tank
$EMSP$	Évora Molten Salt Platform
EVA/ECO	Evaporator/Economizer
HTF	Heat Transfer Fluid
$HPS2$	High-Performance Solar 2
IAM	Incidence Angle Modifier
IEA	International Energy Agency
$LCOE$	Levelized Cost Of Electricity
$LCOH$	Levelized Cost Of Heat
LF	Linear Focusing
MS	Molten Salts
$NREL$	National Renewable Energy Laboratory
$O\&M$	Operation and Maintenance
$OPEX$	Operational Expenditure
PCM	Phase Change Material
PF	Point Focusing
PTC	Parabolic Trough Collector
SAM	System Advisor Model
SCA	Solar Collecting Assembly
SCE	Solar Collector Element
SH	Superheater
TES	Thermal Energy Storage
TMY	Typical Meteorological Year
VHC	Volumetric Heat Capacity
YMS	Yara Most molten salts
Partner acronyms	
DLR	Deutsches Zentrum für Luft- und Raumfahrt – German Aerospace Center
ELT	Eltherm
ESK	ESKOM
FLG	TSK FlagSol
RIO	Rioglass
STE	Steinmüller
UEV	University of Évora
YAR	Yara Company

Variables		
A	Area	m²
Ap	Aperture	m
Cp	Specific heat	$J.kg^{-1}.K^{-1}$
D	Diameter	m
e	Thickness	m
H	Height	m
h	Heat transfer coefficient	$W.m^{-2}.K^{-1}$
I	Electrical Current	A
L	Length	m
M	Mass	kg
$\dot{m}$	Mass flow	$kg.s^{-1}$
Q	Heat	W
R	Resistance	$K.W^{-1}$
r	Radius	m
S	Section	m^2
T	Temperature	°C, K
U	Electrical Voltage	V
v	Velocity	$m.s^{-1}$
Greeks		
k	Thermal conductivity	$W.m^{-1}.K^{-1}$
ρ	Density	$kg.m^{-3}$
μ	Dynamic viscosity	Pa.s
θ	Angle	°
η	Efficiency	-
Δ	Difference	-
π	Pi number	≈ 3.14159

Subscripts	
a	Absorber
avg	Average
C	Cold
c	Glass cover
col	Collector
$cond$	Conduction
$conv$	Convection
CS	Cold Source
dry	Ambient dry
eq	Equivalent
ex	Exergy
ext	External
f	Fluid
fr	Friction factor
gap	Space between collectors
H	Hot
hdr	Headers
hl_{pm}	Head losses per meter
$hsec$	Headers section
HS	Hot Source
$heat$	Heating
i, ins	Insulation
in	Inner
int	Internal
$IOCop$	Inlet, Outlet and Cross over pipe
l	Loss
max	Maximum
p	Pipe
PB	Power Block
rec	Receiver
$Rough$	Relative roughness
run	Runners
$runsec$	Runner section
spd	speed
t	Tank
th	Thermal
tot	Total

1

Introduction

Due to the population increase and the industrial development that the world has undergone over the last decades, energy consumption has increased exponentially. According to studies carried out by International Energy Agency (IEA), between 1970 and 2015 the energy consumption has doubled (**Figure 1**) while the electricity consumption increased by a factor of 4 (**Figure 2**). The main responsible for this increase are, in order of relevance, industry, households, public and commercial services and the transports.

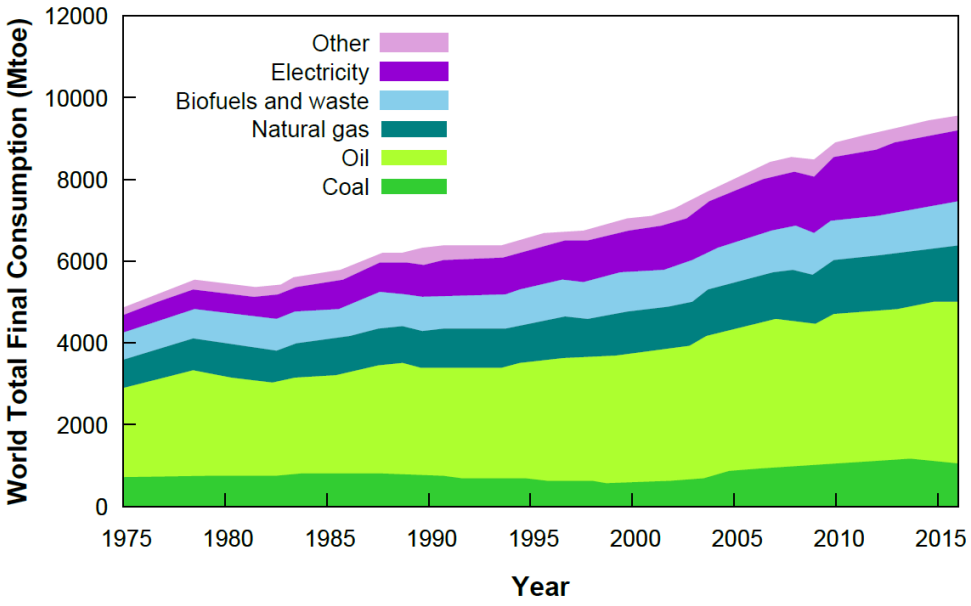

***Figure 1**: Evolution of energy consumption [1].*

This increase of energy consumption generates an increase in demand for fossil fuels, doubling CO_2 emissions during the same period [1]. As a consequence, a climatic change that brings worrying consequences for the planet is observed.

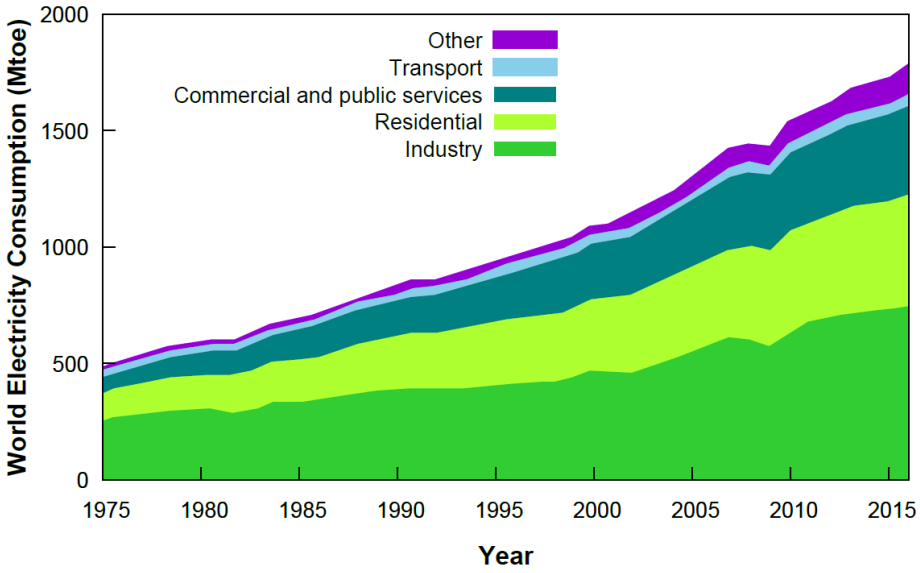

***Figure 2**: Evolution of electricity consumption by sector [1].*

In addition to that, high demand for fossil fuels has led to a reduction in world reserves, and consequently to higher prices. With these changes it becomes increasingly important to look for other solutions that enable energy sustainability. Renewable energy comprises for instance solar energy, wind energy, hydro energy, biomass and geothermal. Among the mentioned renewables energies, wind energy and solar photovoltaic currently lead the market [2].

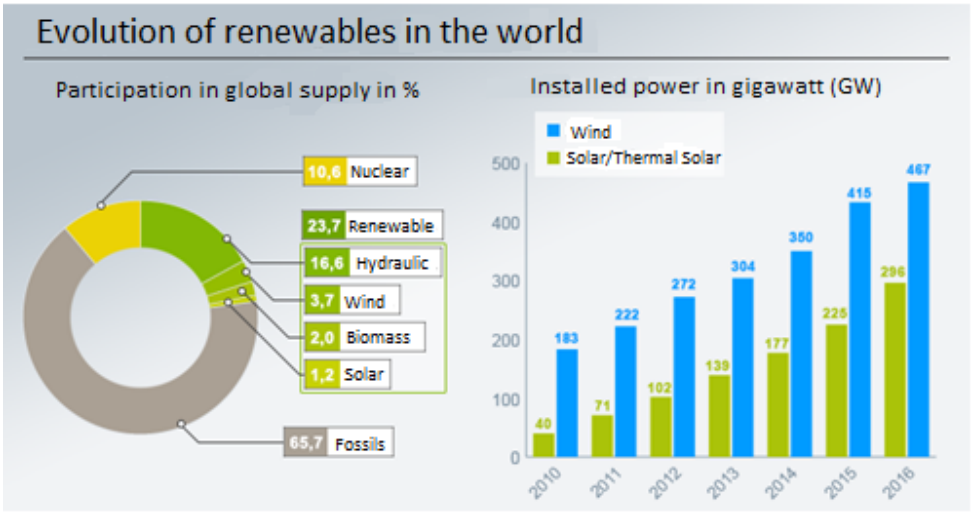

***Figure 3**: Evolution of renewable energies in the world [2].*

Between 2010 and 2016 there was an increase of 284 GW of installed wind power capacity and an increase of 256 GW of installed solar power/solar thermal power worldwide [2].

Concentrated Solar Power (CSP) is still an expensive technology and so it is still at a relatively early stage. Spain and the United States are the countries that have contributed most to the development of this technology (**Figure 4**) [3].

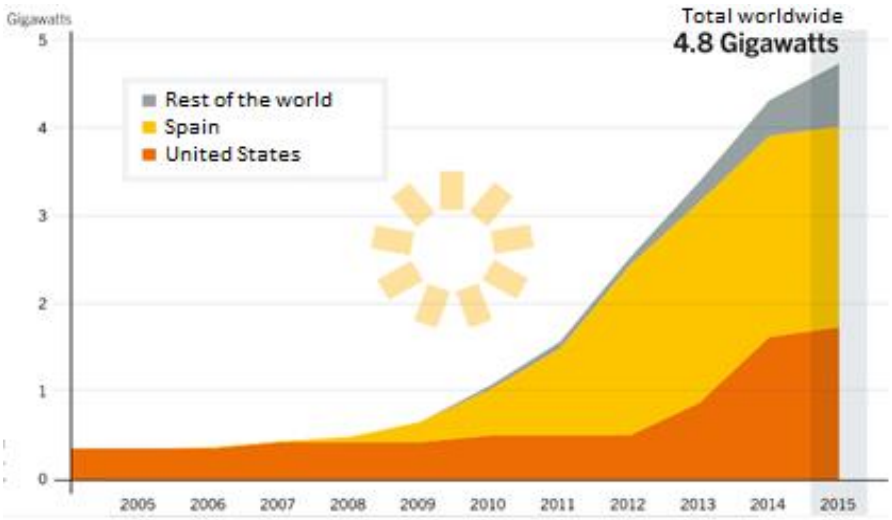

***Figure 4**: Development of CSP between 2005 and 2015 [3].*

However, this technology presents the possibility of storing thermal energy cheaply and efficiently, allowing the production of energy not only during the period of solar irradiation but also during times of greater demand. Thermal Energy Storage (TES) solves the solar intermittency problem that can cause disturbances in the electrical grid.

Most of the commercial CSP systems installed around the world use parabolic trough collectors as concentration elements and thermal oils as heat transfer fluid (HTF). Those having storage use molten salts (MS) as energy storage fluid, yet many do not have a thermal storage system [4]. The thermal efficiency of the current parabolic trough power plants is limited by the HTF maximum operating temperature, which is generally below 400 °C when using thermal oils. Molten salts are already widely used, but only as heat storage fluid because of their high thermal capacity, their lower cost and their thermal stability (no risks of fires).

However, the possibility of using molten salts also as HTF has been the subject of various investigations, since these have several advantages such as the possibility of increasing the output temperature of the solar field to 450-565 °C (compared to a conventional value of 393 °C with thermal oils). Thus, the Rankine cycle's efficiency can be increased from 37.6% to 40% [5]. Moreover, molten salts have low vapor pressure at high temperatures, high boiling temperature, relatively high thermal conductivity and high thermal capacity. Their use as HTF not only reduces the physical size of the storage system but also allows the reduction of the investment costs since their use implies no need for a heat exchanger between the HTF and the storage medium. On the other hand, its use as HTF requires a careful evaluation of certain aspects such as melting point, corrosivity and cost, among others.

The present study goes along with the construction of a 3.6 MW_t parabolic trough plant, called High Performance Solar 2 (HPS2), whose website can be visited through the link http://www.emsp.uevora.pt/, that will use molten salts (YaraMost) as HTF.

With the elaboration of this project it is pretended here to verify the viability of the use of molten salts as HTF in parabolic trough power plants. To assess the associated advantages and drawbacks of such solution, different evaluations will be performed.

First, in Chapter 2 and 3, a comparison between different properties, namely, melting point, maximum operating temperature, density, viscosity, specific heat, conductivity and costs, will be performed. For this comparison, one synthetic oil, Therminol VP-1* was chosen because it is one of the most used in CSP plants and because other thermal oils that are used have very similar properties [1]. Three different molten salts were considered: Solar Salt (60% $NaNO_3$ and 40% KNO_3), Hitec (7% $NaNO_3$, 53% KNO_3 and 40% $NaNO_2$) and Hitec XL (7% $NaNO_3$, 45% KNO_3 and 48% $Ca(NO_3)_2$ [2], as it is not clear yet what salt will be implemented in future commercial plants. Solar Salt is currently the market leader for central receiver solar tower plants, while the two others have been developed to reduce freezing risks. Hitec XL has a very similar composition than of the Yara Most salt used in HPS2.

Then, in Chapter 4, SAM (System Advisor Model) software, developed by the NREL (National Renewable Energy Laboratory) [3], will be used to perform simulations of the general operation of HPS2 solar plant. Both the software and its inputs introduced to carry out the simulation will be presented. Subsequently, a comparison of the general operation of the plant (consumption for antifreeze protection, net global electrical production, possible problems, particular days, long periods of sun, among others) will be performed with the different HTF that are considered.

Consequently, in Chapter 5, the large temperature difference that is allowed by the use of molten salts will have an impact on the power block. Therefore, possible configurations and related efficiencies will be assessed and compared to those of the current commercial plants using thermal oil as HTF.

Finally, in Chapter 6, all the obtained conclusions and recommendations drawn from this project will be summarized in a final chapter.

1.1. Concentrated Solar Power

The concentration of solar energy consists of the reflection of direct solar irradiance by means of a system of mirrors, called collectors. These collectors track the position of the sun throughout the day and concentrate the reflected irradiance at a “point” or a “line”, called receiver. In a CSP power plant, the concentrated flux is transformed into heat that is absorbed in this receiver and transmitted to a heat transfer fluid. Thereafter it can be used for process heat or for electricity generation.

There are several types of heat transfer fluids which are divided into several groups: synthetic and organic thermal oils, molten salts, water, air/gases and liquid metals.

These HTFs work in different temperature ranges; the choice of working fluid being made according to the needs of each system.

Usually, liquid water is used in low concentration systems (until 100 °C if not pressurized and 200 °C if pressurized), thermal oils in low-medium concentration systems (until 400 °C with a pressure up to 14 bars) and molten salts in medium-high concentration systems (until 600 °C in tower plants, with no pressurization). Air and liquid metals are used for high concentration systems with operating temperatures above 800 °C.

Compared to other conventional thermal power plants, which burn fossil fuels to produce steam, CSP plants have a large number of components. They need a field of solar concentrators to produce heat, a storage system to prevent the oscillations in the electrical production that the lack of resource can cause in the grid, and a heat exchanger to produce the vapor. This makes CSP plant operation an apparently complicated and expensive process, though very versatile. However, this type of energy production has two advantages over other renewable energy technologies: production of multiple types of energy (heat, cold, electricity) and thermal storage [4]. In other words, the thermal energy produced in the solar field can be directly used to feed a steam cycle (e.g. a Rankine/Hirn cycle) to generate electricity or it can be stored in a thermal storage system to be used when it is most convenient.

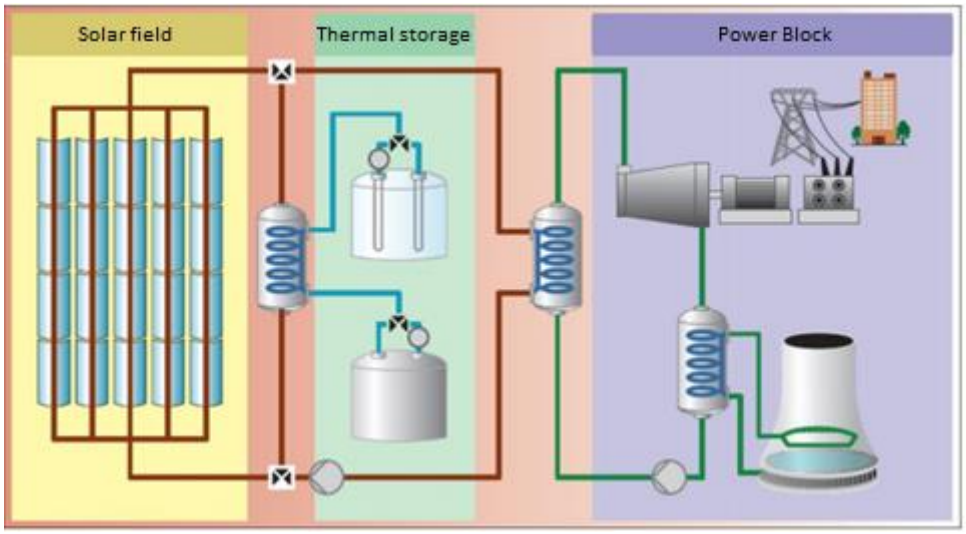

***Figure 5**: Elements of a CSP power plant [5].*

Solar concentration systems are divided into two types of configurations, linear focusing systems (LF) and point focusing systems (PF). The linear focusing systems include parabolic troughs and Fresnel collector systems, while point focus systems include parabolic dishes and tower plants:

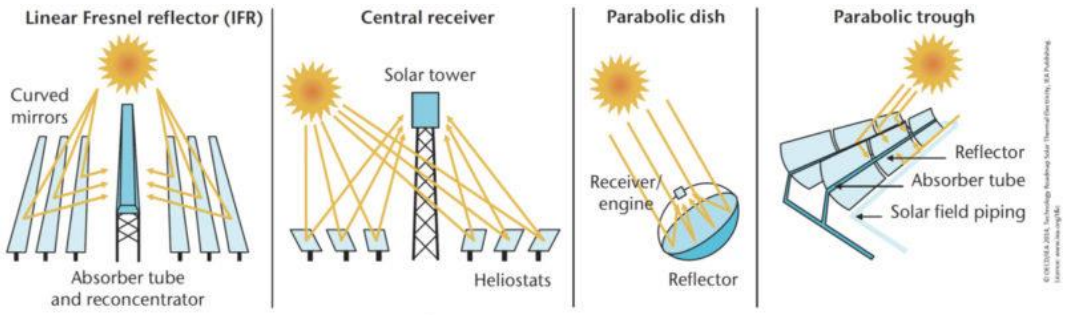

***Figure 6**: Different systems of solar concentration [5].*

Typically, as said above, commercial linear CSP plants use thermal oils as heat transfer fluid and their operating temperature ranges within 290 °C and 390 °C, the high temperature being limited by the stability of the thermal oil that is used. The efficiency of the annual peak conversion of solar energy into thermal energy of this type of power plant is around 14 - 20 % [6].

In commercial central receiver plants, as the concentration factor is higher, the use of molten salts as HTF is more frequent since they allow reaching higher operating temperatures: between 290 °C and 565 °C. In this way, both the power cycle and the direct TES are beneficiary. Increasing the operating temperature allows to improve peak conversion efficiency to 23-35% due to increased power cycle efficiency (37.7% in LF *vs.* 41.6% in PF systems [6]). In central receiver plants, the use of molten salts as HTF is a viable solution because molten salts only circulate between the storage tank and the solar tower. Those are very short paths in which it is relatively easy to implement an external heating source to ensure that the salts' temperatures do not lower close to their melting point, compromising the entire plant.

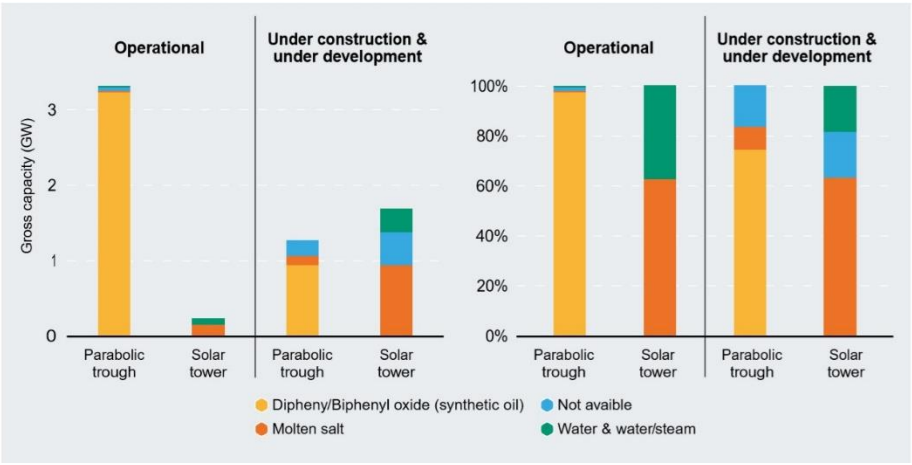

***Figure 7:** Heat transfer fluids used in operational and developing CSP plants [7].*

The implementation of MS as HTF also in LF plants is a hypothesis that arouses great interest by the possibility of increasing the operating temperature and consequently the efficiency of this type of plants. Nevertheless, in this case, the HTF circulates through several kilometres of receiver tubes and needs an external heating sources to ensure that they do not freeze inside the pipes during periods without sun. This

equipment is complex and expensive and can significantly increase Operation and Maintenance (O&M) costs. In this way, several projects have been developed with the objective of finding salts with a lower melting point that make this hypothesis a viable solution.

1.2 Energy Storage

Energy storage is the accumulation of some form of energy that can later be used to perform useful operations. Energy appears in many forms: potential (e.g. chemical or gravitational), kinetic, electrical or thermal. All these forms of energy can be stored with appropriate methods, systems, or technologies. More information about this subject is available in [8]. In this work, focus is given to thermal energy storage.

1.2.1 Types of thermal energy storage

TES has the potential to increase the production of thermal power plants and facilitate large-scale switching. it is useful for correcting the temporal lag between supply and demand of energy. There are basically three types of TES systems, sensible heat storage systems, latent heat storage systems and thermochemical storage systems.

Sensible heat represents the energy released (or absorbed) by a material as its temperature is reduced (or increased). The amount of sensible heat that a material can store is given by **equation (1):**

$$Q = M \cdot Cp \cdot \Delta T \quad \textbf{(1)}$$

Where *M* (in kg) is the mass of the material, *Cp* (in J.kg.K^{-1}) is the specific heat of the material and ΔT (in °C or K) is the temperature range. When the temperature of a material increases, its energy content also increases. The bigger the amount of mass, the thermal capacity or the temperature range, the greater the amount of energy that can be stored.

On the other hand, the latent heat represents the energy associated with phase changes of the materials. The energy required to convert a solid material into a liquid material or a liquid material into a gas (different phase changes) is called heat of fusion and heat of vaporization, respectively. The materials used for this type of storage are called Phase Change Materials (PCMs).

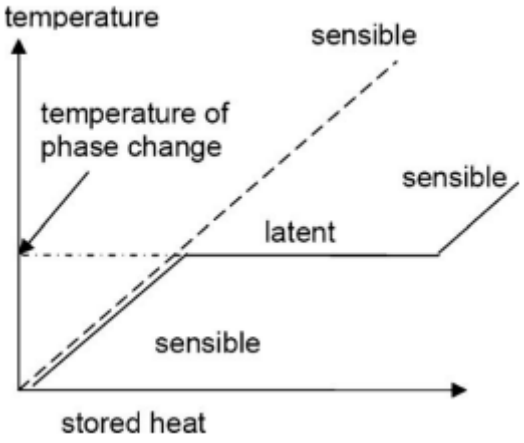

Figure 8: *Sensible and latent heat storage [9].*

The last category of heat storage is achieved through the use of reversible endothermic chemical reactions. Chemical heat is associated with these reactions, where the heat is needed to dissociate a chemical product. All this heat (or almost all) will be recovered later, when the synthesis reaction occurs. An example of this reaction is:

$$2NH_3 + heat \rightarrow N_2 + 3H_2, \qquad \textbf{(R 1)}$$

$$N_2 + 3H_2 \rightarrow 2NH_3 + \text{heat}. \qquad \textbf{(R 2)}$$

A complete storage process involves at least three stages: charging, storing and discharging. Out of the three types of storage systems that were mentioned, heat storage through chemical reactions is the one with the highest energy storage capacity, between 722 kWh.m^{-3} and 1220 kWh.m^{-3} [10]. Second is latent heat, with between 68.1 kWh.m^{-3} and 127.5 kWh.m^{-3} [10], and sensible heat appears as the method with the lowest storage capacity: 50-60 kWh.m^{-3} (for operating temperatures between 200 °C and 400 °C). However, with the use of the molten salts the value of storage capacity in the form of sensible heat can be increased, for example with solar salt (commercially used molten salt), which operates between 290 °C and 565 °C, this value is 250 kWh.m^{-3} [10]. With carbonate salts, whose temperatures can reach 850 °C, this value can even attain 430 kWh.m^{-3}.

Despite storage in the form of latent heat and through chemical reactions generally have storage capacities higher than sensible heat, systems with these types of thermal storage are still in development. As they are not widely marketed they still have very high costs. In this way, the focus is directed to sensible heat with special attention to the molten salts that present a storage capacity of sensible heat quite interesting, due to possible high temperature differences.

1.2.2 Active and passive storage systems, direct and indirect storage systems

Energy storage systems can be classified as active systems or passive systems.

An active system is characterized by the forced convection heat transfer into storage material, i.e., the storage medium itself circulates through a heat exchanger (this heat exchanger can also be a solar receiver or a steam generator). This type of system typically uses one or two storage tanks. The active systems are divided into direct systems and indirect systems. In direct active systems the heat transfer fluid also serves as storage fluid, in indirect active systems, the HTF and the storage fluid are distinct.

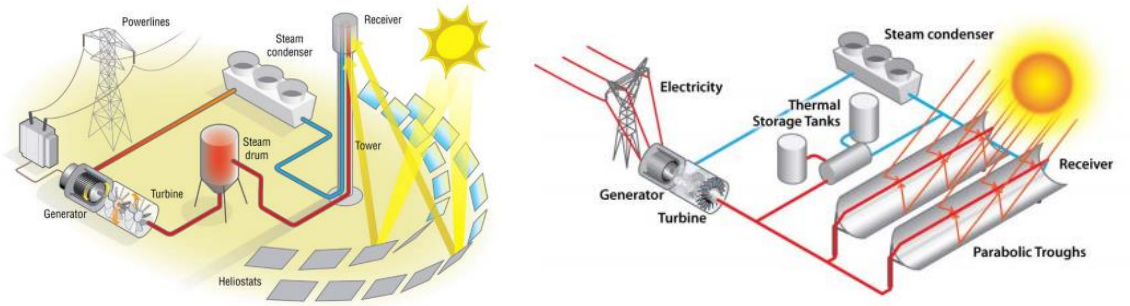

***Figure 9**: Direct storage system (left) and indirect storage system (right) [12].*

In a passive storage system, the HTF circulates through the storage system, usually a solid material, promoting heat exchange between the two without using a heat exchanger [11]. An example of this type of storage is the “concrete block” in which the same fluid that circulates in the solar field also circulates inside the block promoting its heating.

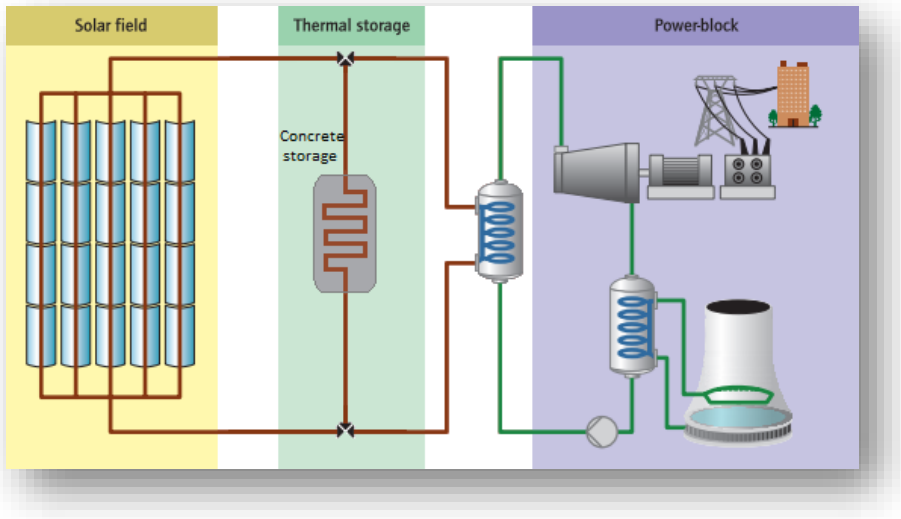

Figure 10: Passive storage system (concrete block).

It is possible to observe several references of plants with diverse types of storage in [11].

1.2.3 Sensible storage system choice

Several factors must be considered when deciding the type and design of any thermal storage system. A very important point in designing a TES system is its thermal capacity. Nonetheless, selection of the appropriate system depends on many considerations such as cost, technical and environmental criteria. The cost of a TES system depends mainly on the following items: storage material, heat exchanger and cost of the space and/or enclosure for the TES [11].

From the technical point of view, the most important criteria in the selection of a storage system are the high energy density of the storage material (storage capacity), good heat transfer between the HTF and the storage medium (efficiency), mechanical and chemical stability of the storage material (must withstand several loading/unloading cycles), compatibility between HTF, heat exchanger and/or storage medium (security), complete reversibility of multiple charge/discharge cycles (service life), low thermal losses and ease of control [11].

In addition to the already mentioned criteria, there are others that are specific to the storage of sensible heat: specific heat, operating temperature, thermal conductivity, vapor pressure, thermal losses and storage fluid costs.

1.3 HPS2 Project

HPS2 is a project under development at the University of Évora (UEV), integrating a consortium of companies led by DLR (German Aerospace Center), whose objective is

the construction of an experimental solar plant in the Évora Molten Salt Platform (EMSP). The aim of this project is to erect and operate a thermal plant with parabolic trough solar concentrator field using molten salts as heat transfer and storage fluid. The consortium of the HPS2 project is constituted by: **DLR**, project's coordinator; **UEV**, proprietary of EMSP; **TSK Flagsol Engineering**, responsible for the development and installation of solar collectors HelioTrough; **Yara Company** (**YAR**) that has developed and provided the ternary salts with low melting temperature (YARA MOST). Are also part of the consortium **Eltherm** (responsible for impedance heating system of the absorber tubes), **Steinmuller Engineering** (responsible for the steam generator) and **Rioglass** (responsible for the absorber tubes compatible with molten salts circulation and high temperature).

This project intends to increase the working temperature of the solar power plants by using MS as HTF and therefore directly circulate them in the solar field. This implementation will allow the removal of the thermal oil circuit and an increase in the efficiency of the electrical production, resulting in a significant reduction of the electricity production cost.

Figure 11: Évora Molten Salt Platform;

The solar field consists of four Solar Collectors Assemblies (SCA), each with a 171 m length and with an aperture of 6.77 m (more information about this topic will be detailed in **3.1 Information about HPS2 Project**). The MS that will be used as heat transfer and storage fluid, Yara MOST, consists of a ternary mixture based on potassium nitrate (KNO_3), sodium nitrate ($NaNO_3$) and as source of calcium nitrate Yara NitCal-K, a patented double salt $KNO_3.5Ca(NO_3)_2.10H_2O$; with a proportion of 43% KNO_3, 15% $NaNO_3$ and 42% $Ca(NO_3)_2$. This ternary mixture has the same composition

as the Hitec XL salt and has a melting point of 131 °C, being able to reach 80 °C without full solidification due to super cooling effect; which reduces the risk of freezing in specific situations [12]. In this way, the minimum process temperature is set to 170 °C to ensure that the temperature of the fluid in the pipes does not approach these values. Storage will be done thanks to a two-tank system: a cold tank at 290 °C and a hot tank at 500 °C.

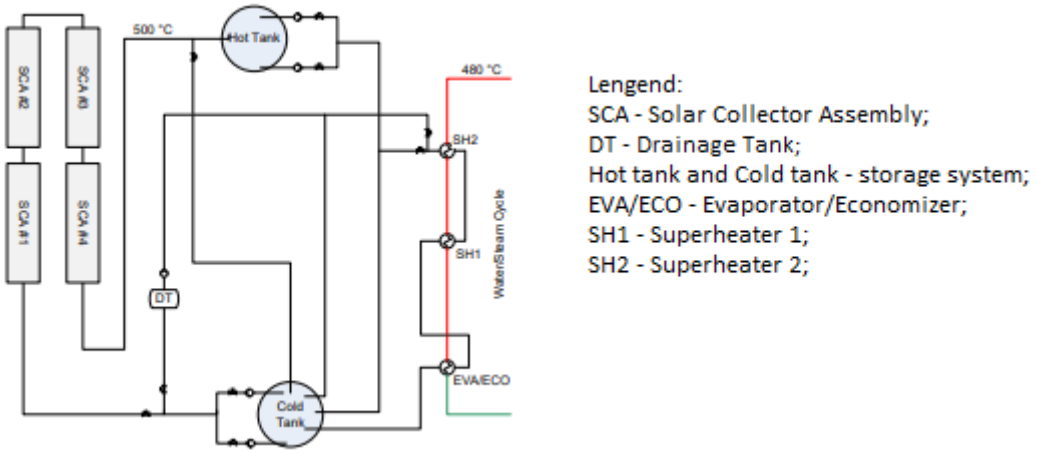

Figure 12: *Simplified design plant [12].*

Some aspects should be tested during the operation of the platform [12]:

- Demonstration of the stable operation of the plant both under normal solar irradiance conditions and in critical situations, such as during night or cloudy periods;
- Verification of the properties of the HTF, namely, viscosity, density, specific heat, thermal conductivity, melting temperature, thermal stability at 500 °C (or higher) and corrosion of the plant components;
- Ensure stable steam production;
- Simulation of daily starts and subsequent stops, as well as night operation;
- Ensure optimized operation to reduce plant costs and at the same time ensure safe and reliable operation.

1.3.1 Solar field heating systems

Due to the high melting point of the HTF it is necessary to implement an electric heating system in order to ensure the supply of heat to all surfaces in contact with the MS in conditions where the solar irradiance and the thermal energy stored in the system are not sufficient to maintain the set input temperature. This heating system will be made in two ways:

- Interconnecting piping: all interconnecting piping and associated instrumentation is heated by electrical heat tracing. The cables are placed around the surface of the pipes and covered with thermal insulation.

- Receiver tubes: to heat the receiver tubes without shading their surface, and to overcome the problems of placing the heat tracing in a vacuum and electrical resistance receiving solar flux, the heating is made by impedance. A voltage is applied at the ends of the receiver tubes and it is necessary to ensure proper electrical insulation of the absorbers supports.

1.3.2 Thermal storage system

Thermal storage tanks play a key role in this type of systems. They allow storing the hot MS in order to increase the steam generation overall duration, and they provide thermal inertia and therefore can be used for antifreeze operation during night. Finally, they offer the possibility of producing energy when it is more convenient. This is the most positive aspect of solar thermal energy that gives it competitiveness with other forms of renewable energy, such as photovoltaics.

2

Heat Transfer Fluid (HTF)

2.1 The different heat transfer fluids that are investigated

The HTF used or considered in CSP plants can be separated into different groups: air, water, steam, thermal oils, molten salts and liquid metals.

Air: The main advantages of using air as HTF are that it can reach very high temperatures and be free. However, the air has a very low density, is a bad thermal conductor and does not allow the storage of energy. Its use as a possible HTF in tower plants is under investigation.

Water: Liquid water has excellent characteristics to be used as HTF, such as low viscosity, high storage capacity due to its high specific heat (*Cp*) and density and can be considered essentially free. Although, the use of water is usually limited to low concentration systems, because of its low boiling point (100 °C @ 1 atm).

Steam: The use of steam as HTF allows operating at very high temperature. It is basically free and sometimes its use allows to save a heat exchanger by directly using the steam generated in the solar field to drive the turbine. Despite of this, it is very difficult to store energy with this fluid. Indeed, water undergoing a phase transition inside the pipes is very difficult to control, steam causes high pressure losses and steam density is very low. Furthermore, the heat transfer coefficient (h) of the steam is very low and this triggers problems for receiver tube design.

Thermal oils: The thermal oils can be divided into mineral oils, silicone oils and synthetic oils [1]. The thermal oils have low melting points (around 0 °C [13] and 12 °C [14] for the oils that are often used in CSP) and can be thermally stable up to approximately 400 °C [14]. They are therefore used as HTF in many commercial parabolic trough systems. However, they have a low density, are toxic, flammable and expensive, so they are not a good storage medium.

Molten salts: The main advantage of the use of molten salts as HTF is their thermal stability and high operating temperature range, which allows operating a CSP plant at temperatures up to 565 °C. They are also a great storage medium due to their low vapor pressure, high density and good thermal capacity. However, they have very high melting points (120 °C to 220 °C) and they are corrosive, whose arise O&M issues.

Liquid metals: Liquid metals have been used in nuclear industries since the 1940's [15] and are currently being studied for a use in solar thermal systems as HTF and TES medium. Until now, liquid metals have not yet been used in commercial CSP applications, however they have several promising properties, including extensive operating temperature range, low viscosity and good heat transfer coefficient. For example, the liquid sodium has an operating temperature range of 98-883 °C [15, 16]. Still, the main drawbacks of liquid metals are their relatively high cost when compared to MS or other HTFs, and their high combustibility when in contact with water [16]. In addition, thermal capacity of these liquid metals is relatively smaller than the nitrate salts and, therefore, are less favourable to be used as a storage medium [17].

Among the different HTFs that were mentioned here, the ones that are of most interest to LF solar plants are the thermal oils and the molten salts. On one hand, thermal oils are the most used HTFs in CSP commercial plants [11], and their behaviour is already well known. On the other hand, molten salts offer higher operating temperatures and therefore improve cycle efficiency and allow direct storage.

2.2 Heat transfer fluid main properties

Some of the most important properties to analyse in a heat transfer fluid are:

- Melting temperature.
- Maximum operating temperature.
- Density.
- Viscosity.
- Specific heat.
- Conductivity.
- Volumetric Heat Capacity (VHC).

Melting Temperature

The melting temperature is a very important factor in the selection of a HTF, because higher temperatures require more precautions to ensure safe operation of the platform. For example, MS present high melting temperatures (between 120 °C for HitecXL and 220 °C for Solar Salt) [2] when compared with thermal oils (12 °C for Therminol VP-1) [14]. The higher this value, the greater care is needed and consequently higher O&M costs.

Melting point and freezing of a substance do not always occur at the same temperature. The melting point of a solid is the temperature at which the liquid phase and the solid phase are equal and at equilibrium. Increasing the temperature of a solid will induce its melting but decreasing the temperature of a liquid past the same temperature will not necessary imply its freezing, due to supercooling effect. It is for this reason that in this work will be used the melting temperature as a performance indicator and not the freezing temperature.

Maximum operating temperature [°C]

The efficiency of a CSP plant is directly related to its maximum operating temperature. The maximum efficiency of a heat engine is given by the efficiency of the Carnot's engine and is directly related to its operating temperature range. This maximum efficiency is obtained by Equation **(2)**:

$$\eta_{Carnot} = \left(1 - \frac{T_{CS}}{T_{HS}}\right) \cdot 100\% \quad \textbf{(2)}$$

Where T_{CS} and T_{HS} represent the temperatures of the cold source (CS) and the hot source (HS), respectively, that are used to drive the thermodynamic cycle. Typically, the cold temperature corresponds to the ambient temperature while the hot source corresponds to the HTF temperature coming from the receiver(s). The greater the difference between HS temperature and CS temperature, the higher the thermal machine's efficiency. Although higher temperatures correspond to greater thermal losses, these losses are compensated by the increased cycle efficiency, as well as the storage systems physical size reduction.

Dynamic viscosity [Pa.s]

The viscosity of the HTF is a very important factor since it directly affects the mass flow and the thermal performance of the system. It is important that the fluid does not have a too high viscosity to be a good HTF. The viscosity tends to decrease with increasing fluid temperature and the lower the viscosity, the better the transport conditions of that fluid. Usually, the thermal oils have a viscosity value which is much lower than the MS when subjected to the same conditions, i.e. at the same operating temperature range. But, a remark should be made that in CSP applications MS operate at temperatures 100 °C higher than the thermal oils, as it will be discussed below in **4.1 Analytic comparison between thermal oils and molten salts**.

Density (or specific mass) [$kg.m^{-3}$]

The density represents the amount of mass per volume unit. In terms of storage, the higher the density of the fluid, the more interesting it is, since it allows having a greater amount of mass in a smaller volume which allows reducing the size of the

tanks. However, the density value also has an influence on the consumption of the pump to circulate it within the pipes. Hence, to be a good HTF, this value cannot be exaggeratedly high.

Specific heat (thermal capacity) [J. $kg^{-1}.K^{-1}$]

This property favours the operation of the system both with respect to the HTF and the storage fluid. Indeed, it directly influences the amount of heat that can be stored, as well as the convection heat transfer coefficients. Therefore, in order to increase the efficiency of the system as a whole, a fluid with high thermal capacity is required.

Volumetric Heat Capacity (VHC)

Volumetric Heat Capacity (VHC) represents the amount of energy that a determined volume of fluid stores when it increases its temperature by one degree. It is obtained by multiplying the density by the specific heat ($\rho.Cp$) of the fluid and its unit is [$J.m^{-3}.K^{-1}$]. This property allows making a relevant comparison between different storage fluids. Indeed, a fluid with higher VHC will necessitate less volume to store the same amount of heat.

Thermal conductivity (k) [$W.m^{-1}.K^{-1}$]

Thermal conductivity quantifies the capacity of materials to conduct thermal energy, i.e. materials with higher thermal conductivity conduct heat quicker and more efficiently than materials with a lower value. In this way, this property is directly related to the absorption of heat by the HTF inside the receiver tubes, as well as the heat exchange with the water in the steam generator.

2.3 Costs

HTF is one of the most important components for the overall performance of CSP, it is used in great quantity and its cost can completely prevent its use from a commercial point of view.

3

HPS2 detailed information and simulation inputs for SAM software

In this chapter it will be presented all information relevant to the simulation of the operation of HPS2 solar plant with the SAM software. Initially, the CSP Parabolic Trough (physical) model was tried, but, in fact, the Process Heat Parabolic Trough model showed to be better as it enabled to specify the piping length. As such, throughout this chapter information about the project will be given, a small presentation of the software will be made, and inputs introduced to carry out the simulation will be explained. In addition, it will be explained the calculations made to estimate thermal losses in the interconnecting piping and in the receiver tubes during nominal operation of the plant, as well as, during nights. In order to define operation strategies, thermal losses from the storage system and piping will be assessed, as well as, thermal inertia capacity of the cold tank to maintain the piping heated.

3.1 Information about HPS2 Project

3.1.1 General information

The HPS2 solar plant was developed with the aim of studying the impact of the use of MS as HTF on the operation of such plants. The HPS2 solar plant consists of a single loop with 4 solar collector assemblies (SCA), 2 of them with 10 solar collector elements (SCE) and the other 2 with 8 solar collector elements (SCE), having a total length of 684 m of solar collectors. The aperture area of the collectors is 6.77 m which makes a total aperture area of the solar field of 4631 m^2 and the nominal power of the solar field is 3.6 MW_t.

The particularity of the plant is the use of MS (YaraMOST) as HTF. The solar field inlet temperature during nominal operation will be 290 °C and the outlet temperature 500 °C. To achieve this higher working temperature, the concentration factor of the

developed collector is higher than the one of typical parabolic trough collectors (PTC) (C ≈ 31 *vs.* C ≈ 26), thanks to a higher Aperture (Ap = 6.77 m *vs.* 5.77 m) and an identical absorber external diameter ($D_{a,ext}$ = 0.07 m), see **equation (*3*)**

$$C = \frac{A_{col}}{A_{rec}} = \frac{Ap}{\pi \cdot D_{a,ext}} = \frac{6.77}{\pi \cdot 0.07} = 30.8 \quad \textbf{(3)}$$

The steam generator is composed of an evaporator and two superheaters. The power and pressure of the steam generator are 1.8 MW_t and 150 bars, respectively.

A table summarizing the main parameters of the plant is presented below (**Table 1**). As it is a research project and because the power of the plant is low, it is difficult to find appropriate turbines and their performance will be lower than the ones used in actual solar thermal plants. Besides, the production of electricity is not a goal for HPS2 so there is no turbine in this plant yet and steam exits the steam generator directly into the condenser.

***Table 1**:The main parameters of HPS2 plant.*

Nominal power [MW_t]	3.6
Expected maximum power [MW_t]	3.2
Low temperature [°C]	290
High temperature [°C]	500
Steam generator power [MW_t]	1.8
Steam generator pressure [bar]	150

Details on heat transfer fluid properties, solar field dimensions and storage system will be given in the following sections.

3.1.2 Heat Transfer Fluid (HTF)

The HTF used in this project is Yara Most molten salt. This salt has the same composition than HitecXL, $Ca(NO_3)_2$-$NaNO_3$-KNO_3, and therefore very similar physicochemical properties. Yara Most supplier performed comparisons between thermal properties of the two fluids and they confirmed that both salts are very akin [18]. As a consequence, in SAM simulations Hitec XL will be used, since its thermal properties are well known and it is already incorporated in the software's fluids list. Main thermal properties of HitecXL can be assessed with the following equations [30] and with the fluid temperature T_f in Celcius:

$$\rho_{HitecXL}(kg.m^{-3}) = 2240 - 0.727 \cdot T_f, \quad \textbf{(4)}$$

$$Cp_{HitecXL}(J.kg^{-1}.K^{-1}) = 1440, \quad \textbf{(5)}$$

$$k_{HitecXL}(W.m^{-1}.K^{-1}) = 0.52, \quad \textbf{(6)}$$

$$\mu_{YMS}(Pa.s) = 1372144.977 \cdot T_f^{-3.36406}, \quad \textbf{(7)}$$

$$L_{HitecXL}(kJ.kg^{-1}) = 120.5 \text{ (latent heat)}. \quad \textbf{(8)}$$

Conductivity and specific heat typically vary with temperature, however YAR considers these variations to be negligible. In this way, the values mentioned are considered constant with respect to temperature variations.

3.1.3 Solar Field

As previously mentioned, the solar field consists of a single loop with North-South orientation collectors. The arrangement of the solar concentrators, as well as the main distances, can be observed in the following scheme **(Figure 13):**

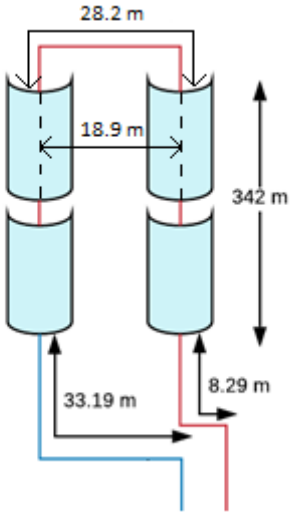

***Figure 13**: HPS2 Solar field scheme with lengths of piping and receivers.*

As can be seen in **Figure 13**, the collector lines are separated by an estimated 28.2 m cross over pipe and the actual distance between centres of collectors is 18.9 m. The receiver tubes have an outer diameter of 0.070 m and a length of 3.8 m each. Interconnection pipes have an outer diameter of 0.0889 m (3 inches). **Table 2** summarizes the main parameters of the solar field dimensions.

Table 2: The main parameters of solar field.

Total length of the solar field [m]	684
Length of one SCE [m]	19
Aperture of SCE [m]	6.77
Absorber tube´s diameter [m]	D_{a_in} = 0.064 and D_{a_ext} = 0.070
Dimensions of glass cover [m]	D_{c_in} = 0.119 and D_{c_ext} = 0.125
Length of a single receiver tube [m]	3.8
Space between lines' center [m]	18.9
Number of SCA	4
Number of SCE per SCA	2 SCA with 10 SCE and 2 SCA with 8 SCE
Diameter of interconnecting piping [m]	0.0889 (3 inches)

Additional information relevant for the analysis will be provided and explained later in the thesis; in the section 3.4 Software inputs.

3.1.4 Storage

The storage of this plant will be direct, i.e. the HTF will be used both in the solar field and in the energy storage tanks. Storage will be performed through two tanks: hot tank at ~500 °C and cold tank at ~290 °C. Inside each of these tanks, two pumps (main and back-up) will enable the circulation of the salts from the cold tank (bigger pump) to the solar field and from the hot tank (smaller pump) to the steam generator. In each tank, four thermal resistances of 5 kW each will ensure that the salts have always temperatures higher than the designed safety temperature. Each tank has an internal height of 5 m and internal diameter of 3.1 m. The minimum level of salt in each tank is 0.7 m while the maximum level is 4.5 m. Thus, the tanks have a maximum effective fluid volume of 29 m^3. With these values, 4.4 MW_th or 2.44 full load hours of energy storage capacity are estimated. **Table 3** gathers the main information about the storage system.

Table 3: Main information about the storage system.

Full load TES capacity [hours]	2.44
TES capacity [MW_th]	4.4
Tank height (inside) [m]	5
Tank diameter (inside) [m]	3.1
Minimum level of salt [m]	0.7
Maximum level of salt [m]	4.5

3.2 HPS2 thermal study

3.2.1 Thermal losses in the piping

Thermal losses are calculated for the piping zones appearing on **Figure 14**. Zone 1 and 4 are the interconnecting piping between the solar field and the tanks; zone 2 and 3 connect the tanks to the steam generator system; zone 5 is the crossover piping between the two lines of collectors. Calculations were made for each zone, according to their characteristics (HTF temperature and length), in order to calculate thermal losses as accurately as possible.

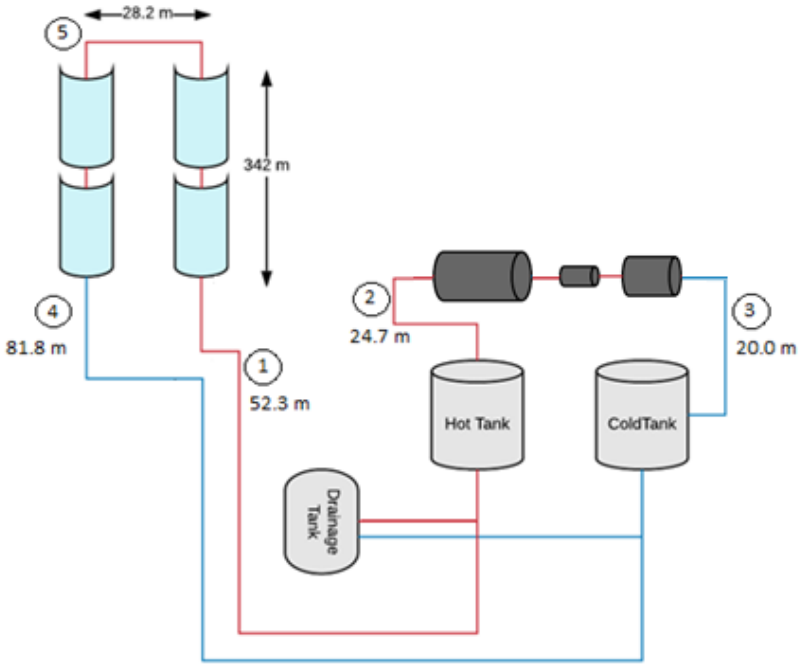

Figure 14: Diagram of the plant with the 5 different pipe zones marked. Hot lines appear in red and cold lines in blue.

It is assumed that all pipes have the same diameter of 3'' (although about 5 % of the plant is composed of 2" pipes where equipment, such as valves, are located) and an insulation thickness of 15 cm. The considered fluid temperature, in each piping zone marked in **Figure 14**, is given in the following table:

Table 4: Value of the temperature in each of the zones.

Zone	Temperature [°C]
1	500
2	500
3	290
4	290
5	400

In order to calculate thermal losses in the piping, three processes must be considered: 1) convective heat exchange between fluid and pipe; 2) conduction through the piping insulation; 3) convective heat exchange between the outer insulation and the air. Radiative losses depend on the surface emissivity, the system temperature and the temperature difference between the surface and the environment. As ambient and surface temperatures are very close **and the piping is protected by a low emissivity aluminium surface** [19], the radiative losses can be neglected. Conduction resistance through the metal piping is also neglected because its thickness is very small and its thermal conductivity is very high.

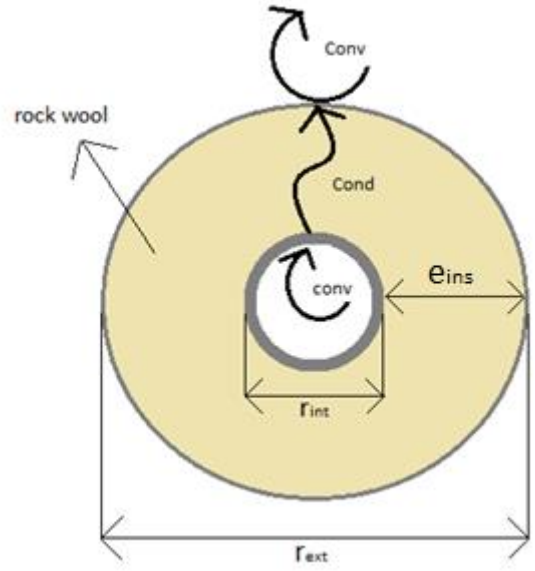

Figure 15: Heat transfer modes occurring for piping heat losses.

To determine the thermal losses occurring in the piping, its thermal resistance must be determined. In electricity, the electrical resistance, R, is calculated from the electrical voltage, U, and the electrical current, I, through Ohm's law, **equation (10)** ,

$$U = R \cdot I. \qquad \textbf{(9)}$$

In thermal analysis, similar equations hold by substituting the electrical voltage by the temperature difference between the two fluids, ΔT, and the electrical current by the thermal losses, P_{th}:

$$\Delta T = R_{th} \cdot P_{th}, \quad \textbf{(10)}$$

$$P_{th} = \frac{\Delta T}{R_{th}}, \quad \textbf{(11)}$$

R_{th} representing the equivalent thermal resistance. Moreover, the insulation is composed of rock wool, with 15 cm thickness (e_{ins}) and thermal conductivity that has been assumed to be k_{ins} = 0.06 $W.m^{-1}.K^{-1}$ (value obtained for the average operating temperature).

To calculate the thermal resistances the following expressions are used:

1) Convection heat exchange from the fluid to the pipes

The convective resistance is obtained by **equation (12)**:

$$R_{conv} = \frac{1}{h_{conv} \cdot S}. \quad \textbf{(12)}$$

Where h_{conv} corresponds to the heat transfer coefficient by convection and S to the heat transfer area. Parameter, h_{conv}, is obtained from **equation (13)** [20]:

$$h_{conv} = \frac{k_f}{D_h} \cdot Nu, \quad \textbf{(13)}$$

k_f corresponding to the thermal conductivity of the fluid, D_h being the hydraulic diameter of the pipe and *Nu* the fluid's Nusselt number. The Nusselt number is a quantity widely used to determine the convection heat transfer coefficients and depends on the fluid properties and its velocity. For a **fluid inside a tube and in a turbulent regime**, the following expression can be used [20],

$$Nu = 0.023 \cdot Re^{0.8} \cdot Pr^{n}, \quad \textbf{(14)}$$
$$Re > 10\,000\,; 0.7 < Pr < 160$$

Where *Pr* corresponds to the number of Prandtl, obtained through the expression [21],

$$Pr = \frac{\mu \cdot C_p}{k}, \quad \textbf{(15)}$$

here μ is the viscosity, C_p the specific heat and *k* the thermal conductivity of the fluid. The number of Prandtl is raised to 0.3 (n = 0.3) when it comes to cooling the fluid and elevated to 0.4 (n = 0.4) when it comes to heating the fluid. And *Re* corresponds to the Reynolds number, obtained through the following expression [20]

$$\mathrm{Re} = \frac{\rho \cdot v \cdot D_h}{\mu}. \quad \textbf{(16)}$$

In order to obtain the heat transfer coefficient between the fluid and the pipe, the properties of Hitec XL molten salt at the different operating temperatures of the plant were used. Convective resistances between the fluid and the pipe, R_{conv}^{f-p}, were estimated from these properties, considering a nominal mass flow rate of 11 kg.s^{-1} and the defined equations, and are presented in the **Table 6**.

2) Conduction through the insulation

For this case it has to be considered the equation for conductive resistance:

$$R_{cond}^{i} = \frac{\ln\left(\frac{r_{ext}}{r_{int}}\right)}{2 \cdot \pi \cdot k \cdot L_{pipe}}, \quad \textbf{(17)}$$

here r_{int} corresponds to the inner radius of the pipe and r_{ext} corresponds to the outer radius of the insulation,

$$r_{int} = 0.04445 \text{ [m]},$$

$$r_{ext} = 0.04445 + 0.15 = 0.19445 \text{ [m]}.$$

For the calculation of the conductive resistance in the piping insulation, R_{cond}^{i}, it was considered the fluid's temperature at which zone (according to the values shown in **Table 4**) and the mentioned insulation conditions. Results appear on **Table 6**.

3) Convection between the pipes and the air

The convective resistance is obtained by the **equations (12)** and **(13)**, considering **air outside the tube** and a cylindrical surface. The Nusselt number is obtained through the empirical relation described by Hilpert [22] and referenced by [23]:

$$Nu_D = c \cdot Re_D^m \cdot Pr^{1/3}. \quad \textbf{(18)}$$

Where the constants *c* and *m* are given in **Table 5**, and with all properties evaluated at the air film temperature T_{air}. The air film temperature is the temperature of the air that is very close to the tube. In the present case, since the pipe is really well insulated, it has been assumed to be the ambient temperature.

Table 5: *Constants of* ***Equation 18*** *at different Reynolds numbers [23].*

Re	c	m
0.4 – 4	0.989	0.33
4 – 40	0.911	0.385
40 – 4000	0.683	0.466
4000 – 40,000	0.193	0.618
40,000 – 400,000	0.027	0.805

To obtain the heat transfer coefficient between the piping and the air, the air thermal properties at 20 °C were used (see attached table in **Appendix 5: Air properties**). In addition, an average wind speed of 3.34 $m.s^{-1}$ was considered; which is obtained from an average of local meteorological data of Évora. According to the mentioned properties, the value obtained for the heat transfer coefficient is 15.2 $W.m^{-2}.K^{-1}$. Using this coefficient, the pipe section and its length, it was possible to obtain the value of convective resistance between the pipe and the air, R_{conv}^{i-a}, in the different zones of the solar field, please, see **Table 6**.

4) Equivalent heat resistance and thermal losses in the piping

Finally, it is possible to calculate the thermal losses in the piping from the equivalent resistance equation:

$$R_{eq}^{pipe} = R_{conv}^{f-p} + R_{cond}^{i} + R_{conv}^{i-a} \quad \textbf{(19)}$$

and **equation 10**; considering again ambient temperature to be 20°C.

Table 6: *Results of the thermal losses obtained in the interconnecting piping.*

Zone	Length [m]	$R_{conv}^{f-p}\ [K.W^{-1}]$	$R_{cond}^{i}\ [K.W^{-1}]$	$R_{conv}^{i-a}\ [K.W^{-1}]$	$R_{eq}[K.W^{-1}]$	$P_{th}^{pipe}[W]$
1	52.3	0.0000283	0.074851	0.00103	0.075909	6323
2	24.7	0.0000599	0.15849	0.00218	0.16073	2986
3	20	0.000182	0.195735	0.002692	0.198609	1359
4	81.8	0.0000445	0.047857	0.000658	0.04856	5560
5	28.8	0.000021	0.135927	0.00187	0.137818	2757
					Total	**18987**

A total thermal loss from piping of about 19 kW has therefore been calculated. Considering a total piping length of 207.6 m, it is possible to assess the average value of the thermal losses per meter of piping (or linear heater losses),

$$P_{th,l}^{pipe} = \frac{P_{th}^{pipe}}{L} = \frac{18987}{207.6} \approx 91.5\ [\mathrm{W.m^{-1}}] \quad \textbf{(20)}$$

3.2.2 Thermal losses in the solar field

The linear heat loss values, with respect to the absorber tube temperature, that are given by the receiver manufacturer are shown in **Table 7**:

Table 7*: Thermal losses associated with the receiver tubes.*

Absorber tube temperature [°C]	Thermal Losses [W.m^{-1}]
150	40
200	70
300	120
350	175
400	250
450	340
500	430
520	530
550	650

From the manufacturer data, a polynomial relation between linear heat losses and the fluid temperature was obtained. Since the losses are directly related to the ambient temperature, the correlation was obtained considering a ΔT between the fluid temperature and an ambient temperature of 20 °C. This correlation is given by the following expression:

$$P_{th,l}^{receiver} \approx (1.912 \cdot 10^{-8}) \cdot (\Delta T_{r\to a})^4 - (1.336 \cdot 10^{-5}) \cdot (\Delta T_{r\to a})^3 + (4.088 \cdot 10^{-3}) \cdot (\Delta T_{r\to a})^2 - 0.0467 \cdot (\Delta T_{r\to a}) \ [\mathrm{W \cdot m^{-1}}]. \quad \textbf{(21)}$$

Additionally, knowing that the inlet temperature in the solar field is 290 °C, that the outlet temperature is 500 °C and that the solar field has a total length of 684 m, it is possible to obtain the mean value for thermal losses in the receiver tubes.

$$P_{th}^{receiver} = P_{th,l}^{receiver} \cdot L = 250.5(W \cdot m^{-1}) \cdot 684\ (m) \approx 171.5\ [\mathrm{kW}] \quad \textbf{(22)}$$

3.2.3 Total thermal losses

Considering all the calculations made and taking the values of thermal losses obtained in the piping during the nominal operation of the platform, the total losses can be obtained:

$$P_{th}^{total} = P_{th}^{pipes} + P_{th}^{receivers} \approx 190.4\ [\mathrm{kW}]$$

In fact, linear thermal losses in the receiver tubes are 2.7 times greater than the linear thermal losses in interconnecting piping. Since the receivers are 3.3 times longer than the pipes, thermal losses in the receivers are approximately 9 times higher; representing about 90% of the total losses.

In addition, the total amount of thermal losses that are occurring in the interconnecting piping and receiver tubes during nominal operation accounts approximately for 5% of the solar field's nominal power.

3.2.4 Night Thermal Losses

During night and cloudy periods, heat losses could lead to salt solidification. To tackle this issue it is possible to use electrical heat tracing to maintain the tubes at a safety temperature and/or using heat stored in the cold tank by circulating the salts in the solar field at a very low flow rate. In principle, the second option will be preferred as no extra electrical consumption will be required. However, it will reduce the net heat production of the plant. Thus, to understand the capacity of the cold tank to maintain the platform's piping and receivers heated at night, thermal capacity of the tank and thermal losses in the piping and receivers during the night must be calculated. From these values it is possible to determine how many hours heat stored in the cold tank can maintain the piping and receivers heated without running the risk of freezing.

3.2.5 Thermal inertia capacity of the cold tank

To determine the available energy in the tank, the following information must be considered:

***Table 8**: Important information to determine the capacity of the tank.*

Tank Volume [m^3]	29
Density of the Hitec XL molten salt at 290 °C[1] [$kg.m^{-3}$]	2000
Specific heat of the Hitec XL molten salt at 290 °C [$J.kg^{-1}.K^{-1}$]	1450
Minimum safety temperature[2] [°C]	200

[1]Initial temperature at which the cold tank is.
[2]To ensure that the temperature of the salt does not approach its freezing temperature to avoid it.

Thermal inertia capacity of the cold tank is given by **equation (23)**:

$$E_{th}^{tank} = V_{tank} \cdot \rho \cdot Cp \cdot \Delta T. \quad \textbf{(23)}$$

From this expression, where ΔT is the value between the initial temperature of the cold tank (290 °C) and the minimum set safety temperature (200 °C), and the given values, it is possible to calculate thermal inertia capacity of the cold tank: $\mathrm{E}_{\mathrm{th}}^{\mathrm{tank}} \approx 2.10\ [\mathrm{MWh}]$. This value, along with the assessed thermal losses during night, will allow estimating how many hours the cold tank can be used to maintain the salts above the minimum allowed temperature.

3.2.6 Thermal losses from tanks

Thermal losses of the tanks are important parameters to evaluate, since these losses have influence on the number of hours which the cold tank can maintain piping and receivers heated. Moreover, it is a fundamental calculation to determine the coefficient of thermal losses in the tanks which is an input that must be inserted in the simulation software. To determine thermal losses in the tanks it is necessary to consider the height of the tanks, their diameter and their insulation. Besides, it will only be determined the losses on the sides and tops of the tanks; the bottom losses being considered negligible. The tanks have the following presentation:

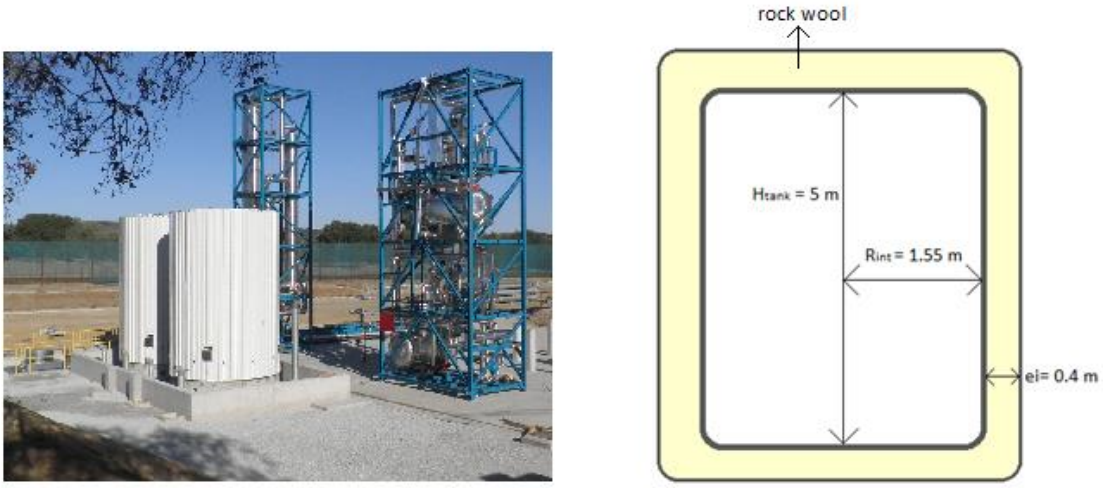

Figure 16:Scheme of the storage tanks.

To calculate heat losses, the following assumptions were made:

- The wall of the tank is at the fluid temperature;
- The ullage space is not considered, i.e. the tank is considered to be full of fluid.

Thus, the predicted heat losses are overestimated. However, since they don´t take into account a lot of thermal bridges (structure, sensors, etc.), the latter assumption may lead to a correct final estimation.

Eventually, the following information will be considered:

Table 9: The main information about the tanks.

Tanks characteristics	
r_{in} [m]	1.55
r_{ext} [m]	1.95
H_{tank} [m]	5
e_i [m]	0.4
k [$W.m^{-1}.K^{-1}$]	0.06

1) Conductive resistances:

Through the data provided in previous table and using the expressions **(24)** and **(25)**,

$$R_{cond}^{t,side} = \frac{\ln\left(r_{ext}/r_{int}\right)}{2 \cdot \pi \cdot k_{ins} \cdot H_{tank}}, \quad \textbf{(24)}$$

$$R_{cond}^{t,top} = \frac{e_i}{k \cdot \pi \cdot r_{tank}^2}, \quad \textbf{(25)}$$

it is possible to obtain the value of conductive thermal resistance for the side, $R_{cond}^{t,side} \approx 0.121793$ [K·W^{-1}], and top, $R_{cond}^{t,top} \approx 0.883274$[K·W^{-1}], of the tanks.

2) Convective Resistances

To determine the convective resistance between the tanks walls and air, it is necessary to consider the values presented in **Table 9**, as well as, air properties, available in the attached table (**Appendix 5**: **Air properties**). Initially the heat transfer coefficient between the walls of the tanks and air is calculated by **equation (13)**. In this case, to calculate the Nusselt number, the Zhukauskas relation is used (for Reynolds number $2x10^5 < Re < 2x10^6$ and Prandtl number $0.7 < Pr < 500$) [23]:

$$Nu = c \cdot Re^m \cdot Pr^n. \quad \textbf{(26)}$$

Where the correlation constants are presented in **Table 10**.

***Table 10**: Constants used in Zhukauskas correlation.*

Relation of Zhukauskas [23]	
c	0.076
m	0.700
n	0.370

From the heat transfer coefficient between the wall of the tank and the air and using **equation (12)**, the values of convective resistances are obtained: for the side of the tank, $R_{conv}^{t,side} \approx 0.002589$ [K·W^{-1}], and for the top, $R_{conv}^{t,top} \approx 0.013278$ [K·W^{-1}].

With these values it is then possible to determine the equivalent thermal resistance of the tanks, knowing that the conductive and convective resistances at the side and at the top of the tank are in series with each other, and the side of the tank is in parallel with the top of the tank.

$$R_{eq}^{tank} = \left(\frac{1}{R_{cond}^{t,side} + R_{conv}^{t,side}} + \frac{1}{R_{cond}^{t,top} + R_{conv}^{t,top}} \right)^{-1} \approx 0.109228 \text{ [K·W}^{-1}\text{]}, \quad \textbf{(27)}$$

Finally, considering ambient air temperature of 10 °C (night temperature), hot tank temperature to be 500 °C and cold tank temperature 290 °C, the following values for thermal losses from the tanks are obtained:

Table 11: Values of thermal losses from the tanks.

Thermal losses of the tanks	
	$P_{th}^{tanks}\ [kW]$
Hot Tank	4.5
Cold Tank	2.6
Total	7.1

Using the table values, total thermal loss coefficient of the tanks ($h_{storage}$) can be obtained by **equation (28)**:

$$P_{th}^{tanks} = h_{storage} \cdot S \cdot \Delta T \qquad \textbf{(28)}$$

Where S corresponds to the total heat transfer surface and ΔT the temperature difference between the tank and air. The value obtained through the equation is 0.163 $W.m^{-2}.K^{-1}$ and this will be the value entered in the software to perform the simulations.

3.2.7 Pipe thermal losses at night

To calculate the pipe thermal losses during night, it is important to consider fluid's path during this period, see **Figure 17**.

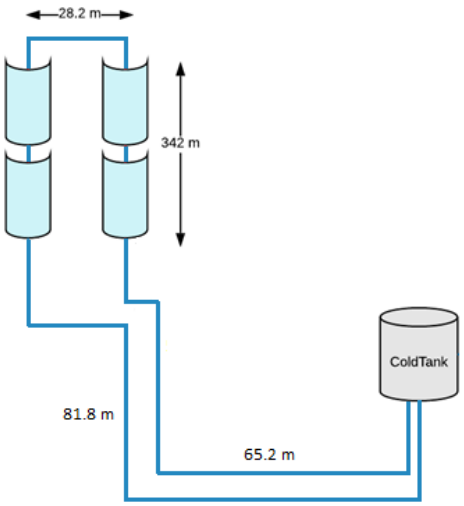

Figure 17: Trajectory of fluid during the night.

1) Conduction heat resistance

The conduction heat resistance of pipe insulating material can be calculated knowing information presented in **Table 12**.

Table 12: Information about the pipe.

r_{in} of the piping [m]	0.04445
Thickness of the insulation [m]	0.15
r_{ext} of the piping [m]	0.19445
Conductivity of insulation (k) [W.m^{-1}.K^{-1}]	0.06
Length of piping [m]	175.2

Using **equation (17)**, a value of $R_{cond}^{i} = 0.022344\ K{\cdot}W^{-1}$ is obtained.

2) Convection heat resistance

For the calculation of the convection resistance between the fluid and the piping, the properties of the fluid at 290 °C, shown in the attached table (**Appendix 6: Hitec XL molten salt properties**), and very low flow rate of 1 kg.s^{-1} are considered. With the obtained heat transfer coefficient, ~202 W.m^{-2}.K^{-1}, and using **equation (12)**, the value of convection resistance between the fluid and the pipe ($\mathrm{R}_{\mathrm{conv}}^{\mathrm{f-p}}$) obtained is $0.000132\ [\mathrm{K}\cdot\mathrm{W}^{-1}]$.

Likewise, to obtain the convection resistance between the tube and the air during the night properties of the air at 10 °C, shown in **Appendix 5: Air properties**, are considered. To obtain the heat transfer coefficient during night, it was considered that the circulation of the salts is performed with a very low flow rate of 1 kg.s^{-1}. With this value, a coefficient of ~15.2 W.m^{-2}.K^{-1} is obtained. Using again **equation (12)**, the value of convection resistance between the pipe and air ($\mathrm{R}_{\mathrm{conv}}^{\mathrm{i-a}}$) is $0.000307\ [\mathrm{K}\cdot\mathrm{W}^{-1}]$.

3) Thermal Losses in piping at night

Through the sum of conduction and convection resistances, the equivalent resistance value is obtained:

$$R_{eq} = 0.022783\ [K\cdot W^{-1}].$$

Knowing the value of the equivalent resistance and using the **Equation (*11*)**, the thermal losses are obtained:

$$P_{th}^{pipes} = \frac{\Delta T}{R_{eq}} = \frac{(290-10)}{0.022783} = 12290\ [W].$$

The thermal loss value during the night in the interconnecting piping is therefore ~12.3 kW.

4) Thermal losses in receiver tubes at night

Using **Equation (21)** and considering that the average ambient temperature at night is 10 °C and that the receiver tube is at 290 °C, the following value of linear thermal losses in the receiver tube at night is obtained:

$$P_{th}^{receivers} = 131.7\ [W \cdot m^{-1}].$$

Considering that the receiver tube has a total length of 684 m then the value of the thermal losses at night in the receiver tubes is:

$$P_{th}^{receivers} = 131.7 \cdot 684.0\ = 90060.0\ [W] \approx 90\ [kW].$$

5) Total thermal losses at night

Adding the losses in the interconnecting piping with the losses in the receiver tubes and in the tanks, the total heat loss value is:

$$P_{th}^{total} = P_{th}^{pipes} + P_{th}^{receivers} + P_{th}^{tanks} \approx 109399.5\ [W] \approx 109.4\ [kW].$$

Having this value and knowing that the thermal inertia capacity of the cold tank between 290 °C and 200 °C is 2.1 MWh, it is expected that it will be able to maintain the system heated during about 21.2 hours, without solar irradiation. A more accurate estimation can be made by accounting for the total system heat loss decrease as the fluid temperature decreases. In addition to that, if fluid temperature is allowed to decrease down to a lower value, for instance 170 °C, the number of hours will increase to 28.3 hours.

It should be noted that in this calculation, losses through pipe supports were not included; it was assumed that supports are well thermally insulated and, in this way, losses in these points can be neglected. To avoid severe heat losses in the pipe supports, that can lead to local salt freezing, these supports must be pre-insulated with calcium silicate rods, as calcium silicate offers the necessary thermal and mechanical resistances, despite being expensive.

3.2.8 Operation Strategies

The main problem of using MS as HTF in CSP plants is their high melting point[1]. Thus, operating strategies of this type of platform are largely directed in maintaining salts at temperatures above safety temperature (in this project defined as 50 °C above freezing point [12]), spending as little electricity as possible in this process. In this

[1] As explained above melting and freezing point can be different, since some supercooling effect can occur, however here they will be considered identical in order to ensure an additional safety margin during operation.

sense, there are numerous strategies that can be defined, as is the case of circulating the MS from the cold tank through solar field piping during night and cloudy periods, as described above. This strategy reduces the necessity to use impedance heating and electrical heat tracing and thus reduce electricity consumption. To extend the period that the cold tank can maintain the piping heated without using electricity there are several strategies that can be defined, as is the case of the already mentioned example of reducing the minimum temperature of the tank to increase its thermal inertia capacity.

Another possibility is to leave some energy stored in the hot tank and to use this energy to heat the cold tank when the temperature of the latter is too low. In addition, in the periods of the year with less solar irradiation, a strategy that can be considered is to store the small amount of thermal energy that is obtained from the solar field at these times, instead of sending it to the steam generator, for later use to maintain the system heated and to avoid long periods of electricity consumption.

3.3 System Advisor Model (SAM)

In this work the System Advisor Model software was used to simulate the operation of the HPS2 project as well as testing its operation with different HTFs.

SAM was developed by NREL in order to model a range of renewable energy technologies for electricity generation, including photovoltaic systems, solar thermal parabolic troughs, power towers and Stirling dish systems. SAM also includes models for wind turbines, biomass plants, and geothermal systems and allows comparing renewable energy projects with conventional power projects. SAM uses an hourly performance model to estimate a power system's total annual output, and a cost and financial model. In addition, reports performance and financial metrics in tables and graphs, which can be exported for use in reports or for further analysis in other tools [24].

The SAM software is free and can be downloaded through the website [25]. The current version of System Advisor Model is **SAM 2017.9.5**. Help tutorial can be obtained with a PDF file through the same link and the technical manual for the SAM Physical Trough Model on [26].

3.4 Software inputs

In order to make the HPS2 simulation as close as possible to its actual operation, there are some fundamental inputs that have to be introduced into the software. In addition to the introduced inputs that are placed directly in the software, which will be available in **Appendix 4: Inputs of SAM**, a meteorological data file was created and

collector and receiver specifications defined. These were inserted into the program's library so that they can be selected during simulations.

3.4.1 Weather Data file:

For the weather data file, hourly values of normal direct solar irradiance (beam), ambient dry temperature (T_{dry}), relative humidity (RH), atmospheric pressure (Pres) and wind speed (w_{spd}), were used for a full year. The dataset for this work was obtained through the meteorological station of the Institute of Earth Sciences in Évora, Portugal (N38.567686, W7.91172), being a reference station for the region. The meteorological data that were used are the result of a compilation between years 2016, 2017 and 2018 [27]

3.4.2 Collector File

The collectors used in HPS2 are an innovative technology called HelioTrough from the company TSK-Flagsol. These collectors increase the concentration factor, C≈31 (compared with C≈26 typical for this type of systems), suitable for the use of molten salts, thanks to an aperture of~6.77 m instead of the usual ~5.77 m. Details about data entered into the collector data file are provided in **Appendix 2: Collector file**; this section aims to give details about their main features, such as the average surface to focus path length ($L_{f,avg}$) and the optical attenuation coefficient (k_θ), called Incidence Angle Modifier (IAM) in SAM.

1) Average surface to focus path length

Until sun rays reach the receiver tube they travel different paths with different lengths. These lengths will influence the optical efficiency, since a longer path will induce a large cone diameter for the reflected rays. Average surface to focus path length represents average path that solar rays cross until they reach the receiver tube, as can be seen in the **Figure 18**. A mean value for this path can be obtained depending on the focal length, *a*, and aperture of the collector, *w*.

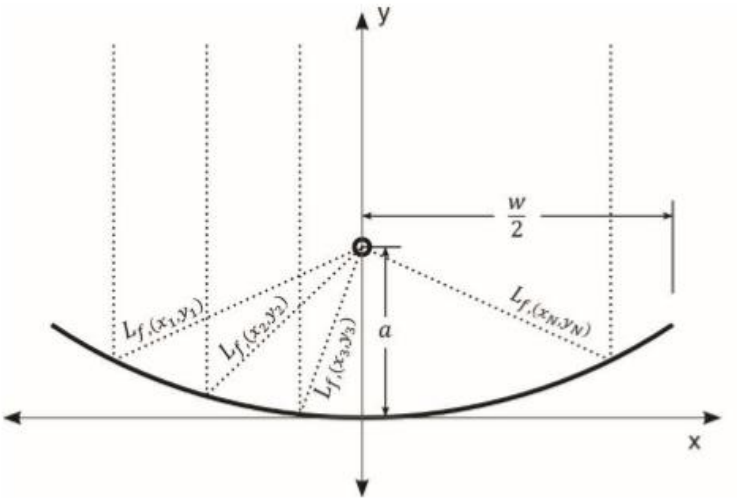

Figure 18:Focal length geometry for calculating the average focal length; extracted from SAM's tutorial [26].

According to these parameters, the average surface-to-focus path length is given by the equation **(29)**:

$$L_{f,avg} = \sqrt{\frac{(4a^2 + \left(\frac{w}{2}\right)^2)^2}{a^2}} \cdot \frac{12a^2 + \left(\frac{w}{2}\right)^2}{12\left(4a^2 + \left(\frac{w}{2}\right)^2\right)} = \frac{12a^2 + \left(\frac{w}{2}\right)^2}{12a}. \qquad \textbf{(29)}$$

In the present case, a = 1.71 m and w = 6.77 m; substituting these values in **Equation (29)**, an average surface-to-focus path length of ~2.27 m is found.

2) Attenuation coefficient (k_θ)

The attenuation coefficient, k_θ (in SAM it is called IAM), is the variation of the optical performance of a solar collector due to different incidence angles between the sun's rays and the normal surface to the collector.

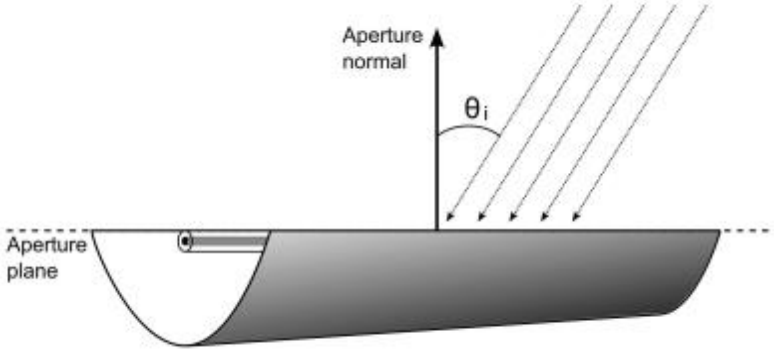

Figure 19: The angle between the solar irradiation and the normal vector to the collector aperture plane. [26]

Mathematically it is represented by the division between the efficiency of the collector for a certain angle of incidence and its maximum efficiency:

$$k_\theta(\theta_i) = \frac{\eta(\theta_i)}{\eta_{max}}. \quad \textbf{(30)}$$

Thus, this value is maximum, $k_\theta(\theta_i) = 1$, when θ_i is equal to zero and decreases as θ_i increases. Its variation with the angle of incidence can be generally expressed as a second-degree polynomial function:

$$k_\theta = a_0 + \frac{a_1 \cdot \theta + a_2 \cdot \theta^2}{\cos\theta}. \quad \textbf{(31)}$$

Where the values of a_0, a_1 and a_2 are obtained through dedicated experimental tests. Since the studied solar field is still under development, the optical qualification tests are not yet carried out to obtain these values. Therefore, for the present work, the **equation (32)** determined by L. Valenzuela in [28] is used.

$$k_\theta = 1 - \frac{(7 \pm 4) \cdot 10^{-4} \cdot \theta + (36 \pm 6) \cdot 10^{-6} \cdot \theta^2}{\cos\theta}, \quad \textbf{(32)}$$

with incidence angle, θ, expressed in degrees. For θ expressed in radians is used the **equation (33)**:

$$\mathrm{k_\theta} = 1 - \frac{0.040107 \cdot \theta + 0.118181 \cdot \theta^2}{\cos\theta}. \quad \textbf{(33)}$$

The term cos(θ) represents the fraction between the solar energy density that actually reaches the collectors and the energy density that reaches a surface that is perfectly perpendicular to the sunbeams. In SAM, it has been separated from other optical losses (slope error, curvature error, receiver tube position error, etc.) since it is independent from the collector geometry and material quality.

3.4.3 Receivers specifications

The receiver tubes that are used in this project were developed by Rioglass (Spain) and called PTR 70-5G (fifth generation). They have an external diameter of 0.070 m, an internal diameter of 0.064 m, contained in vacuum and protected by a glass cover with an external diameter of 0.125 m and an internal diameter of 0.119 m. The file with all the information about the receivers introduced in the software can be seen in **Appendix 3: Receiver specifications (Rioglass PTR 70-5G)**.

Taking into account thermal losses provided by Rioglass and the relation obtained through **equation (21)**, previously shown in section **3.2.2 Thermal losses in the solar field**, thermal losses of the solar receivers can be calculated from:

$$P_{th,l}^{receiver} = (1.912 \cdot 10^{-8}) \cdot (\Delta T_{r\to a})^4 - (1.336 \cdot 10^{-5}) \cdot (\Delta T_{r\to a})^3 + (4.088 \cdot 10^{-3}) \cdot (\Delta T_{r\to a})^2 - 0.0467 \cdot (\Delta T_{r\to a}) \; [W \cdot m^{-1}]. \quad \textbf{(34)}$$

Considering that:

i) $\Delta T_{r\to a}$ represents the difference between the average temperature of the receiver and ambient temperature;
ii) ii) HTF enters the solar field at 290 °C and leaves at about 500 °C;
iii) iii) an average ambient temperature of 20 °C;

and the mean receiver heat losses, obtained by integrating **equation (34)** between 270 °C and 480 °C, linear heat losses from receivers are estimated to be ~250.5 $W.m^{-1}$.

3.4.4 Remaining SAM inputs

All other inputs that were introduced into the software and that are considered important are presented in **Appendix 4: Inputs of SAM**.

3.5 Length of piping

In order to understand how SAM calculates pressure and thermal losses and to get HPS2 simulations as close to reality as possible, it is necessary to understand how the program calculates piping length. In SAM's technical manual it is possible to find the values that the software assumes for piping lengths in the pumping system and in the steam generator; these values are shown in **Table 13**.

Table 13: The assumed piping lengths for the pumping system and steam generator *[26]*.

Description	Length [m]
1 - Pump suction header to pump inlet	45
2 - Pump discharge to discharge header*	45
3 - Pump discharge header*	100
4 - Collector field to expansion vessel/TES	120
5 - Steam generator supply header	80
6 – Inter-steam-generator piping	120
7 - Steam generator exit to exp. Vessel/TES	80

* Pump discharge length are divided between the piping that is necessary to connect the pump(s), valves, etc., and the piping to connect the first one to the first headers

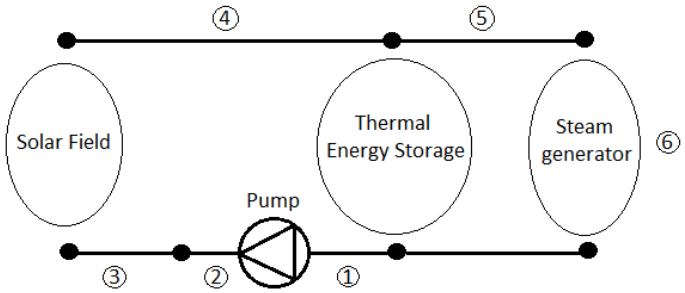

Figure 20*: Diagram demonstrating the lengths indicated in* ***Table 13****.*

To calculate the remaining piping lengths the software uses the expressions that will be presented below. Before going to that and in order to clarified pipe lengths calculation that will be done later, different piping sections, i.e. loops, headers and runners, are represented in **Figure 21**.

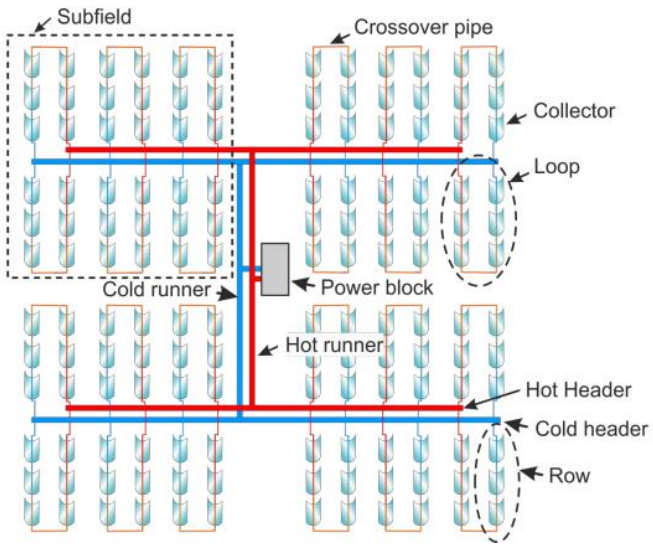

Figure 21*: Different piping sections extracted from SAM's tutorial [29]*

Considering the different piping sections shown in the **Figure 21**, the length of each of them is calculated by the following expressions:

1) For piping length corresponding to inlet and outlet of the collectors and between the collectors (L_{IOCop}), the length is calculated by:

$$L_{IOCop} = 40\ [\mathrm{m}] + L_{spacing}. \quad \textbf{(35)}$$

Where $L_{spacing}$ represents the distance between two rows of collectors.

2) To determine total length of the loop ($L_{loop,tot}$):

$$L_{loop,tot} = \sum_{i=1}^{N_{SCA}} (L_i + L_{SCA,gap}), \quad \textbf{(36)}$$

here N_{SCA} represents the total number of SCA, L_i the length of each assembly and $L_{SCA,gap}$ the space between collectors.

3) To determine the length of piping that carries the fluid to the inlet of the collectors, called headers (L_{hdr}), the following expression is used:

$$L_{hdr} = \sum_{i=1}^{N_{hsec}} 2 \cdot \left(L_{spacing} + 4.275\ [\mathrm{m}]\right). \quad \textbf{(37)}$$

Where N_{hsec} represents the number of headers of the solar field and the value 4.275 [m] represents the normalized piping length per loop required for thermal expansion/contraction compensation.

4) To determine the length of pipe between the power block and the headers, called runners, it is used:

$$L_{run,tot} = \sum_{i=1}^{N_{runsec}} L_{runsec,i}. \quad \textbf{(38)}$$

Where N_{runsec} is the number of runners and $L_{runsec,i}$ is its length. For $L_{runsec,1}$, the software considers a value of 50 m; $L_{runsec,1} = 50\ [m]$. As HPS2 plant is small it only has one runner section and the flow rate is the same in all the piping, SAM considers $L_{run,tot}$ = 50 m.

Using the above equations, it is possible to verify SAM's pipe lengths in this design and check with the actual pipe lengths to see if they are identical or if the software has deviations that may be significant for later calculations of pressure and thermal losses.

3.5.1 Observing the diagram of the plant

In the image below, it is possible to observe the piping lengths that make the connections between the various elements of the plant,

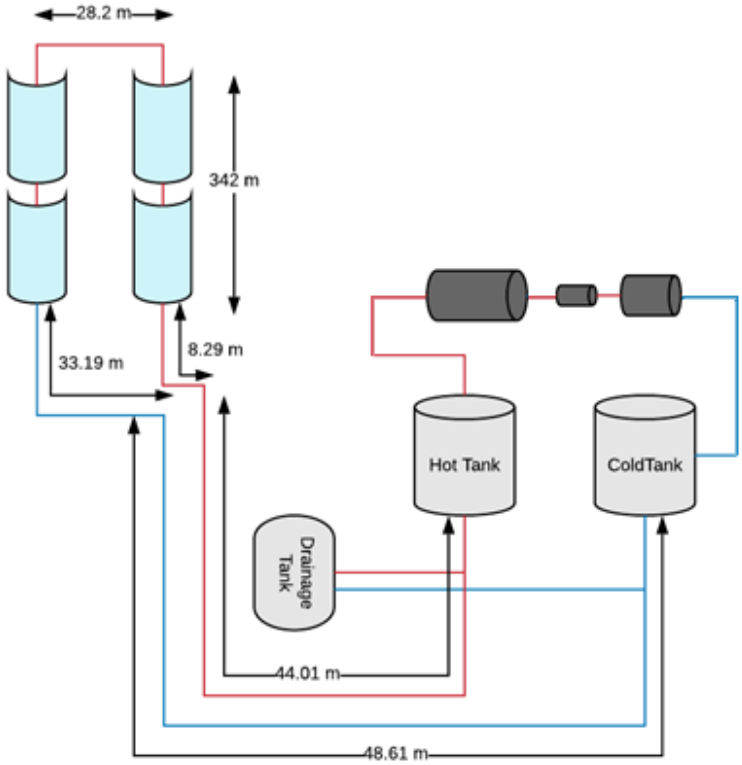

***Figure 22**: Diagram of the plant with the piping lengths marked.*

In the following table it is possible to see the actual piping length values of the Inlet-Outlet and Cross over piping (IOCop), loop, headers and runners calculated based on the plant diagram and compare with the values obtained through the SAM equations:

***Table 14:** Piping length using the SAM equations and the plant diagram.*

	Length with SAM equations [m]	Length with plant diagram [m]
L_{IOCop}	58.9	28.2
$L_{loop,tot}$	684	684
$L_{IOCop} + L_{loop,tot}$	742.9	712.2
L_{hdr}	46.4	41.48
$L_{run,tot}$	50.0	92.62
Total	839.3	846.3

Observing the values of **Table 14**, obtained through calculations made using previous equations, it can be verified that the SAM assumes a total piping length of 839.3 m while the measured length of the plant diagram is 846.3 m. The values calculated by

the two methods are identical. However, since the HPS2 project is a small plant with only one loop, and the software is designed for commercial scale projects, in CSP parabolic trough model the minimum number of field subsections that the software allows to choose is two. In order to overcome this problem, instead of using "CSP parabolic trough model" option it was used "Process heat model"; this option allows piping length to be set as well as control better all parameters. With this option simulations do not predict electricity that would be produced, but since HPS2 will not have turbine[2], this option fits better the simulation needs. Electricity production is predictable simply by multiplying heat production by a defined turbine efficiency, for example, Siemens SST-050 turbine.

3.6 Summary

The objective of this chapter was to specify all the inputs that were used for the simulations with SAM software, as well as giving substantial details about HPS2 plant. Therefore, a complete thermal study of HPS2 has been performed, including thermal losses during day and night and operation strategies.

Now that all needed information has been provided, the following parts will focus on the scientific studies that were actually performed during this work, i.e. comparing performances of thermal oils and molten salts as HTF in LF systems.

[2] The inclusion of a turbine is now being considered for installation in a future project.

4

Comparison between the use of thermal oil, solar salt and YaraMOST/HitecXL salts as Heat Transfer Fluids

Throughout this chapter various comparisons will be made between thermal oil and molten salts. Initially, an analytical comparison will be made between the most relevant properties to evaluate the performance of the different fluids as HTF. Later, an analysis of the results obtained in the simulations carried out with SAM will be done in order to compare HPS2 performance with different HTF in terms of production, operation and electrical consumption. Finally, the impact of these changes in the Levelized Cost Of Heat (LCOH) will be analysed.

4.1 Analytic comparison between thermal oils and molten salts

4.1.1 Properties

In order to perform an analytic comparison between Therminol VP-1, Solar Salt, Hitec and Hitec XL; it is essential to consider the properties mentioned in **Section 2.2** for each of the fluids. These properties, at 300 °C, are presented in **Table 15**:

Table 15: *Heat transfer fluid properties: [(1)] reference [2]; [(2)] reference [1]; [(3)] reference [30].*

	Therminol VP-1	*Solar Salt*	*Hitec*	*HitecXL*
Melting point[(1)] [°C]	13	220	142	120
T_{max}[(1)] [°C]	400	600	535	500
Density[(1)], ρ [kg.m^{-3}] @ 300°C	815	1899	1640	1992
Viscosity[(1)], μ [mPa.s] @ 300°C	0.2	3.26	3.16	6.37
Specific heat[(1)], Cp [J.kg^{-1}.K^{-1}] @ 300°C	2319	1447	1560	1450
Conductivity[(2)], k [W.m^{-1}. K^{-1}] @ 300°C	~0.1	0.55	0.48 [(3)]	0.52
Cost[(1)] [$. Kg^{-1}]	2.2	0.49	0.93	1.19
Volumetric Heat Capacity [MJ.m^{-3}. K^{-1}] @ 300°C	1.89	2.75	2.56	2.89

Observing these values it is verified that the salts present a VHC considerably higher than thermal oil: Hitec XL is the one that presents the greater heat capacity. Compared with Therminol VP-1, Hitec XL allows to store 54 % more heat in the same volume; which allows reducing significantly the size of the storage system for the same energy storage requirements. In addition, another interesting aspect in this table is that molten salts have significantly lower costs than Therminol VP-1.

4.1.2 Heat transfer coefficient

The heat transfer coefficient allows estimating the efficiency of the fluid heat collection from the solar heated receiver tube. Furthermore, as receiver tubes collect more solar irradiation from the collector facing side, this side tends to reach higher temperatures. A too low heat transfer coefficient would cause a non-uniform thermal expansion of the receiver tubes making them to bend and possibly break the protective glass cover. In this perspective, heat transfer properties of the HTF are crucial to prevent such problems from happening and to ensure maximum efficiency.

In order to analyse how the salts behave as HTF, heat transfer coefficients (*h*) of thermal oil and molten salts were calculated to verify if there are significant

differences between them. To do that, for each HTF, **Equation (13)** is used considering Nusselt, Prandtl and Reynolds numbers calculated for each HTF using **Equations (14)**, **(15)** and **(16)**, respectively.

• **For a first approach** it was considered important to verify how the studied fluids behave when subjected to the same operating conditions. Therefore, considering that all fluids flow at a velocity of 3 $m.s^{-1}$ (intermediate value between the nominal velocity of the two types of fluids for the HPS2 project conditions) in the receiver tubes and operate in the same temperature range (300 °C to 400 °C). The obtained values are presented in **Table 16:**

***Table 16**: Heat transfer coefficient (h) of the HTFs and respective intermediate calculations for the first approach.*

	Therminol VP-1	*Solar Salt*	*Hitec*	*HitecXL*
Re	806850	115338	102760	61918
Pr	4.6	8.6	10.3	17.8
Nu	2258	609	597	495
h [$W.m^{-2}.K^{-1}$]	3421	5075	4340	3903

Observing the values obtained, it can be verified that the three molten salts that are studied have a value of heat transfer coefficient (h) higher than the thermal oil if they circulate at the same velocity inside the pipes. However, the salts have higher density and lower specific heat than the thermal oil which means that to achieve the same output power, with the same length of piping, the salts will have to circulate at a lower velocity. And this factor, along with the higher viscosity, will influence the heat transfer coefficient (*h*).

• The velocity at which each fluid circulates within the receiver tubes depends on its mass flow, which in turn is defined according to its specific heat (*Cp*), the operating temperature range and the power to be obtained at the end. Thus, **for a second approach** a power was set (3.6 MW- nominal power of the HPS2 project) and the heat transfer coefficient (*h*) was calculated for each case. The velocity at which each fluid needs to circulate to achieve this power, an inlet temperature of 300 °C and an outlet temperature of 400 °C (since the thermal oil does not allow operation at higher temperatures) was considered. The results obtained are presented in **Table 17:**

Table 17: *Heat transfer coefficient (h) of the HTF and respective intermediate calculations for the second approach.*

	Therminol VP-1	*Solar Salt*	*Hitec*	*HitecXL*
$\dot{m}$ [kg. s^{-1}]	15.5	24.9	23.1	24.8
v [$m.s^{-1}$]	5.6	3.8	4.1	3.6
Re	1497400	147225	140883	75190
Pr	4.6	8.6	10.3	17.8
Nu	3703	740	768	579
h [$W.m^{-2}. K^{-1}$]	5610	6170	5587	4560

Observing the values in the table, it is verified that in these conditions the HitecXL salt is the one with the lowest heat transfer coefficient, which is explained by the fact that this is the one with the highest viscosity. However, in general it can be considered that there is no significant loss in heat transfer within the receiver tubes using salts instead of thermal oil. Although the Hitec XL is the fluid that under these conditions has the lowest heat transfer coefficient, it compensates for the plant efficiency since it allows operating temperatures above 400 °C. In addition, with this temperature increase there will be a reduction in the viscosity of this fluid which also provides an increase of this coefficient.

• A third approach is considering the same ΔT, but with the properties of the salts at 400 °C (average operating temperature) and of the thermal oil at 350 °C. **The result of this approach is a value of *h* for the thermal oil of 5261 $W.m^{-2}.K^{-1}$ and for the Solar Salt, Hitec and HitecXL of 7403 $W.m^{-2}.K^{-1}$, 6894 $W.m^{-2}.K^{-1}$ and 6690 $W.m^{-2}.K^{-1}$, respectively**. This increase is due to the fact that the viscosity of the salts is relatively lower at 400 °C than at the 300 °C used for the calculations of the previous approach.

• However, in addition to the properties of the salts at 400 °C, it is important to note that the operating temperature range (ΔT) in the case of the salts increases to approximately 210 °C. **In this way a last approach can be made considering an inlet temperature of 290 °C and an outlet temperature of 500 °C for the salts**. This increase in the operating temperature range implies the use of lower operating flow rates, i.e., the salts circulates more slowly and this causes a significant decrease in the heat transfer coefficient (*h*).

Table 18: *Heat transfer coefficient (h) of the HTF and respective intermediate calculations for the last approach.*

	Therminol VP-1	*Solar Salt*	*Hitec*	*HitecXL*
$\dot{m}$ [kg. s^{-1}]	14.7	11.3	11.1	12.2
v [$m.s^{-1}$]	5.6	1.8	1.8	1.9
Re	1598898	120258	113491	93369
Pr	5.1	5.3	6.1	6.8
Nu	4038	519	524	469
h [$W.m^{-2}. K^{-1}$]	5261	4089	3808	3695

In this case, the value of *h* for Solar Salt, Hitec and Hitec XL is 4089 $W.m^{-2}.K^{-1}$, 3808 $W.m^{-2}.K^{-1}$ and 3695 $W.m^{-2}.K^{-1}$, respectively (against 5261 $W.m^{-1}.K^{-1}$ for the oil).

Analyzing the values obtained, for the same output power, considering the operating conditions of the thermal oil and the operating conditions of the salts (ΔT and properties at the average operating temperature of each one), the thermal oil presents a heat transfer coefficient (*h*) higher than the molten salts. However, for such high values of *h* this difference does not have a significant impact on the operation of the plant.

The manufacturers of the receiver tubes claim that a $Re > 20\ 000$ is sufficient to standardize the temperature around the receiver tube avoiding the problems of expansion. As *Re* values are much higher than required ($Re > 20{,}000$), although the molten salts have a lower *h* value than the thermal oil and it is always preferable to have a higher value, they do not present any risk to the receivers or proper operation of the system.

All calculations made to determine the values mentioned, as well as the tables with values of the properties used are available in **Appendix 1: Explanations about convection coefficient differences** for consultation.

4.1.3 Pressure losses

Since the thermal oils have lower density and viscosity than the molten salts, they are expected to have lower pressure losses in the solar field when subjected to the same conditions. However, some approaches were realized in order to have a better

perception of the actual differences between them. First, in order to understand the behaviour of the fluids when subjected to the same operating temperature range, the power of the plant was set to 3.6 MW_{th}, similarly to what was done for calculations of the heat transfer coefficient. Considering the velocity at which each fluid circulates to achieve this power with an inlet temperature of 300 °C and an outlet temperature of 400 °C (typical values of a power plant using thermal oil as HTF), pressure losses in the solar field are obtained with the following equations:

$$\Delta p_{pipe} = hl_{pm} \cdot \rho \cdot g \cdot L_{pipe}. \quad \textbf{(39)}$$

Where ρ represents the fluid density, *g* the gravitational acceleration, L_{pipe} the pipe length and hl_{pm} (head loss per meter) is given by **equation (40)**:

$$hl_{pm} = \frac{fr \cdot \bar{v}^2}{2 \cdot D_{pipe} \cdot g}. \quad \textbf{(40)}$$

To obtain the value of hl_{pm} it is necessary to know the friction factor *fr*, the mean velocity of the fluid inside the tube, $\bar{v}$, and its diameter, D_{pipe}. The velocity of the fluid inside the tube is determined by **equation (41)**:

$$\bar{v} = \frac{\dot{m}}{\rho \cdot \pi \cdot \frac{D^2}{4}}. \quad \textbf{(41)}$$

Where $\dot{m}$ represents the mass flow rate. On the other hand, the friction factor is given by the following **equation (42)**,

$$fr = \frac{1}{X^2}. \quad \textbf{(42)}$$

Where *X* is obtained by the following **equation (43)**:

$$Fx = X + 2 \cdot \log_{10}\left[\frac{Rough}{3.7} + 2.51\frac{X}{Re}\right]. \quad \textbf{(43)}$$

X value is calculated when F_x equals to zero ($F_x = 0$), with *Rough* being the relative roughness of the tube, i.e. the roughness of the tube divided by its internal diameter (Rough = ε/D). In this case, the value of roughness of commercial new steel pipe (ε = 0.046 mm) and the Reynolds values previously calculated for the same conditions were used.

The values of the intermediate calculations as well as the values of the pressure losses in the receiver tubes using thermal oil and MS, in $Pa.m^{-1}$, are shown in **Table 19:**

Table 19: *Pressure losses values per meter [$Pa.m^{-1}$] obtained for each HTF in the same operating conditions.*

	Therminol VP-1	Solar Salt	Hitec	HitecXL
X	7.39	7.02	7.01	6.77
fr	0.018	0.020	0.020	0.022
h [$m_f.m^{-1}$]	0.438	0.230	0.266	0.224
Δp [$Pa.m^{-1}$]	3500	4278	4279	4376

Comparing the value obtained with Therminol VP-1 to those obtained with Hitec XL an increase of 25% in pressure losses using this salt as HTF instead of the thermal oil is observed. However, doing again the calculation, but taking into account that the ΔT between inlet and outlet of the solar field is approximately 100 °C when using thermal oil and 210 °C when using MS, the obtained values are shown in **Table 20**:

Table 20*: Pressure losses values per metre [$Pa.m^{-1}$] obtained for each HTF in their operating conditions.*

	Therminol VP-1	Solar Salt	Hitec	HitecXL
X	7.39	6.95	6.93	6.86
fr	0.018	0.021	0.021	0.021
h [$m_f.m^{-1}$]	0.438	0.052	0.052	0.058
ΔP [$Pa.m^{-1}$]	3500	937	918	1079

Analyzing through this last table the pressure loss values in the solar field for each fluid according to its operating conditions, it is verified that contrary to what was predicted, the pressure losses in the solar field are smaller when using MS as HTF. Although thermal oils are less dense and less viscous, MS have a higher operating ΔT which allows reducing the flow velocity of the fluid in the receiver tube resulting in the decrease of pressure losses.

4.1.4 Vapor pressure

The vapor pressure is the pressure exerted by vapor when it is in thermodynamic equilibrium with the liquid that gave rise to it. In other words, the vapor pressure represents a measure of the tendency of the liquid to evaporate. The higher the vapor pressure, the more volatile the liquid is, and the lower its boiling temperature relative to other liquids with lower vapor pressure at the same temperature.

The thermal oil tends to reach very high vapor pressures and therefore has a very low boiling point when compared to the molten salts. The increase of Therminol VP-1 vapor pressure with temperature can be seen in **Figure 23.**

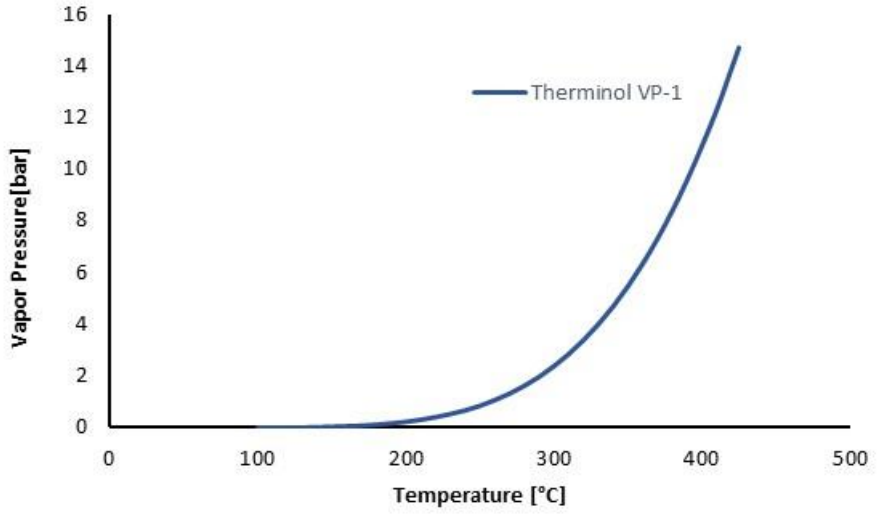

***Figure 23**: Therminol VP-1 vapor pressure evolution with increasing temperature [14].*

Boiling temperature of Therminol VP-1 is relatively low: at 1 bar it is 257 °C and reaches very high vapor pressures with increasing temperature.

From the graph, it can be seen that at 400 °C Therminol VP-1 has a vapor pressure of 11 bars. To ensure that the thermal oil does not evaporate inside the solar field piping, it is necessary to ensure that the pressure is never lower than this value in any part of the plant. This implies very high-pressure values at the entrance of the solar field in order to overcome pressure drops while keeping that minimum pressure.

Considering that the MS do not present problems of vapor pressure [31], (they have a high boiling point of about 800 °C [32]), they present here an advantage over the thermal oil. Their use as HTF allows reducing pressure levels in the solar field and thus reducing pump investment costs, energy costs for pump operation, leakage risks, piping thickness, insulation materials costs and risk of accidents due to both high temperatures and high pressures.

In addition, thermal oils are flammable, toxic and quite expensive which in turn justifies the interest in using MS as HTF.

4.1.5 Problems associated with the use of molten salts as HTF

As already mentioned in previous points, using MS as HTF implies several problems that must be considered. Particularly the high melting point and the corrosion rate, which require extra care about the protection against freezing of the fluid in the piping as well as materials that are more resistant to corrosion. This all leads to higher O&M expenses.

If the salt temperature drops considerably and they freeze in the piping, it can cause clogging, which can cause irreversible damages in the pumps. In addition, when the salts freeze, they dilate and may even end up breaking the receiver tubes which compromises the integrity of the whole plant. It is for this reason that it is very important to implement an auxiliary heating system in the piping that can ensure protection against freezing.

One way to control the temperature in the piping during nights and days with absence of direct solar irradiance is to circulate the salts stored in the cold tank through the solar field. Nevertheless, the heat collection elements as well as the remaining solar field piping require electric heating systems. These systems aim to preheat the piping before the salt is circulated in order to minimize the transient thermal tensions [2], as well as to ensure the protection temperature if the energy stored in the tanks is not sufficient.

The main doubts about this issue is whether the efficiency improvement that the salts provide to the plant compensates or not the investment costs in materials that are more resistant to corrosion, the heat systems as well as energy spent in piping heating.

4.1.6 Partial conclusion: General comparison between the fluids

Making a brief analysis between the thermal oil and the molten salts, in order to understand the advantages and drawbacks of the implementation of molten salts in parabolic trough thermal concentration systems, the following points are highlighted:

- The most promising aspect in the implementation of MS as HTF in CSP LF plants is that the salts allow an increase in the operating temperature of these systems to 500 °C, in case of Hitec and HitecXL, and up to 565 °C, in the case of Solar Salt, instead of the 400 °C that thermal oils currently offer in commercial power plants of this type. This increase in the output temperature of the solar field allows an improvement in the steam cycle efficiency.

- MS have higher VHC than thermal oils, which means they are an excellent energy storage material. It is for this reason that they are used in many commercial CSP LF power plants as energy storage medium since their use allows to reduce significantly the volume of storage required for the same amount of energy. In short, their use as HTF and storage medium not only improves storage efficiency, but also saves investment of the heat exchanger between the solar field and the storage system. Reduction of tank side along with heat exchanger removal results in a reduction of the initial investment costs.

- As can be seen in previous calculations, the mass flow in the solar field is considerably smaller when MS are used, which in turn leads to lower pressure losses in the solar field piping. In addition, MS do not present vapor pressure issues such as thermal oils. Low pressure losses coupled with low vapor pressure lead to a significant reduction of total pump losses.

- It is expected that with temperature increase in the solar field the thermal losses are also higher. Higher thermal losses imply lower thermal efficiency. The higher temperature difference between the inlet and the outlet of the solar field also induces a lower heat transfer coefficient (because mass flow and therefore velocity are lower for the same power). However, it is expected that these factors only represent a small deficit in the system performance: as mentioned above, the decrease in the value of *h* will not cause any significant change in the receiver tubes.

- The greatest problem associated with the use of MS as HTF is their high melting point; that are 220 °C for Solar Salt and 120/130 °C for Hitec XL [2, 10]. With the melting point of Therminol VP-1 of 13 °C, it will be expected that in this aspect the use of the salts will lead to an increase of O&M costs in order to ensure that the salts do not freeze inside the piping. Although the salts of the cold tank can be used to maintain the pipes heated during the night, electric power is only as back-up option, this represents thermal energy consumption; which will not be used for electricity production. It also implies the cost of installing the electrical heating system, compulsory for guarantying pipe preheating, in particular, for commissioning.

- Among the selected, Solar Salt is currently the most commonly used in commercial plants as energy storage medium. However, this salt has a very high melting point (220 °C) so when it comes to the use of salts as HTF, both Hitec and Hitec XL appear as more viable solutions. Hitec XL is the fluid that has the lowest melting point and highest VHC, and Hitec is more interesting in the remaining points. Although Hitec has good characteristics to be used as HTF, the choice of Hitec XL for HPS2 project is due to the fact that it has the lowest

melting point as well as good thermal stability at 500 °C. While in some references it is mentioned that Hitec has good thermal stability up to 550 °C; in Hitec datasheet [33] it is mentioned good thermal stability only up to 450 °C.

4.2 Therminol VP-1, Solar Salt and YaraMOST/Hitec XL simulation and LCOE calculations

To simulate the performance of the plant in the SAM software, only three fluids, Therminol VP-1, Solar Salt and Hitec XL, were used. It is considered that these are enough to study the operation differences between thermal oils and molten salts.

4.2.1 Annual production of energy

In the simulation model that was used, "Process heat parabolic trough", the annual production of energy represents the amount of thermal energy that the plant produces during a year and the value is given in $MW_{th}h$.

Using the meteorological data of Évora and HPS2 project information, simulating the operation of the platform with each fluid under study, the following values of annual production of thermal energy are obtained:

Table 21: *Values of annual production of thermal energy with each fluid.*

	Annual energy [$MW_{th}h$]
Therminol VP-1	4544
Solar Salt	4559
Hitec XL	4540

As can be seen from the values obtained in **Table 21** the annual production of thermal energy is very similar for the three fluids. This parameter is influenced by the project characteristics, as it is the case of installed power and storage capacity, and not so much by the heat transfer fluid that is used.

4.2.2 Capacity factor

Capacity factor is a comparative measure of the amount of energy produced by a plant with the maximum energy that could be produced if the plant was operating at nominal power during the same duration (**equation (*44*)**).

$$CF = \frac{\text{Annual Energy Produced}}{\text{Maximum energy that could be produced}}. \quad \textbf{(44)}$$

In this case, considering the steam generator power of 1.8 MW, the capacity factor is obtained by the following **equation (*45*)**:

$$CF = \frac{\text{Annual Energy Produced}}{(1.8 \times 10^6) \cdot 8760 \text{ hours}}. \quad \textbf{(45)}$$

Through this value it is possible to determine how much equivalent hours the plant is producing at nominal power during that year. The capacity factor obtained through the values provided by SAM for the platform for each HTF, as well as, the corresponding number of hours at nominal power production are presented in **Table 22**.

Table 22: *Capacity factor values obtained and corresponding number of hours with production at nominal power.*

	Capacity Factor	Hours
Therminol VP-1	0.288	2524
Solar Salt	0.289	2533
Hitec XL	0.288	2522

These parameters are directly related to the annual energy production. Consequently, there are no big changes in the plant capacity factor with the use of different fluids. Solar salt is the one that presents the greatest number of equivalent hours with a difference of 11 hours in relation to Hitec XL (worst case). This difference represents 0.1 % of the total so it can be considered insignificant.

4.2.3 Annual thermal power freeze protection

Annual thermal power freeze protection is one of the values provided in the SAM summary table. It represents the thermal energy required to heat the storage system as well as the solar field, always ensuring the safety temperature range of the HTF. In this way, the amount of thermal energy required to heat the plant with the different operating fluids is presented in **Table 23.**

Table 23: *Quantity of thermal energy needed to heat the storage system and the solar field with the different HTF.*

	TES freeze protection [$MW_{th}h$]	Solar field freeze protection [$MW_{th}h$]	Annual total freeze protection [$MW_{th}h$]
Therminol VP-1	15.664	0.137	15.801
Solar Salt	23.300	231.282	254.581
Hitec XL	9.104	18.655	27.759

From the values shown in the **Table 23** it can be seen that the fluid with less losses in the storage system is Hitec XL molten salt. These differences are explained in the case of Therminol VP-1 by volumetric heat capacity and temperature range, which are significantly lower than the salts. This implies much higher storage system dimensions to ensure the same storage thermal capacity, and consequently greater losses. In case of Solar Salt, the losses are higher than those of Hitec XL because its melting point is very high and thus it requires maintaining the tanks at relatively high temperatures; above 250 °C. In case of the solar field, the thermal oil practically does not need heating due to its low melting temperature when compared to the molten salts. Observing the two salts, using Solar Salt requires about 12 times more thermal energy per year for freeze protection than Hitec XL.

4.2.4 Annual electricity consumption

In the annual electricity consumptions determined by SAM's simulations are included the electric energy spent to: 1) circulate the HTF along the solar field; 2) circulate fluid into the steam generator; 3) collector daily tracking; 4) TES freeze protection. The values found are shown in **Table 24.**

Table 24*: Values of annual electricity consumption for each HTF.*

	Annual electricity load [kW_eh]
Therminol VP-1	45036
Solar Salt	35668
Hitec XL	31446

Observing these values, it can be verified that surprisingly thermal oil is the fluid that presents the highest electricity costs. However, in order to have a better perception of the difference in the electricity spent with the pump system for each fluid, an infinite thermal resistance was assumed in the tanks in order to remove the TES freeze protection from the electricity consumption. The obtained values are:

***Table 25**: Values of annual electricity consumption for each HTF without the value of TES freeze protection.*

	Annual electricity load [kW_eh]
Therminol VP-1	30239
Solar Salt	10967
Hitec XL	18891

Analysing these values it can be verified that the thermal oil continues to be the fluid that presents the greatest costs of electricity. The energy spent in daily solar tracking is essentially the same for the three HTF and almost insignificant; this implies that the electricity spent to pump the fluid into the solar field is the main component contributing to the overall electricity consumption. For a better perception of these consumptions, the following graphs show the energy spent to pump each HTF along the solar field (**Figure 24**) and through the heat sink **(Figure 25**).

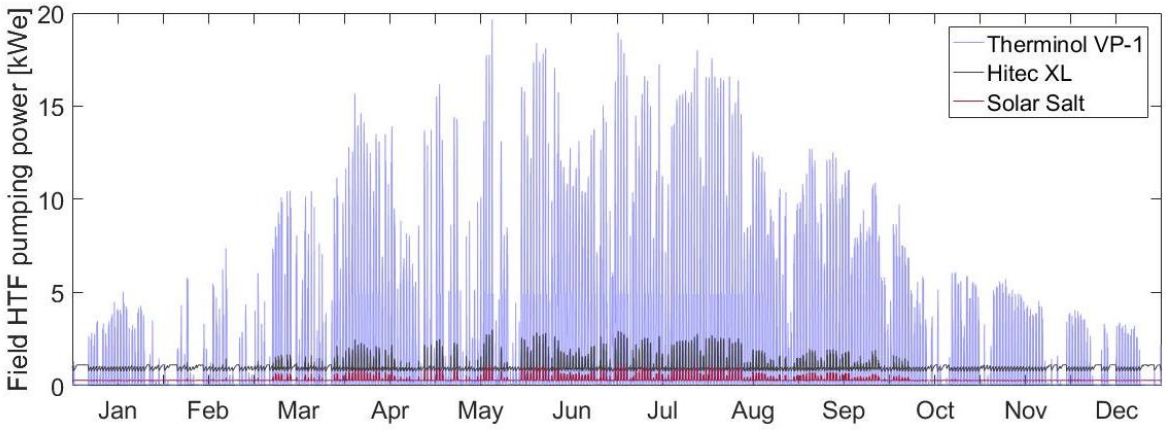

***Figure 24**: Annual field HTF pumping power for each HTF. From highest to lowest values: Therminol VP-1, Hitec XL and Solar Salt.*

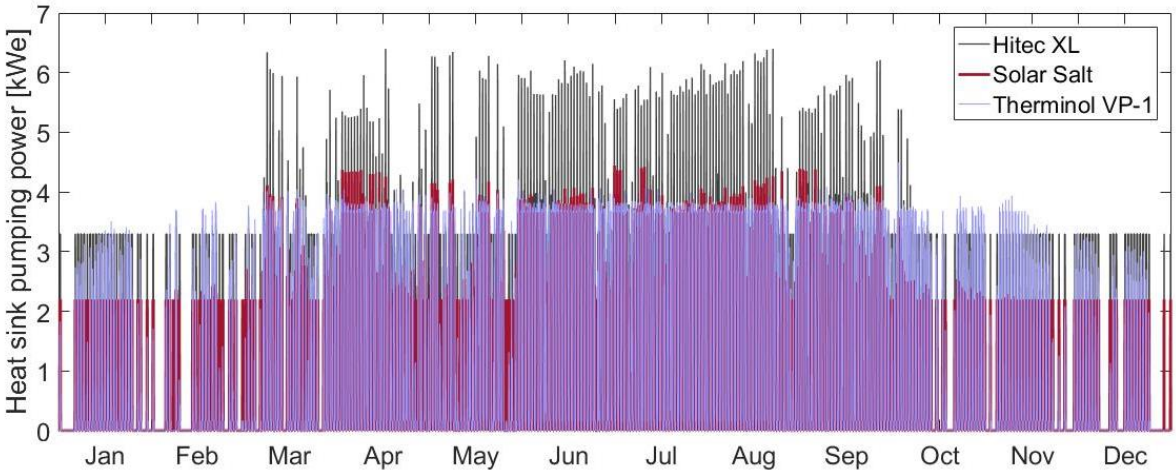

***Figure 25** :Annual heat sink pumping power for each HTF. From highest to lowest values: Hitec XL, Solar Salt and Therminol VP-1.*

The molten salts have clearly lower pump consumptions. This is mainly due to the fact that they reach higher temperatures (for the same low operating temperature), allowing circulation at lower flow rates and resulting in lower pressure losses. Of the two salts, Solar Salt is the one that needs less energy, both in the solar field and in the heat sink, mainly because its maximum operating temperature is higher than that of Hitec XL and its viscosity is lower.

However, as solar field heating will be done by impedance and electrical tracing, i.e., using electricity, it is important to count the annual thermal power freeze protection at this point. For this it is considered that the electrical resistances have an efficiency of 99% and total values of annual electricity consumption are shown in **Table 26.**

Table 26: Annual electricity consumption counting solar field heating.

	Annual electricity load [kW_eh]	Annual electricity consumption for solar field freeze protection [kW_eh][3]	Total annual electricity load [kW_eh]
Therminol VP-1	45036	138	45174
Solar Salt	35668	233618	269286
Hitec XL	31446	18843	50289

Observing the values obtained it can be seen that there is a great discrepancy between the Solar Salt electric consumption and the other two fluids. This value is a result of the high heating requirement in the solar field when using this fluid due to its high melting point. **Figure 26** allows analysing in more detail the needs for solar field heating according to the fluid used.

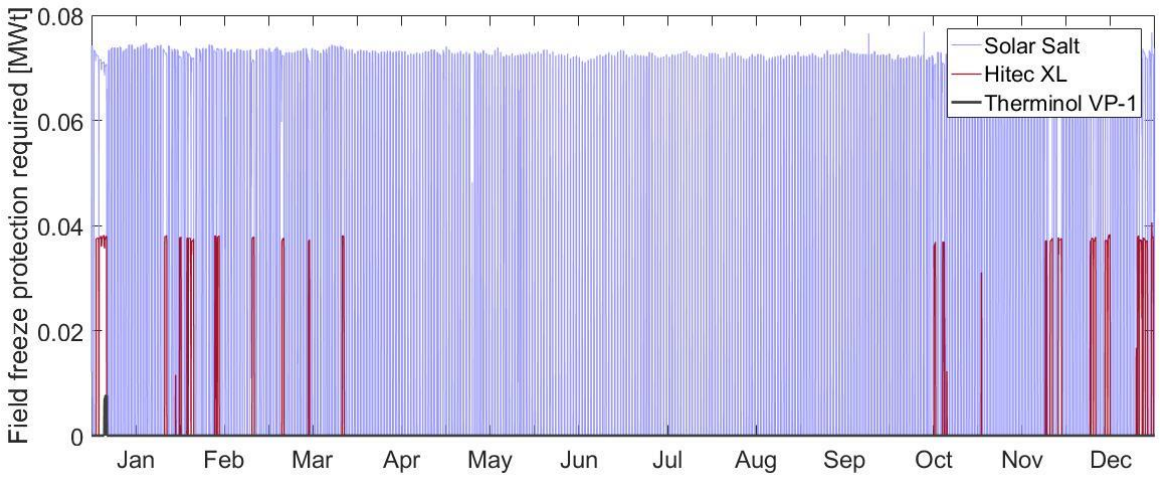

Figure 26: Annual field freeze protection required in MW_t. From highest to lowest values: Solar Salt, Hitec XL and Therminol VP-1.

However, this is the worst-case scenario. No operation strategy, as for example the circulation of salts from the cold tank through the piping during the night, is considered. And this latter strategy can significantly reduce the amount of electricity spent on solar field heating.

[3] Value obtained through the SAM software where it is called "Annual thermal power for field freeze protection".

4.2.5 Electricity costs estimate

Considering annual consumptions and that electricity has an estimated cost of 0.192 €/kWh, a guess of annual electricity costs for the different fluids can be made:

Table 27: *Estimation annual electricity costs of the HPS2 project with each HTF.*

Annual electricity costs [€]	
Therminol VP-1	8673
Solar Salt	51703
Hitec XL	9656

Even without considering any operating strategy, the Hitec XL molten salt does not have much higher electricity consumption than thermal oil Therminol VP-1, so the electricity costs are similar. This means that, even considering the energy spent in solar field heating, it might be possible to spend less electrical energy with low melting point MS than with thermal oils. In addition, when these values are translated into a commercial scale, the impact of electric power consumption will be even greater on thermal oils. This is because the energy spent in the pumping increases proportionally with the plant size increase; whereas the increase in heat consumption with salts is not so significant since the tanks' thermal capacity will also increase.

4.2.6 LCOE calculation

In order to calculate LCOE (Levelized Cost of Energy) of a direct storage plant with molten salts and compare it with a conventional power plant, a parabolic trough power plant of 50 MW_e with 7.5 hours of storage was considered. Several researches were carried out in order to find reference costs for the various elements of conventional plants. In addition, some calculations were based on information obtained from HPS2 partners. The results obtained are detailed in **Table 28.**

Table 28: *Costs of conventional power plant and direct storage with molten salts plant.*

	CONVENTIONAL POWER PLANT	DIRECT STORAGE WITH MOLTEN SALTS
Capital Expenditure (CAPEX)		
Labour : Site and solar field	62.4 M$|55.9 M€	62.4 M$|55.9 M€
Solar Field	103.9 M$|93.1 M€	103.9 M$|93.1 M€
Synthetic oil	7.8 M$|7.0 M€	-
Molten Salts[4]	26.4 M$|23.7 M€	16.1 M$|14.4 M€
Piping&Insulation	11.4 M$|10.2 M€	11.4 M$|10.2 M€
Pre-insulated piping supports	-	0.20 M$|0.18 M€
Heat tracing	-	13.4 M$|12M€
Pumps	Oil: 3 M$\|2.7 M€ Salts: 1.6 M$|1.4 M€	Only salt but bigger: 2.5 M$|2.2 M€
Storage tanks (with insulation and foundation)	9.6 M$|8.6 M€	5.4 M$|4.8 M€
Oil-to-salt heat exchanger	5.1 M$|4.6 M€	-
Electronics, controls, electrical and balance of system	12.6 M$|11.3 M€	12.6 M$|11.3 M€
Power block	20.8 M$|18.6 M€	20.8 M$|18.6 M€
Balance of plant and grid connection	31.2 M$|28 M€	31.2 M$|28 M€
Others*	71.0 M$|63.6 M€	71.0 M$|63.6 M€
Operational Expenditure (OPEX)		
Pumping	572662$|513435 €	298179$|267340 €
Temperature maintain	0 M$|0 M€	0 M$|0 M€**
Others	3 M$ |2.7 M€	3 M$ |2.7 M€
Production		
Power block efficiency	39.1%	43.5%
Heat losses	3.94 MWh_{th}	3178 MWh_{th}
Heat exchanger efficiency	95.3%	-

*project development and management, financing, allowances** with proper operation (salt circulation during night), electrical heat tracing system is not used

The references used to obtain the values presented in **Table 28** were [34, 35, 36], as well as, some contacts made with suppliers. The costs of synthetic oil correspond to Therminol VP-1 [2] and the cost of molten salts corresponds to Hitec XL molten salt [2]. The energy spent in the pumping of the fluid in the solar field and the value of heat

[4] In this value are included the cost of salts necessary for the storage in the case of conventional plant and for the storage and HTF in the case of direct storage with molten salts plant.

losses are obtained through SAM's results. The power block efficiency is calculated using the **equation (46)** and considering an exergy efficiency of 0.7 for both cases.

$$\eta_{PB} = \eta_{ex} \cdot \eta_{Carnot} \quad \textbf{(46)}$$

With,

$$\eta_{ex} = 0.7; \eta_{Carnot} = 1 - \frac{T_{CS}}{T_{HS}} \quad \textbf{(47)}$$

Where T_{CS} corresponds to the cold source (ambient) temperature and T_{HS} to the hot source temperature (in K).

Two different methods were used to calculate LCOE of the two plant types. The first one using SAM, in the *CSP parabolic trough model - LCOE calculator*, and a second method using algebraic calculations. For both cases an operating period of 25 years was considered [37]. Normally the LCOE calculation is performed using the solar irradiation values of a typical meteorological year (TMY). In this case, since we do not have a series of solar irradiation data long enough to determine a TMY in Évora, the LCOE has been determined by averaging the values obtained from 2016, 2017 and 2018 solar irradiation years.

• In the first method, using SAM, the values of CAPEX and OPEX resulting from **Table 28** were inserted in the "financial parameters" section and the results obtained are presented in **Table 29**. Most of CAPEX values that were used correspond to relatively old projects (2008) from which data is available. Current data shall lead to lower LCOE; in fact, current project LCOE in Middle East and Morocco are about 7-10 c$/ kWh however detail of costs is not available. Nevertheless, a comparison between the two fluids in terms of cost is still relevant.

Table 29: *LCOE values obtained through the simulations in SAM.*

	CAPEX [M$]	OPEX [M$]	Annual Energy [MWh]	LCOE [c$/kWh]/[c€/kWh][5]
Conventional CSP power plant	366.80	3.57	191043	17.69/15.80
Direct storage with molten salts (Hitec XL)	349.48	3.30	194169	16.57/14.80

Observing this table, it can be verified that despite the extra anti-freezing protection requirements for the use of molten salts as HTF (namely electrical tracing, impedance,

[5] Conversion rate: 1 EUR = 1,11844 USD|1 USD = 0,894103 EUR

and pre-insulated piping supports), the CAPEX value of this type of plant is lower. This is due to the savings in synthetic oil, storage tanks and molten salts, pumps and heat exchanger. The increase of the solar field output temperature allows the reduction of the storage size and consequently the amount of required salt. Money is saved on the pump acquisitions because there is only one working fluid and thus a single system pump (plus a back-up one) is enough for both the solar field and the storage system, while with thermal oil there are two working fluids and thus two pump systems (plus back-up ones). Finally, no heat exchangers are needed between the solar field and the storage. Adding to this the fact that the value of OPEX is slightly lower for the salts due to the lower consumption of pumping, and the higher electricity production due to the power block efficiency, it is possible to reduce the LCOE of this type of technology by about 6.3 %. This value can even become bigger as a consequence of price reductions associated with scaling up of molten salts technologies manufacturing.

• In the second method, LCOE calculation was made using the values in **Table 28**, in Euros, considering a discount rate of 2 % (value of the Portuguese rate), a lifespan of 25 years and the energy production values obtained through the simulation performed with SAM for Évora. In these calculations the value of the energy consumed to heat the solar field when using MS is discounted from the total value of produced energy. In addition, the degradation of the thermal oils that occurs in conventional plants is also taken into account [38]. As such, the cost of an oil exchange every 5 years has been included in the OPEX.

Considering the **equation (48)** to calculate the LCOE value,

$$LCOE = \frac{\sum_{n=0}^{N} C_n (1+r)^{-n}}{\sum_{n=0}^{N} E_n (1+r)^{-n}}. \quad \textbf{(48)}$$

whereby,

- C_n – total cost for year n;
- E_n – annual electricity production (kWh) for year n;
- N – lifespan;
- r – discount rate.

The values obtained through the calculation are presented in the **Table 30,**

Table 30: *LCOE values obtained through the second approach.*

	CAPEX [M€]	OPEX [M€]	Annual Energy [MWh]	LCOE [c€/kWh]
Conventional power plant	328.89	3.20	191043	13.00
Direct storage with molten salts (Hitec XL)	313.36	2.96	190526	11.49

Observing the obtained values, a reduction of 11.6 % in the LCOE value is estimated using Hitec XL instead of Therminol VP-1 as HTF. This reduction is lower than the value envisaged by D. Kearney et al [2] (17.6%). However, the LCOE values may actually be even lower since a large part of the costs presented in **Table 28** were obtained using references already with a few years old [34, 35, 36] and these values should currently be lower.

4.2.7 Partial conclusion: SAM results and LCOE calculations with different HTF

The use of MS as HTF in a parabolic trough power plant implies extra care regarding freezing protection. The expected cost of such power plant might be therefore higher than for conventional technology. However, it has been shown in this section that additional costs due to possible freezing are relatively modest, while the use of MS enables to reduce the pumping and the TES costs. Besides, thanks to higher operating temperatures, the power block efficiency can be improved. This resulted in an expected lower LCOE for power plants with MS as HTF.

Building new LF systems with molten salts will require the design of several components such as impedance heating systems, pre-insulated piping supports, etc. One of the purposes of HPS2 project is to get experience on those issues. Nevertheless, new power block designs will also be required. Indeed, the use of MS implies a different temperature range for the system. This is why the last section of this work aims to give some clues about what those new power blocks could be.

5

Power block with high T_H and high ΔT

One of the most interesting aspects in the use of molten salts as HTF is the fact that they allow to reach temperatures higher than the thermal oils. Such temperatures in the order of 500 °C to 565 °C enable higher ΔT of operation, decreasing TES size while increasing power block efficiency. Thus, it is important to understand what changes this increase will cause in the thermodynamic cycle. To achieve this goal, first reminders about thermodynamic cycles will be given, then the cycles that are currently used in CSP LF plants with thermal oil as HTF will be studied. Finally, different cycles for the temperatures that are achieved with molten salts will be proposed.

5.1 Thermodynamic cycle efficiency, Carnot cycle and real cycle

A thermodynamic cycle is composed of a compression, a heat input, an expansion and a heat output. The efficiency of a thermodynamic cycle producing electricity is defined as the ratio between the produced work (net value: expansion work within turbine minus compression work within pump or compressor) and the input heat:

$$\eta_{cycle} = \frac{W_{out,net}}{Q_{in}}. \quad \textbf{(49)}$$

The produced work can be rewritten as the difference between the input heat and the output heat, respecting first law of thermodynamics.

$$\eta_{cycle} = \frac{Q_{in} - Q_{out}}{Q_{in}}. \quad \textbf{(50)}$$

1) Ideal cycle

In an ideal cycle, also called Carnot cycle, the compression and expansion work are isentropic while heat exchanges are isothermal and reversible.

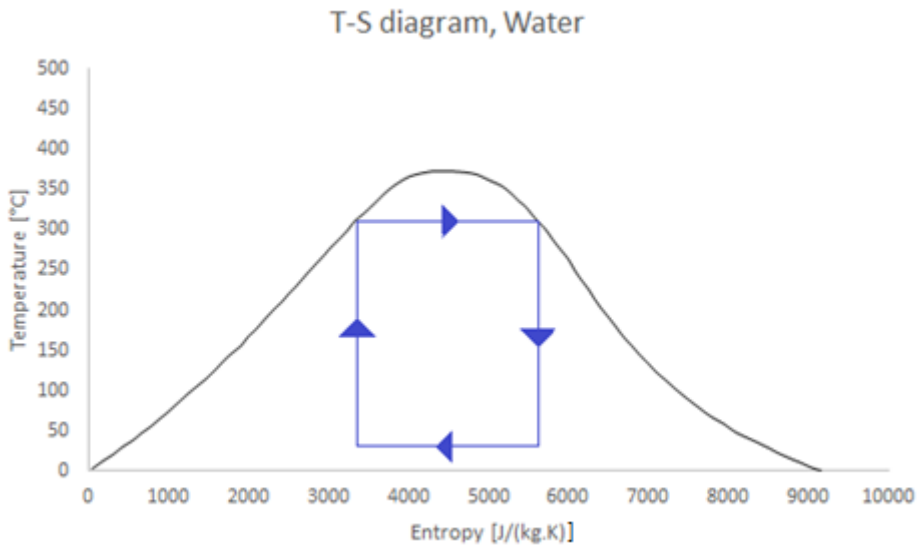

***Figure 27**: A Carnot cycle in the water diagram.*

Because heat exchanges are reversible, the entropy variation can write as follows:

$$dS = \frac{dQ}{T}. \tag{51}$$

The heat exchange rates can therefore be obtained by integrating the product TdS along the fluid path. The result therefore corresponds to the area below the curve corresponding to this path in a Temperature-Entropy (T-S) diagram. Moreover, thanks to the entropy variation definition, the heat ratio can be related to the ratio of the absolute temperatures of the cold and hot sources with which the system is exchanging heat:

$$\eta_{Carnot} = \frac{Q_{in} - Q_{out}}{Q_{in}} = 1 - \frac{Q_{out}}{Q_{in}} = 1 - \frac{T_{CS}}{T_{HS}}. \tag{52}$$

Because Q_{in} and Q_{out} can be related to the areas that are below the condensation and the evaporation horizontal lines, one may also notice that the efficiency is directly related to the area between those two curves.

2) Real cycle

Because of unavoidable irreversibilities and because of technical limitations, an ideal cycle is impossible to realize. For example:

- Compression and expansion generate entropy;

- Compressors and turbines cannot work in diphasic regimes (cavitation and corrosion problems).

This is why actual vapor cycles usually are Hirn cycles, which are a variant of a Rankine cycle with a superheating stage avoiding expansion in a wet regime and allowing pumping in a liquid regime. Comparison between a Hirn cycle and the corresponding Carnot cycle is given in **Figure 28.**

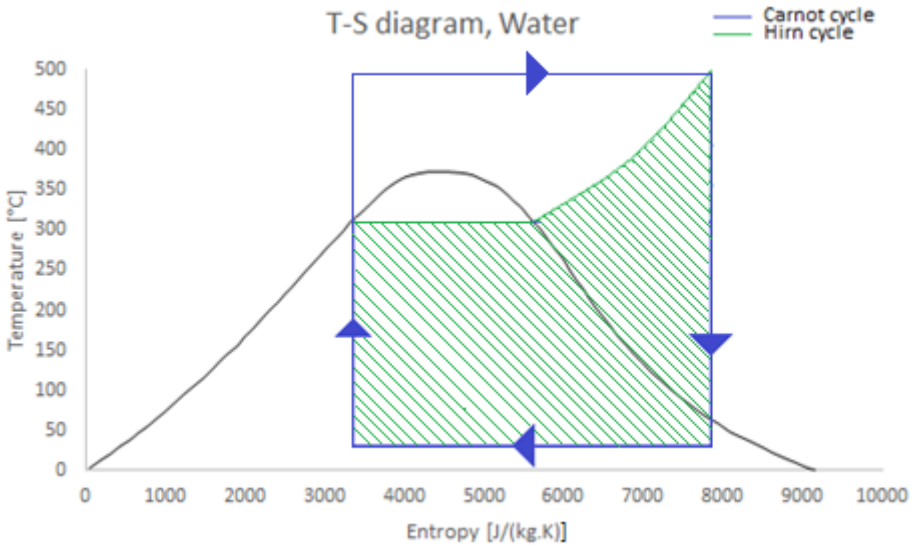

Figure 28: *Hirn cycle with corresponding ideal cycle of Carnot.*

Considering that the Hirn cycle is an internally reversible cycle (quasi-static transformation and entropy variation evaluated at the system temperature, isentropic compression and expansion), the efficiency of the cycle can still be calculated by dividing the area of the cycle by the area below the heating curve.

3) Bleedings

As it will be seen in the following sections, one way to increase the efficiency of a real power cycle is to use bleedings, i.e. extracting a part of the steam from the turbine before being completely expanded in order to preheat the water that will enter the boiler. This kind of method reduces the generated entropy because the average temperature at which the input heat is transferred is higher. Hence, the cycle efficiency increases. The choice of the number of bleeding is only constrained by economic considerations. Current thermal power plants generally have between 5 to 8 bleedings.

5.2 Commercial CSP power cycles: low T_H (400 °C) and low ΔT (T_L = 290 °C) because of oil limitations

First step is therefore to understand how the thermodynamic cycles of actual power plants work. To do so, the cycle that is proposed by Ascensión Piquer *et al*. [39] is decomposed and efficiency improvements throughout its different features will be studied.

5.2.1 Carnot efficiency

As already explained, the efficiency of a Carnot machine represents the maximum efficiency that it can reach when working between two temperatures; using two heat sinks: a hot source (HS) and a cold source (CS). To calculate the maximum theoretical efficiency that the power block of a conventional plant can reach, a hot temperature of 390 °C and an ambient temperature of 20 °C will be considered, as shown in **equation (47)**

$$\eta_{Carnot} = 1 - \frac{T_{CS}}{T_{HS}} = 1 - \frac{293.15}{663.15} = 0.56$$

It can be seen that with this hot source temperature the maximum efficiency that the cycle can reach is ~56%.

5.2.2 Conventional power cycle

The thermodynamic cycle of a commercial power plant of 50 MW is presented by [39] (illustrated in **Figure 29**). Water is pumped up to a pressure of 120 bars, then it is vaporized in the steam generator (15 bars pressure drops) where it is superheated up to 380 °C (10 °C pinch within the heat exchanger). Superheated high pressure steam is then expanded in a multi-stage turbine with one reheating and 6 bleedings. Finally, it is condensed with a pressure of 0.06 bars and a temperature of 36 °C and pumped again. The different bleedings are used to preheat the water through opened and closed feedwater tanks, up to a temperature of 241 °C.

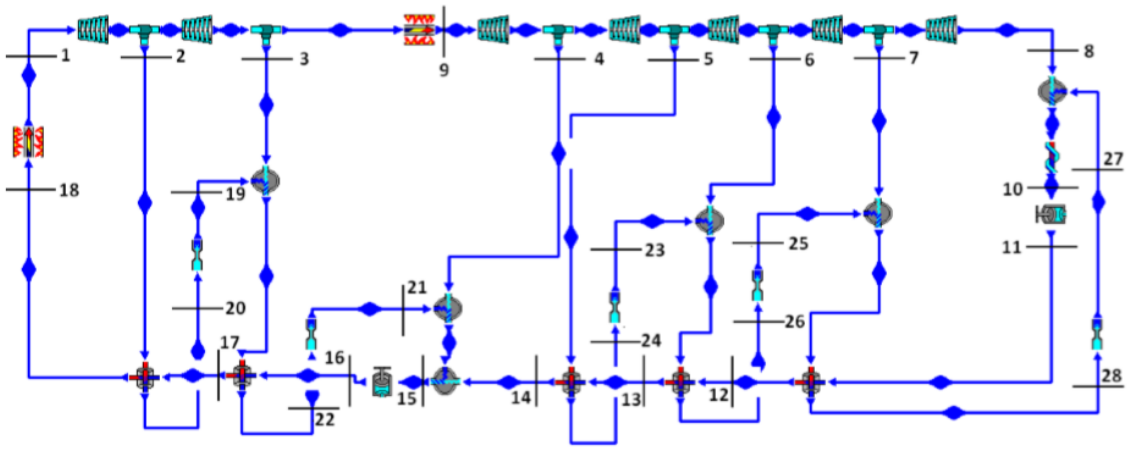

***Figure 29**: Thermodynamic cycle of a current commercial power plant of 50 MW. The diagram was copied from [39]*

Reheating (point 9) and bleedings (points 2, 3, 4, 5, 6 and 7) are carried out with the aim of increasing cycle efficiency. In order to assess the value of each of those enhancements, the following considerations are taken:

- Maximum output temperature of the steam generator is 380 °C (20 °C pinch within the heat exchanger);
- Maximum pressure at the outlet of the pump is 120 bars;
- Turbines are adiabatic and have an isentropic efficiency of $\eta_T = 0.87$ (calculated from enthalpies of points that are considered in [39]);
- The pressure losses are 15 bars during the steam generation and approximately 2 bars during the reheating;
- The steam quality at the outlet of the turbine must be higher than 95% to avoid erosion (calculated from given points in [39]);
- The mass flow rate is determined according to the system conditions.

The values of pressure, temperature, mass flow and enthalpy at each of the points marked in the **Figure 29** and in the T-S diagrams of the Rankine cycles presented throughout the study are given in **Appendix 7: Values used for cycle efficiencies of conventional power plant**, which is provided by [39].

From these values it is possible to calculate the efficiency of each of the cycles. Starting in the basic cycle, then a cycle with reheating and finally adding bleedings until the complete cycle of a conventional plant is obtained in order to understand the impact that the various strategies have on the cycle efficiency.

5.2.3 Basic Cycle efficiency

Basic Rankine cycle (without reheating or bleedings) is shown below in the T-S diagram of **Figure 30.**

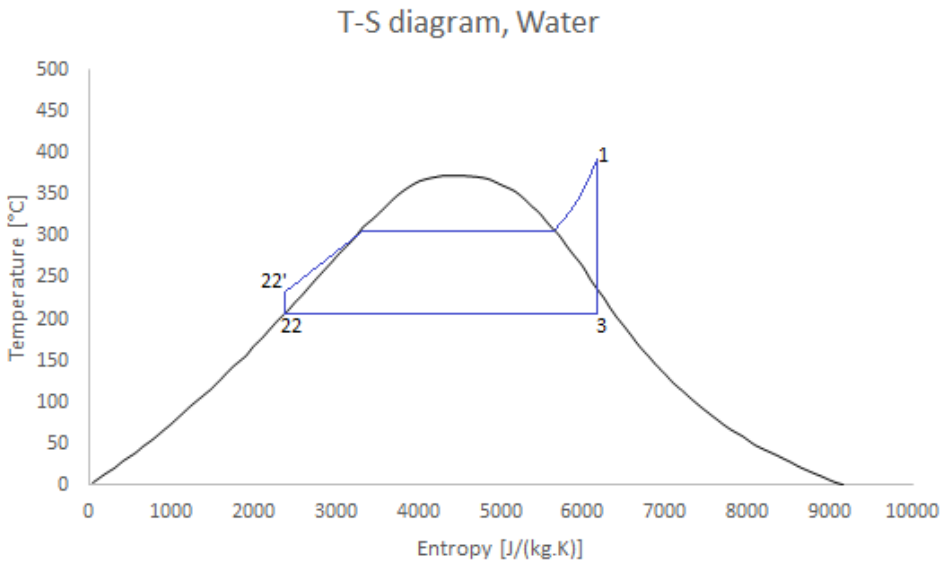

***Figure 30**: Diagram T-S of water with basic cycle.*

The energy spent in heating to generate steam for the turbine is determined by the enthalpy difference between point 1 and point 22' (preheating, phase-change and superheating). The work of the turbine is given by the enthalpy difference between point 1 and point 3. Finally, the work done by the pump is obtained through the enthalpy difference between point 22 'and point 22. The enthalpy in point 22' can be assessed with **equation (53)**

$$h_{22'} = h_{22} + v_{water} \cdot (p_{22'} - p_{22}). \qquad \textbf{(53)}$$

Thus, the efficiency of this cycle is determined by **equation (54)**, knowing that for this simple case, the mass flow is the same in the whole cycle.

$$\eta_{cycle} = \frac{W_{turbine} - W_{pump}}{W_{heat}} = \frac{(h_1 - h_3) - (h_{22'} - h_{22})}{(h_1 - h_{22'})} = 0.1380 \qquad \textbf{(54)}$$

As expected, since the minimum cycle temperature is very high, the efficiency of this cycle is very low. This is the reason why more complex cycles, that allow to achieve higher efficiencies, have been conceived. Several of those cycles will be studied below.

5.2.4 Cycle with reheating

One of the most important methods in increasing the efficiency of the power cycle is reheating, since this will allow the cycle to reach a considerably lower minimum temperature. In **Figure 31** the Rankine cycle with reheating is represented.

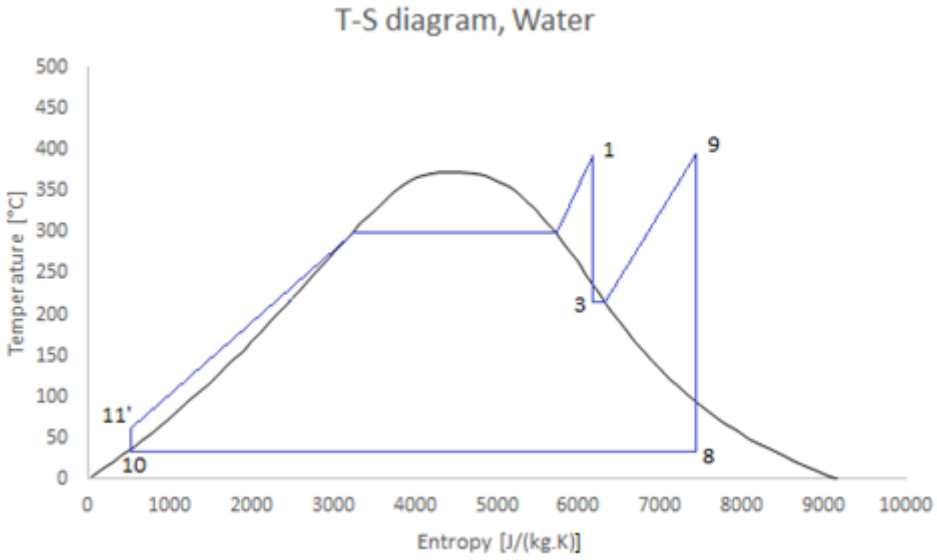

***Figure 31**: Rankine cycle with reheating.*

Reheating is represented in the cycle between points 3 and 9 (vaporization of the residual liquid water, then superheating) To calculate the efficiency of the cycle, the specific enthalpy of fluid at point 11' ($h_{11'}$) must be determined. This enthalpy can be assessed with **equation (55)**.

$$h_{11'} = h_{11} + \nu_{water} \cdot (p_{11'} - p_{11}). \quad \textbf{(55)}$$

Where h_{11} is the enthalpy at point 11, ν_{water} represents the specific volume of water and $p_{11'}$ and p_{11} the pressure at points 11' and 11, respectively. And, the efficiency of this cycle is calculated by **equation (56)**

$$\eta_{cycle} = \frac{W_{turbine\ 1} + W_{turbine\ 2} - W_{pump}}{W_{heat\ 1} + W_{heat\ 2}} \quad \textbf{(56)}$$

$$= \frac{(h_1 - h_3) + (h_9 - h_8) - (h_{11'} - h_{10})}{(h_1 - h_{11'}) + (h_9 - h_3)} = 0.3585$$

As can be seen from the obtained result, the cycle's efficiency has increased by a factor of approximately 2.6 thanks to reheating, which is very significant.

5.2.5 Cycle with reheating and bleedings

Another way to increase efficiency is the use of bleedings. Bleedings allow raising the water temperature before entering the steam generator, reducing the amount of energy required on heating but most of all increasing temperature at which heating is performed, enhancing efficiency. The 6 bleedings of a power cycle of a 50 MW_e conventional parabolic trough power plant are shown in **Figure 32**

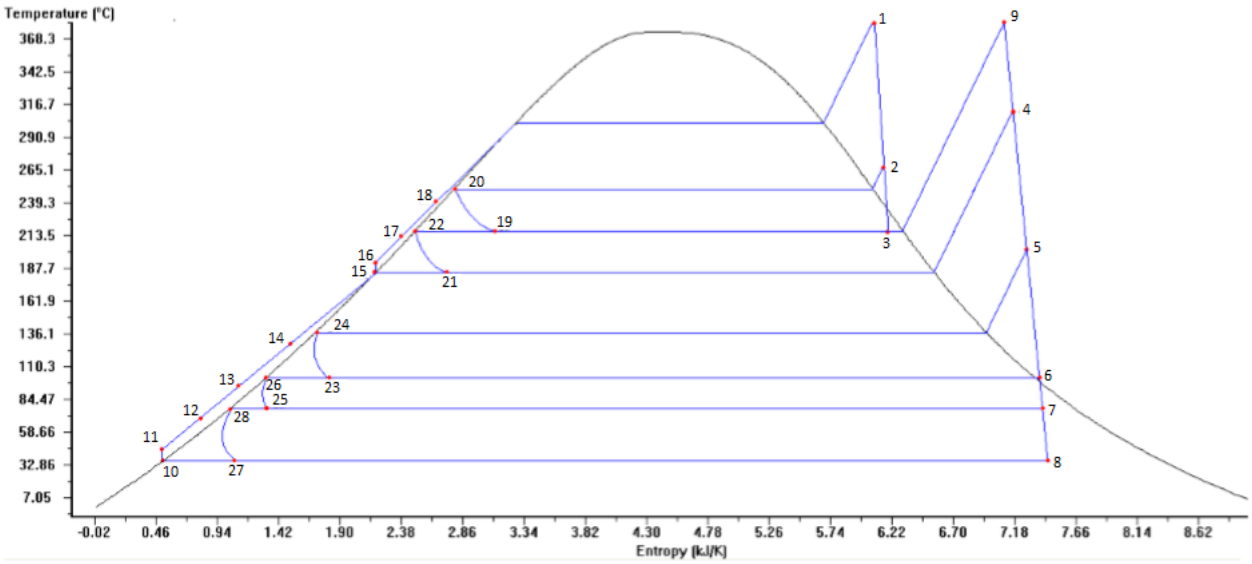

Figure 32:Complete cycle of a conventional power plant.

Through this diagram and the values of **Table 42** (presented in **Appendix 7: Values used for cycle efficiencies of conventional power plant**), the cycle efficiency with reheating and successively 1, 2, 3, 4, 5 and 6 bleedings were determined. The efficiency is determined by the following method (calculation example for the complete cycle):

The work performed by the turbine at high and low pressure is determined by the following **equations (57)** and **(58)**.

$$W_{turbine\,1} = m_{1\to2}(h_1 - h_2) + m_{2\to3}(h_2 - h_3) = 16405.2\ \text{kW} \qquad \textbf{(57)}$$

$$W_{turbine\,2} = m_{9\to4}(h_9 - h_4) + m_{4\to5}(h_4 - h_5) + m_{5\to6}(h_5 - h_6) + m_{6\to7}(h_6 - h_7) + m_{7\to8}(h_7 - h_8) = 38873.75\ \text{kW} \qquad \textbf{(58)}$$

The work performed by the two pumps is determined by the **equations (59)** and **(60)**:

$$W_{pump\,1} = m_{10\to11}(h_{11} - h_{10}) = 59.55\ \text{kW} \qquad \textbf{(59)}$$

$$W_{pump\,2} = m_{15\to16}(h_{16} - h_{15}) = 780.64\ \text{kW} \quad \textbf{(60)}$$

And the energy spent on heating (heat 1) and reheating (heat 2) is obtained through the **equations (61) and (62)**:

$$W_{heat\,1} = m_{18\to1}(h_1 - h_{18}) = 113365\ kW \quad \textbf{(61)}$$

$$W_{heat\,2} = m_{3\to9}(h_9 - h_3) = 23483.46\ kW \quad \textbf{(62)}$$

Finally, the efficiency of the complete cycle is determined by the **equation (63)**:

$$\eta_{cycle} = \frac{W_{turbine\,1} + W_{turbine\,2} - W_{pump\,1} - W_{pump\,2}}{W_{heat\,1} + W_{heat\,2}} = 0.3978 \quad \textbf{(63)}$$

Details about efficiency increase thanks to every bleeding is shown in **Table 31.**

***Table 31**: Values of cycle efficiency with different number of bleedings.*

Number of bleedings	Efficiency
1	0.3658
2	0.3727
3	0.3801
4	0.3845
5	0.3903
6	0.3978

As can be seen from the obtained values, efficiency increases slowly with the increase of bleedings number. Values higher than those initially mentioned in the literature are reached. This may be related both to the fact that references have already been published a few years ago and to the fact that thermal losses in turbine and heat exchangers are not included in this calculation. The choice of the number of bleedings is therefore an optimization between capital expenditure costs and expected incomes from the increase of efficiency throughout the lifetime of the power plant (20-30 years). In addition, the efficiency of the presented power cycle, corresponding to a conventional power plant of 50 MW (with reheating and 6 bleedings), is 39.78%.

5.2.6 Exergy efficiency

Exergy is the maximum useful work which can be extracted from a system as it reversibly comes into equilibrium with its environment. Exergy efficiency is therefore the comparison between the actual efficiency of a system and that maximum. The efficiency of all cycles presented as well as the corresponding exergy efficiency is presented in the **Table 32**.

Table 32: Efficiency of all cycles presented and corresponding exergy efficiency.

	Efficiency	Exergy efficiency
Basic cycle	0.1380	0.2464
Cycle with reheating	0.3585	0.6402
Cycle with reheating and 1 bleeding	0.3658	0.6532
Cycle with reheating and 2 bleeding	0.3727	0.6655
Cycle with reheating and 3 bleeding	0.3801	0.6788
Cycle with reheating and 4 bleeding	0.3845	0.6866
Cycle with reheating and 5 bleeding	0.3903	0.6970
Complete cycle	0.3978	0.7104

From here it can be seen that all the strategies used allow to increase the exergy efficiency of the cycle from 24.6% to 71.0%. This increase has a very significant impact on the energy production of a plant. However, all these strategies also represent a significant increase in the complexity and cost of the power block.

5.3 YARA Most molten salts: TH = 500 °C and TL = 170 °C

As the salts allow to reach a greater high temperature, ~500 °C in the case of YaraMost (Hitec XL) used in the HPS2 project, the power cycle undergoes some changes. These changes are expected to increase cycle efficiency, and this is one of the factors of greatest interest in the use of molten salts such as HTF. Thus, throughout this section, these changes will be analysed and the cycle efficiencies determined using the same method of analysis used in the previous section for a conventional power plant.

5.3.1 Carnot efficiency

Considering that the molten salts allow to reach higher temperatures, it is verified the impact that this temperature increase has on the Carnot efficiency. For this, **equation (47)** is used and is considered the cold source (ambient) at 20 °C and the hot source at ~500 °C.

$$\eta_{Carnot} = 1 - \frac{T_{CS}}{T_{HS}} = 1 - \frac{293.15}{773.15} = 0.62$$

With this temperature range the maximum efficiency that the cycle can achieve is 62%, (vs. 56% for the hot source at 400 °C), showing the interest of increasing high temperature.

5.3.2 Power cycle of direct storage with molten salts plant

Similar to the previous point, efficiency will be calculated for the basic cycle, cycle with reheating, cycle with the various bleedings and for the complete cycle (reheating and 6

bleedings). In this way, it is possible to compare the efficiency of this cycle with the cycle efficiency of a conventional plant.

Some considerations are taken:

- Maximum output temperature of the steam generator is 490 °C;
- Maximum pressure at the outlet of the pump is 150 bars;
- Turbines are adiabatic and have an isentropic efficiency of $\eta_T \cong 0.87$;
- The pressure loss is 15 bars during the steam generation and 2 bars during the reheating;
- The steam quality at the outlet of the turbine must be higher than 95% to avoid corrosion (values determined by the software Coolpack);
- The mass flow is determined according to the system conditions.

The values of pressure, temperature, mass flow and enthalpy at each point marked on T-S diagram of cycles are given in tables available from **Appendix 8: Values used for basic cycle efficiency calculation with MS** to **Appendix 14: Values used for efficiency calculation of complete cycle**.

5.3.3 Basic cycle efficiency

In the following T-S diagram is shown the basic cycle of a direct storage with molten salts (Hitec XL) plant represented in green, and basic cycle of commercial CSP in blue.

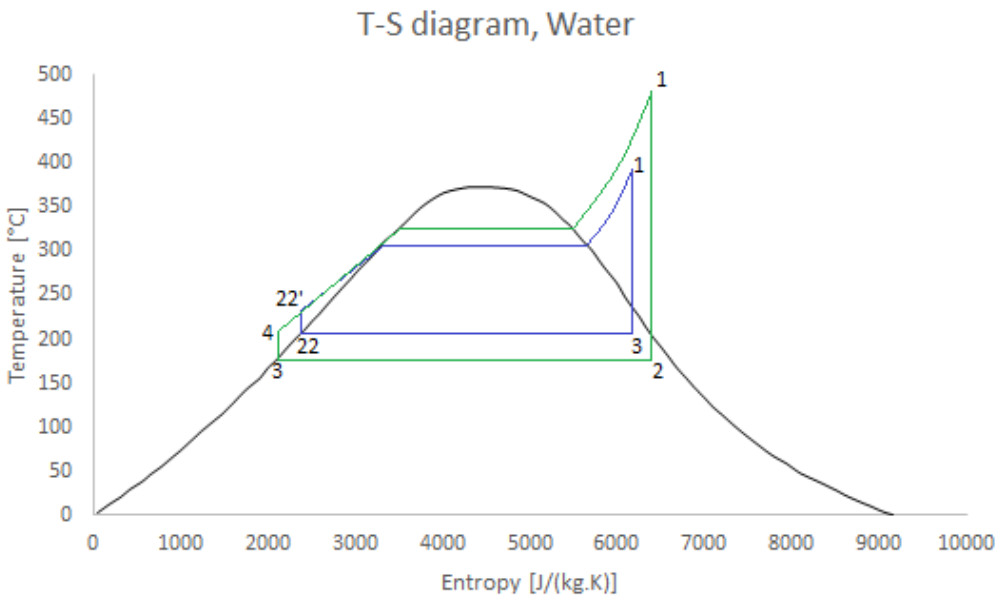

***Figure 33**: Diagram T-S with basic Rankine cycle of a direct storage with molten salts (Hitec XL) plant (green) and basic cycle of commercial CSP (blue).*

By simply observing the diagram, it is possible to verify that the "area" of this cycle is higher than the area of the same cycle of a conventional plant thanks to the increase of ΔT of operation. To calculate this efficiency, the values shown in the table on the **Appendix 8: Values used for basic cycle efficiency calculation with MS** are considered, the obtained efficiency is 21.29%.

This efficiency is significantly higher than the efficiency of the simplest cycle when using thermal oils (13.80%). From here it is possible to confirm that the increase in the high temperature of the cycle has a significant impact on the cycle efficiency.

5.3.4 Cycle efficiency with reheating

In the following **Figure 34**, the Rankine cycle with reheating is represented in the T-S diagram of water.

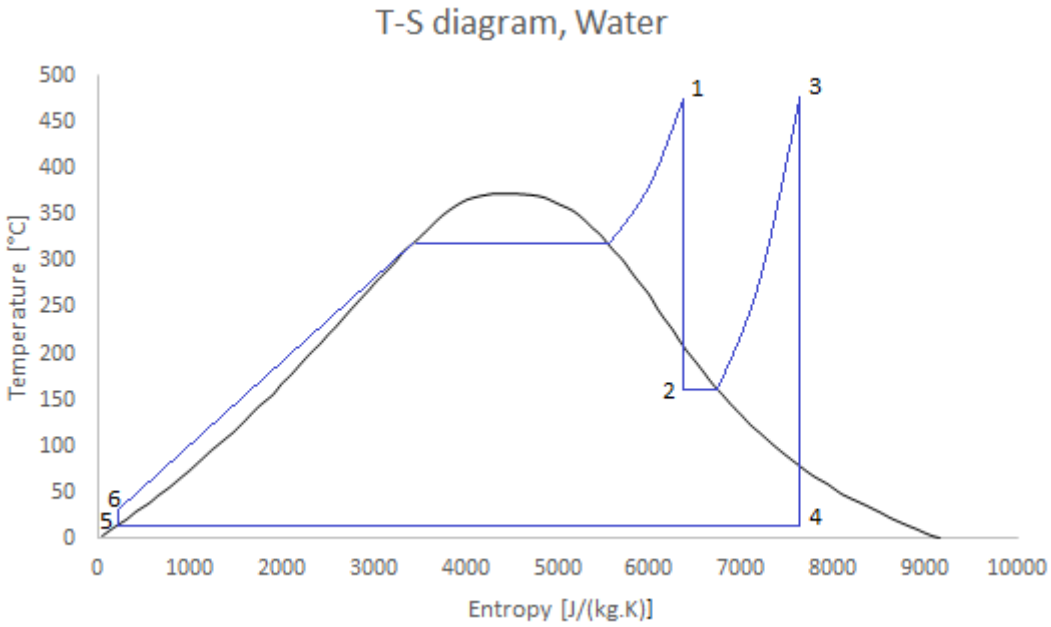

***Figure 34**: Rankine cycle with reheating.*

Reheating is represented in the cycle between points 2 and 3. The values of pressure, temperature, mass flow and enthalpy at each point are shown in table available in **Appendix 9: Values used for cycle with reheating efficiency calculation**. Through these values and equation, also available in this same appendix, an efficiency of 38.11% was determined.

As can be seen, with the increase in the high temperature of cycle, the cycle efficiency only with reheating is already higher than the efficiency of cycle with 3 bleedings of a conventional plant. However, the salts have a high melting point and for this reason it is necessary to heat the water before starting to exchange heat with the salts so that their temperature does not decrease too much. Thus, the same calculation will be done but with a bleeding at 290 °C. In this way it will be possible to solve the question of the high melting point of salts and at the same time increase the efficiency.

5.3.5 Cycle efficiency with reheating and 1 bleeding at 290 °C (74.36 bars)

In the cycle with a bleeding at 290 °C, represented in **Figure 35** by the green line, a mixer is used at point 7. The use of the mixer allows a heat exchange with an efficiency of 100%, however it involves adding a new pump (from point 7 to point 8).

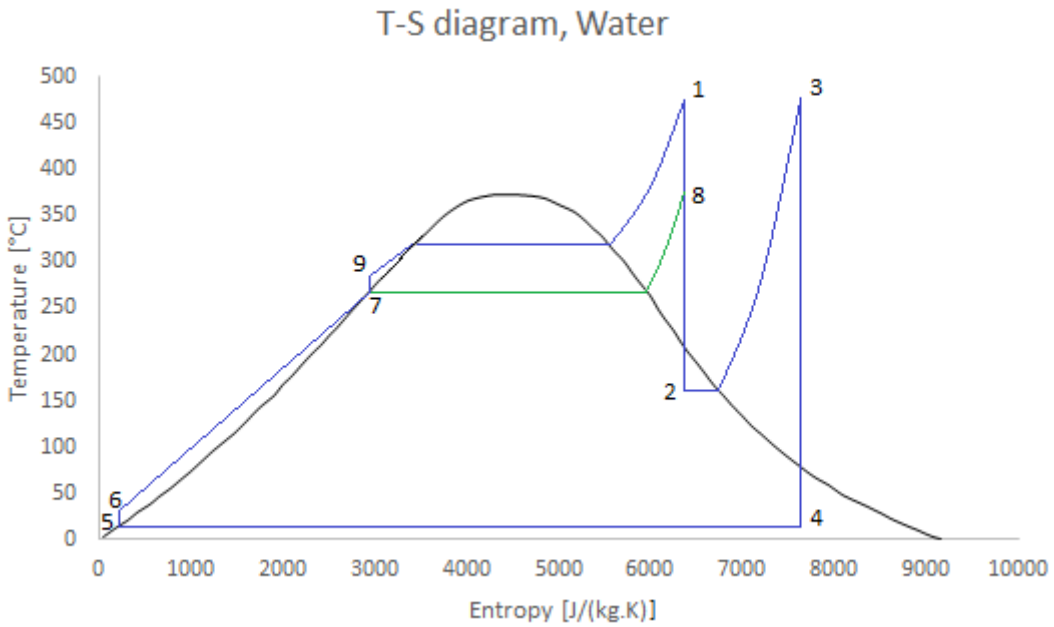

***Figure 35**: Rankine cycle with reheating and 1 bleeding at 290 °C.*

The values of pressure, temperature, mass flow and enthalpy for each point marked in T-S diagram are shown in table available in **Appendix 10: Values used for efficiency calculation of cycle with reheating and 1 bleeding at 290 °C**. Using these values an efficiency of 39.72% was determined.

This bleeding not only solves the problem of the high melting point of salts (raising the water temperature from 37.95 °C to 290 °C) but also increases the cycle efficiency from 38.11% to 39.72%. However, a lot of useful energy is being wasted to heat water at low temperature. In this way, the cycle efficiency with two bleedings will be studied, adding one bleeding at 100 °C, and thus making the water heating more efficient.

5.3.6 Cycle efficiency with reheating and 2 bleeding at 290 °C (74.36 bars) and 100 °C (1.01 bars)

The bleeding at 100 °C that has been added to the previous cycle can be seen in **Figure 36** by the green line between points 10 and 11. In this second bleeding, the heat exchange is done through a heat exchanger with an efficiency of 90%, which allows to increase the temperature from point 6 to point 12.

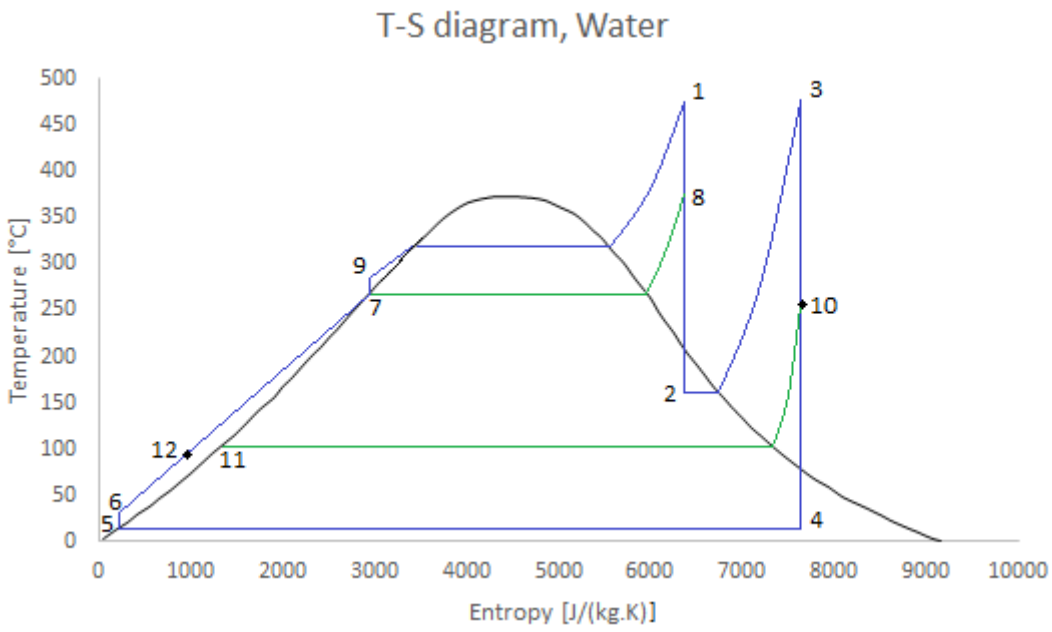

***Figure 36**:Rankine cycle with 2 bleedings at 100 °C and 290 °C.*

The values of pressure, temperature, mass flow and enthalpy determined for each point indicated in diagram are available in table in **Appendix 11: Values used for efficiency calculation of cycle with reheating and 2 bleedings at 100 °C and 290 °C**.

With this second bleeding it was possible to improve the efficiency of heating, allowing to increase the cycle overall efficiency from 39.72% to 41.02%. However, since Yara Most molten salts have a very low melting point of 130 °C, it is interesting to see if a single bleeding at a temperature below 290 °C will increase the cycle efficiency.

5.3.7 Cycle efficiency with reheating and 1 bleeding at 200 °C (15.54 bars)

Since Hitex XL is a low melting point salt, being its safety temperature 170 °C, it is possible to use a cycle with a single bleeding at 200 °C without causing problems on the side of the salts. Similar to what happened in the section **5.3.5 Cycle efficiency with reheating and 1 bleeding at 290 °C**, a mixer is used as heat exchanger medium which implies the use of another pump. The values of pressure, temperature, mass flow and enthalpy used for cycle efficiency calculation as well as the T-S diagram are available in **Appendix 12: Values used for efficiency calculation of cycle with reheating and 1 bleeding at 200 °C**. Through these values, an efficiency of 41.04% was determined.

From this it can be seen that the cycle efficiency, using only one bleeding but at a lower temperature, increases from 39.72% to 41.04%. In addition, this cycle with only one bleeding is as efficient, 41.04%, as the previous cycle with two bleedings (one at 290 °C and another at 100 °C), 41.02%. However, this cycle continues to use energy at 200 °C to heat water at 36.54 °C, which represents a great waste of exergy. Then, as

was done for the previous cycle, the cycle efficiency will be determined by improving the efficiency of the heating using a second bleeding at 100 °C.

5.3.8 Cycle with reheating and 2 bleeding at 200 °C (15.54 bars) and 100 °C (1.01 bars)

As previously, the heat exchange of this second bleeding is done through a heat exchanger with an efficiency of 90%, which allows increasing the water temperature to 93.65 °C. The values of pressure, temperature, mass flow and enthalpy used for cycle efficiency calculation as well as the T-S diagram are available in **Appendix 13: Values used for efficiency calculation of cycle with reheating and 2 bleedings at 100 °C and 200 °C**. Through these values an efficiency of 41.76% was determined, against 41.04% for a single bleeding at 200 °C.

As this second approach revealed to be more efficient, it was chosen to continue the study and to determine efficiency with 3, 4, 5 and 6 bleedings, such as what is done in conventional plants.

5.3.9 Complete cycle

As previously mentioned, bleedings are used to increase cycle efficiency by improving heating efficiency through increases of water temperature before entering the steam generator. In this way, the complete cycle of a conventional plant (with reheating and 6 bleedings) adapted to the pressure and temperature conditions of a plant using molten salts (namely Hitec XL) as HTF is illustrated in **Figure 37**.

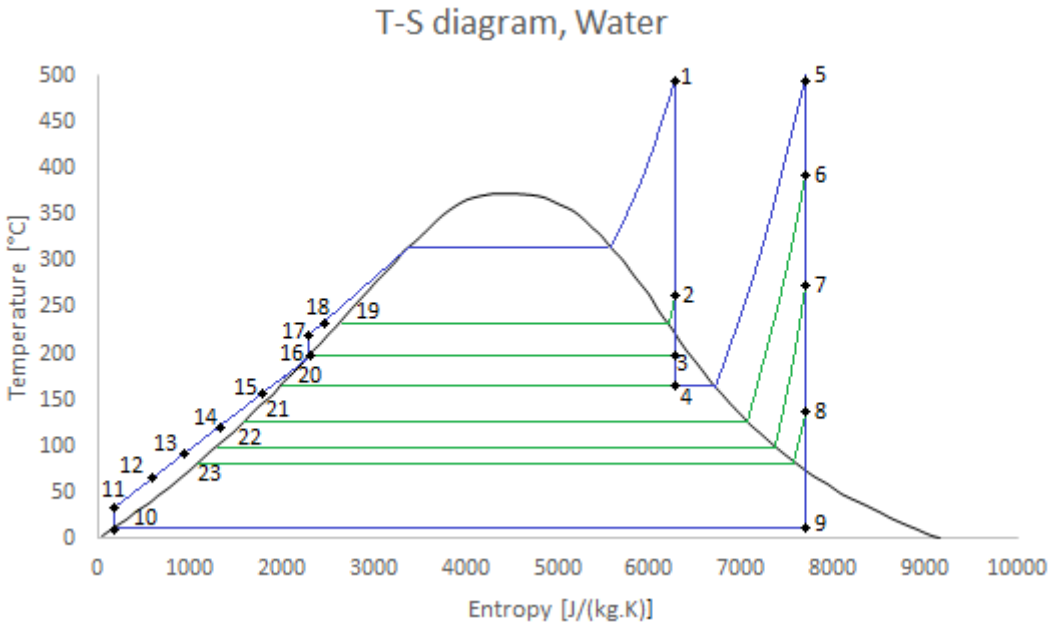

Figure 37: Complete cycle of direct storage with molten salts plant.

The values of pressure, temperature, mass flow and enthalpy at each point were determined and are available in **Appendix 14: Values used for efficiency calculation of complete cycle.**

Using these values and the following equations, it is determined:

- The work carried out by the high-pressure turbine (turbine 1) and the low-pressure turbine (turbine 2).

$$W_{turbine\,1} = m_{1\to2}(h_1 - h_2) + m_{2\to3}(h_2 - h_3) + m_{3\to4}(h_3 - h_4) = 21669\ \text{W}. \quad \textbf{(64)}$$

$$W_{turbine\,2} = m_{5\to6}(h_5 - h_6) + m_{6\to7}(h_6 - h_7) + m_{7\to8}(h_7 - h_8) + m_{8\to9}(h_8 - h_9) = 28331\ \text{kW}. \quad \textbf{(65)}$$

- The work done by the two pumps (pump 1 and pump 2).

$$W_{pump\,1} = m_{10\to11}(h_{11} - h_{10}) = 53\ \text{kW}, \quad \textbf{(66)}$$

$$W_{pump\,2} = m_{16\to17}(h_{17} - h_{16}) = 479\ \text{kW}. \quad \textbf{(67)}$$

- And the work done by the heating (heat 1) and the reheating (heat 2).

$$W_{heat\,1} = m_{18\to1}(h_1 - h_{18}) = 93439\ \text{kW}, \quad \textbf{(68)}$$

$$W_{heat\,2} = m_{4\to5}(h_5 - h_4) = 22880\ \text{kW}. \quad \textbf{(69)}$$

Through these values and using **equation (70)**, the efficiency of the complete cycle is determined.

$$\eta_{cycle} = \frac{W_{turbine\,1} + W_{turbine\,2} - W_{pump\,1} - W_{pump\,2}}{W_{heat\,1} + W_{heat\,2}} = 0.4253 \quad \textbf{(70)}$$

The obtained efficiency value, ~42.53%, is much higher than the one of the complete cycle of a conventional plant, ~39.78%. This increase represents a significant value in the annual production of a plant (6.9%).

5.3.10 Exergy efficiency

The efficiency values determined for each of the cycles as well as the exergy efficiencies corresponding to each of them appear in **Table 33.**

Table 33: Efficiency of all cycles presented and corresponding exergy efficiency.

	Efficiency	Exergy efficiency
Basic cycle	0.2129	0.3434
Cycle with reheating	0.3811	0.6147
Cycle with reheating and 1 bleeding	0.4104	0.6619
Cycle with reheating and 2 bleeding	0.4176	0.6735
Cycle with reheating and 3 bleeding	0.4205	0.6782
Cycle with reheating and 4 bleeding	0.4214	0.6797
Cycle with reheating and 5 bleeding	0.4220	0.6806
Complete cycle	0.4253	0.6860

From this table it can be seen that all the strategies used allow to substantially increase the exergy efficiency of the cycle from 34.34% to 68.60%. However, when compared to the exergy efficiency of the conventional power plant used as reference, 71.04%, this value is lower. This is due to the fact that the superheating of steam is higher in the second case (about 160 °C of temperature difference between the maximum temperature and the vaporization temperature, against around 75 °C). Indeed, superheating is performed because of technical reasons (turbines should not work in humid regime) although it decreases the exergy efficiency of the system.

5.4 Comparative summary table between the two cycles

In order to visualize with better precision all differences between the various cycles of the two types of plants, **Table 34** shows all the results obtained.

Table 34: Summary table with all the results obtained.

	Conventional CSP power plant		Direct storage with molten salts (Hitec XL)	
	Efficiency	Exergy efficiency	Efficiency	Exergy efficiency
Basic cycle	0.1380	0.2464	0.2129	0.3434
Cycle with reheating	0.3585	0.6402	0.3811	0.6147
Cycle with reheating and 1 bleeding	0.3658	0.6532	0.4104	0.6619
Cycle with reheating and 2 bleeding	0.3727	0.6655	0.4176	0.6735
Cycle with reheating and 3 bleeding	0.3801	0.6788	0.4205	0.6782
Cycle with reheating and 4 bleeding	0.3845	0.6866	0.4214	0.6797
Cycle with reheating and 5 bleeding	0.3903	0.6970	0.4220	0.6806
Complete cycle	0.3978	0.7104	0.4253	0.6860

Observing all the values obtained it can be seen that the exergy efficiency of the basic cycle is considerably higher in the cycle of the plant with direct storage with molten salts (Hitec XL) than in the cycle of a conventional plant. However, when cycle enhancements (reheating, bleedings…) are added for both technologies (conventional and direct storage with MS), the obtained exergy efficiencies are quite close. And for the complete cycle, it is slightly lower for the second case (MS). Nevertheless, comparison of all cycles except the complete ones in terms of exergy efficiency is not relevant because their condensing temperature is different (see the efficiency of Carnot).

Knowing that all the strategies that allow to increase the efficiency of the cycle also make it more expensive, the results can be analysed in two ways. The first is that using the molten salts as HTF enables achieving simple power blocks (only 1 bleeding) with superior energy efficiency than the complete cycle (6 bleedings) of a conventional plant (thermal oil as HTF). With this bleeding the problem of high melting point of the salts is solved and an efficiency of 41.40% is reached (against 39.78% for the cycle with oil). Less complexity means lower cost. In summary, it is possible to have a power block more efficient and at a lower cost. The second way of analysing the results is that with the same complexity, i.e. the same initial investment, a higher efficiency is achieved (42.53% with MS, 39.78% with oil).

6

Conclusions

The initial objective of this work was to verify the viability of using molten salts as HTF in parabolic trough power plants, determining the associated advantages and disadvantages. For this purpose, several comparative analyses were developed throughout this work. From a first analysis, using the properties of fluids presented in chapters 3 and 4, the following aspects are highlighted:

- The most promising aspect in the implementation of MS as HTF in CSP LF plants is that the salts allow an increase in the operating temperature of these systems to 500 °C, in case of Hitec and HitecXL, and up to 565 °C, in the case of Solar Salt, instead of the 400 °C that thermal oils currently offer in commercial power plants of this type. This increase in the output temperature of the solar field allows an improvement in the steam cycle efficiency.

- MS have higher VHC than thermal oils, which means they are an excellent energy storage material. It is for this reason that they are used in many commercial CSP LF power plants as energy storage medium since their use allows to reduce significantly the volume of storage required for the same amount of energy. In short, their use as HTF and storage medium not only improves storage efficiency, but also saves investment of the heat exchanger between the solar field and storage system. Reduction of tank size along with heat exchanger removal results in a reduction of the initial investment costs.

- The mass flow in the solar field is considerably smaller when MS are used, which in turn leads to lower pressure losses in the solar field piping. This result was not expected, since MS are more viscous than thermal oils at the same temperature (but not necessarily when used up their maximum operating temperature). In addition, MS do not present vapor pressure issues such as thermal oils and therefore do not need to be pressurized. Low pressure losses

coupled with low vapor pressure leads to a significant reduction of total pump losses.

On the other hand,

- It was expected that with temperature increase in the solar field the thermal losses would be higher, reducing the thermal efficiency of the system. The greater temperature difference between the inlet and outlet of the solar field also induces a lower heat transfer coefficient within the receivers because mass flow and therefore velocity are lower for the same power. However, it is expected that these two factors only represent a small deficit in the system performance and will not cause any significant change in the receiver tubes' mechanical behaviour.

- The greatest problem associated with the use of MS as HTF is their high melting point. It is expected that the use of the salts will lead to an increase of O&M costs in order to ensure that the salts do not freeze inside the piping. Although the salts of the cold tank can be used to maintain the pipes heated during the night and electric power is only as back-up option, this represents a significant thermal energy consumption. It also implies the cost of installing the electrical heating system, compulsory for guarantying pipe preheating, in particular for commissioning.

From the thermal study of the HPS2 project the thermal losses in the solar field piping as well as the receivers during the nominal operation were determined, being 91.5 $W.m^{-1}$ and 250.5 $W.m^{-1}$, respectively. From these values it can be concluded that the greater part of the total thermal losses occurs in receivers; both the value of losses per meter and the length are higher for the receivers. In addition, the thermal inertia capacity of the cold tank and the thermal losses during the night were determined. In this way it was assessed how many hours without direct solar irradiance the cold tank can maintain the piping above its safety temperature. The thermal inertia capacity of the cold tank, cool down between 290 °C and 200 °C, is 2.10 MWh and the total nocturnal thermal losses (pipes, receivers and tanks) is about 109.4 kW. This means that the cold tank between 290 °C and 200 °C can withstand piping losses for 21.2 hours. If the tank temperature decreases to the safety salt temperature (170 °C), the number of hours increases to 28.3 hours.

Observing the results of HPS2 simulations in SAM with Therminol VP-1, Solar Salt and Hitec XL, the first aspect to highlight is the value of solar field freeze protection. This is the aspect that arouses more curiosity and concern in the use of molten salts. As the thermal oil has a low melting point there is no need for freeze protection in the solar field. However, between the Solar Salt and the Hitec XL there is a large discrepancy, 231.28 $MW_{th}h$ and 18.66 $MW_{th}h$, respectively. Solar Salt requires about 12 times more energy to heat the solar field than Hitec XL, which is explained by Solar Salt having a

melting point of 100 °C higher. The second point to take into account is the electric energy spent to pump the HTF. The annual energy spent with Therminol VP-1, Solar Salt and Hitec XL was 30239 kWh, 10967 kWh and 18891 kWh, respectively. This is essentially due to the pressure losses being significantly higher with the thermal oil. Observing the annual electricity costs, without considering any operation strategy, i.e. avoid freezing by using electrical heating system only, the consumptions obtained for HPS2 project with Therminol VP-1, Solar Salt and Hitec XL were 8673 €, 51703 € and 9656 €, respectively. This means that if operating strategies are considered (using the tank to avoid freezing) it is possible to spend less electricity to operate a plant using a low melting point salt than thermal oil. On the other hand, the use of Solar Salt, or other salt of high melting point, requires a more careful analysis since it requires the expenditure of a great amount of energy for heating the solar field.

With the LCOE calculation, it can be verified that despite the extra anti-freezing protection requirements for the use of molten salts as HTF (namely electrical tracing, impedance, and pre-insulated piping supports), the CAPEX value of this type of plant is lower. This is due to the savings in synthetic oil, storage tanks and molten salts, pumps and heat exchanger. Adding to this the fact that the power block is more efficient due to the hot source temperature increase, the LCOE shows an interesting reduction. The LCOE values presented may not be updated due to the fact that the found references have already been published a few years ago. However, the values for both cases were taken from the same references so the obtained reduction can be considered valid.

The maximum operating temperature increase that the use of molten salts as HTF provides implies a modification of the power block configuration. As it has been demonstrated, this change not only increases the power block efficiency, but also allows reaching higher efficiencies with simpler configurations (less bleedings). This offers not only the possibility of increasing cycle efficiency but also reducing power block costs, two very important aspects for LCOE reduction of this type of plants.

References

[1] K. Vignarooban, X. Xu, A. Arvay, K. Hsu and A. Kannan, "Heat transfer fluids for concentrating solar power systems - A review," *Applied Energy,* pp. 383-396, 2015.

[2] D. Kearney, U. Herrmann, P. Nava, B. Kelly, R. Mahoney, J. Pacheco, R. Cable, N. Potrovitza, D. Blake and H. Price, "Assessment of a molten salt heat transfer fluid in a parabolic trough solar fiel," *JSEE,* 2002.

[3] NREL, "National Renewable Energy Laboratory (NREL) Home Page | NREL," [Online]. Available: https://www.nrel.gov/.

[4] P. Gauché, J. Rudman, M. Mabaso, W. Landman , T. von Backstrom and A. Brent, "System value and progress of CSP," *Solar Energy,* vol. 152, pp. 106-139, 2017.

[5] "International Energy Agency," [Online]. Available: https://www.iea.org. [Acedido em 12 2018].

[6] E. González-Roubaud, D. Pérez-Osorio and C. Prieto, "Review of commercial thermal energy storage in concentrated solar power plants: Steam vs. molten salts," *Renewable and Sustainable Energy Reviews,* vol. 80, pp. 133-148, 2017.

[7] IRENA, "Analysis based on SolarPACES," 2017. [Online]. Available: https://www.irena.org.

[8] I. Dinçer and M. A. Rosen, THERMAL ENERGY STORAGE - Systems and Applications, WILEY, 2002.

[9] H. Mehling e L. Cabeza, Heat and cold storage with PCM, Springer, 2008.

[10] A. Gil, M. Medrano, I. Martorell, A. Lázaro, P. Dolado and B. Zalba, "State of the art on high temperature thermal energy storage for power generation. Part 1 - Concepts, materials and modellization," *Renewable and Sustainable Energy Reviews,* pp. 31-55, 2010.

[11] M. Medrano, A. Gil, I. Martorell, X. Potau and L. F. Cabeza, "State of the art on high-temperature thermal energy storage for power generation. Part 2 - Case studies,"

Renewable and Sustainable Energy Reviews, pp. 56-72, 2010.

[12] M. Wittmann, M. Schmitz, H. G. Silva, P. Schmidt, G. Doppelbauer, R. Ernst, P. Santamaria, T. Miltkau, D. Golovca, L. Pacheco, D. Hogemann, M. Meyer-Grunefeldt and B. Seubert, "HPS2 - Demonstration of a Molten-Salt in Parabolic Trough Plants - Design of Plant," *SolarPaces,* 2018.

[13] ARKEMA, "JARYSOL by ARKEMA - Collect solar energy efficiently," [Online]. Available: https://www.arkema.com/export/shared/.content/media/downloads/products-documentations/hydrogen-peroxide/brochure-jarysol.pdf.

[14] SOLUTIA, "THERMINOL VP-1 Datasheet," [Online]. Available: http://twt.mpei.ac.ru/tthb/hedh/htf-vp1.pdf.

[15] J. Pacio and T. Wetzel, "Assessment of liquid metal technology status and research paths for their use as efficient heat transfer fluids in solar central receiver systems," *Solar Energy,* pp. 11-22, 2013.

[16] N. Boerema, G. Morrison, R. Taylor and G. Rosengarten, "Liquid sodium versus Hitec as a heat transfer fluid in solar thermal central receiver systems," *Solar Energy,* pp. 2293-2305, 2012.

[17] J. Pacio, C. Singer, T. Wetzel and R. Uhlig, "Thermodynamic evaluation of liquid metals as heat transfer fluids in concentrated solar power plants," *Applied Thermal Engineering,* pp. 295-302, 2013.

[18] YARA, *Internal comunication - YARA Knowledge grows,* 2018.

[19] ROCKWOOL, "The thickness of ROCKWOOL insulation," 2009. [Online]. Available: https://www.pipelagging.com/pdf/rockwool/Rockwool_Thickness_Guide.pdf.

[20] I. Tosun, Modeling in Transport Phenomena - A Conceptual Approach 2nd Edition, Elsevier Science, 2007.

[21] B. E. Rapp, Microfluidics: Modeling, Mechanics and Mathematics, Elsevier, 2017.

[22] R. Hilpert, "Heat Transfer from Cylinders," Forsch. Geb. Ingenieurwes, 1933, p. 4:215.

[23] "Forced Convection Correlations," Cairo University - Faculty of engineering, [Online].

Available: http://www.pathways.cu.edu.eg/ec/text-pdf/part%20b-9.pdf.

[24] NREL, “NREL System Advisor Model (SAM),” 05 04 2010. [Online]. Available: https://sam.nrel.gov/.

[25] NREL, “NREL System Advisor Model (SAM) - Download SAM,” [Online]. Available: https://sam.nrel.gov/download.

[26] NREL, “Technical Manual for the SAM Physical Trough Model,” [Online]. Available: https://www.nrel.gov/docs/fy11osti/51825.pdf.

[27] F. M. Lopes, R. Conceição, H. G. Silva, T. Fasquelle, R. Salgado, P. Canhoto and M. Collares-Pereira, “Short-Term Forecasts of DNI from an Integrated Forecasting System (ECMWF) for Optimized Operational Strategies of a Central Receiver System,” *energies,* 2019.

[28] L. Valenzuela, R. López-Martín and E. Zarza, “Optical and thermal performance of large-size parabolic-trough solar collectors from outdoor experiments: A test method and a case study,” em *Energy*, 2014, pp. 456-464.

[29] J. Dersch and S. Giuliano, “CSP Bankability Project Report: Draft for an Appendix C – Solar Field Modeling,” 09 01 2017. [Online]. Available: https://www.dlr.de/sf/Portaldata/73/Resources/dokumente/linienfokusssyst/cspbank-solarpaces-guideline/CSPBankProjectReport_Draft_for_AppendixC_SolarField_170109.pdf.

[30] A. Bonk, S. Sau, N. Uranga, M. Hernaiz and T. Bauer, “Advanced heat transfer fluids for direct molten salt line-focusing CSP plants,” *Progress in Energy and Combustion Science ,* pp. 69-87, 2018.

[31] R. Siegel, W. Bradshaw and P. Nathan, “Molten nitrate salt development for thermal energy storage in parabolic trough,” 2008. [Online]. Available: https://pdfs.semanticscholar.org/b188/bd8fa0adc330cf31329e85b5f99efd0a26da.pdf.

[32] N. Pfleger, T. Bauer, C. Martin, M. Eck and A. Wörner, “Thermal energy storage – overview and specific insight into nitrate salts for sensible and latent heat storage,” *BEILSTEIN Journal of Nanotechnology,* pp. 1487-1497, 2015.

[33] L. Coastal Chemical Co., “HITEC® Heat Transfer Salt,” Coastal Chemical Co., L.L.C. , [Online]. Available: http://stoppingclimatechange.com/MSR%20-

%20HITEC%20Heat%20Transfer%20Salt.pdf.

[34] IRENA, “RENEWABLE ENERGY TECHNOLOGIES: COST ANALYSIS SERIES,” 2012. [Online]. Available: https://www.irena.org/documentdownloads/publications/re_technologies_cost_analysis-csp.pdf.

[35] D. Kearney, U. Herrmann, P. Nava, B. Kelly, R. Mahoney, J. Pacheco, R. Cable, N. Potrovitza, D. Blake and H. Price, “Assessment of a Molten Salt Heat Transfer Fluid in a Parabolic Trough Solar Field,” *Journal of Solar Energy Engineering,* vol. 125, pp. 170-176, 2003.

[36] C. Turchi, M. Mehos, C. K. Ho and G. J. Kolb, “Current and future costs for parabolic trough and power tower systems in the US market,” U.S.A, 2010.

[37] DLR, “Concentrating solar power now - clean energy for sustainable development,” 2002.

[38] H. Grirate, N. Zari, A. Elmchaouri, S. Molina and R. Couturier, “Life Time Analysis of Thermal Oil Used as Heat Transfer Fluid in CSP Power Plant,” *AIP Conference Proceedings,* 31 May 2016.

[39] A. A. Piquer, “Determinación del ciclo de vapor de una central solar termoeléctrica CCP de 50MW,” UNIVERSIDAD CARLOS III DE MADRID , Madrid , 2012.

[40] Keenan, Chao, Keyes, G. Tables and Wiley, “Thermophysical Properties of Matter,” em *Vol. 3: Thermal Conductivity*, 1970.

Appendices

Appendix 1: Explanations about convection coefficient differences

This appendix explains the differences between the different obtained convection coefficient, thanks to the comparison of the mathematical formulas. The thermal properties that were used for these calculations are given in the following table.

***Table 35**: Values of thermal properties at 300 °C used in calculations,[(1)] reference [2]; [(2)] reference [1]; [(3)] reference [30].*

	Therminol VP-1	Solar Salt	Hitec	HitecXL
Melting point [°C]	13 [1]	220 [1]	142 [1]	120 [1]
T max [°C]	400 [1]	600 [1]	535 [1]	500 [1]
Density, ρ [kg.m^{-3}] (at 300°C)	815 [1]	1899 [1]	1640 [1]	1992 [1]
Viscosity, μ [mPa.s] (at 300°C)	0.2 [1]	3.26 [1]	3.16 [1]	6.37 [1]
Specific heat, Cp [J.kg^{-1}.K^{-1}] (a 300°C)	2319 [1]	1447 [1]	1560 [1]	1450 [1]
Conductivity, k [W.m^{-1}.K^{-1}]	~0.1 [2]	0.55 [2]	0.48 [3]	0.52 [2]

Using equations **(13)** and **(14)**, the ratio between the salt convection coefficient and the oil one writes:

$$\frac{h_{salts}}{h_{oil}} = \frac{0.023 \cdot \left(\frac{\rho_{salts} \cdot v_{salts} \cdot D}{\mu_{salts}}\right)^{0.8} \cdot \left(\frac{\mu_{salts} \cdot Cp_{salts}}{k_{salts}}\right)^{0.4} \cdot \frac{k_{salts}}{D}}{0.023 \cdot \left(\frac{\rho_{oil} \cdot v_{oil} \cdot D}{\mu_{oil}}\right)^{0.8} \cdot \left(\frac{\mu_{oil} \cdot Cp_{oil}}{k_{oil}}\right)^{0.4} \cdot \frac{k_{oil}}{D}}$$

• For a first approach, it was considered that all fluids circulate at a velocity of 3 m.s^{-1} in the receiver tubes and operating in the same temperature range (300 °C to 400 °C). Thus, by making a comparison between the heat transfer coefficient (h) of the salts and the oil, it is obtained:

$$\frac{h_{salts}}{h_{oil}} = \frac{\left(\frac{\rho_{salts}}{\mu_{salts}}\right)^{0.8} \cdot \left(\frac{\mu_{salts} \cdot Cp_{salts}}{k_{salts}}\right)^{0.4} \cdot k_{salts}}{\left(\frac{\rho_{oil}}{\mu_{oil}}\right)^{0.8} \cdot \left(\frac{\mu_{oil} \cdot Cp_{oil}}{k_{oil}}\right)^{0.4} \cdot k_{oil}}$$

After simplification and regrouping, it writes:

$$\frac{h_{salts}}{h_{oil}} = \left(\frac{\rho_{salts}}{\rho_{oil}}\right)^{0.8} \cdot \left(\frac{\mu_{oil}}{\mu_{salts}}\right)^{0.4} \cdot \left(\frac{Cp_{salts}}{Cp_{oil}}\right)^{0.4} \cdot \left(\frac{k_{salts}}{k_{oil}}\right)^{0.6}$$

It can be seen that although the viscosity (μ) and the specific heat (Cp) of the salts are lower than the oil, the fact that the density (ρ) and the conductivity (k) of the salts are higher has a greater impact and in this condition the salts have higher *h* values.

Solving the equation with the properties of Hitec XL salt and Therminol VP-1 oil, the following relation can be observed:

$$\frac{h_{salts}}{h_{oil}} = \left(\frac{1992}{815}\right)^{0.8} \cdot \left(\frac{0.0002}{0.00637}\right)^{0.4} \cdot \left(\frac{1450}{2319}\right)^{0.4} \cdot \left(\frac{0.52}{0.1}\right)^{0.6} = 1.14$$

Thus, even though the salt viscosity is 31 times higher than the oil and the specific heat is 1.6 times lower, the higher density and the higher conductivity led to slightly higher convection coefficient.

• For the second approach a power (3.6 MW_{th}) was set. In addition, the heat transfer coefficient (*h*) was calculated for each case based on the velocity at which each fluid needs to circulate to achieve that power, considering the same ΔT for all fluids.

Knowing that,

$$v = \frac{\dot{m}}{\rho \cdot S} \qquad \dot{m} = \frac{P}{Cp \cdot \Delta T}$$

The comparison between the two convection coefficients writes:

$$\frac{h_{salts}}{h_{oil}} = \frac{0.023 \cdot \left(\frac{P \cdot D}{Cp_{salts} \cdot \mu_{salts} \cdot S \cdot \Delta T}\right)^{0.8} \cdot \left(\frac{\mu_{salts} \cdot Cp_{salts}}{k_{salts}}\right)^{0.4} \cdot \frac{k_{salts}}{D}}{0.023 \cdot \left(\frac{P \cdot D}{Cp_{oil} \cdot \mu_{oil} \cdot S \cdot \Delta T}\right)^{0.8} \cdot \left(\frac{\mu_{oil} \cdot Cp_{oil}}{k_{oil}}\right)^{0.4} \cdot \frac{k_{oil}}{D}}$$

After simplification and regrouping, it gives:

$$\frac{h_{salts}}{h_{oil}} = \left(\frac{Cp_{oil}}{Cp_{salts}}\right)^{0.4} \cdot \left(\frac{\mu_{oil}}{\mu_{salts}}\right)^{0.4} \cdot \left(\frac{k_{salts}}{k_{oil}}\right)^{0.6}$$

Since in this situation the fluids circulate at different velocities inside the piping and ΔT is the same, the viscosity factor is decisive. The fact that the salts in these conditions have a viscosity significantly higher than the thermal oil, causes the h of the salts to be lower than that of the oil.

Solving the equation with the properties of Hitec XL and Therminol VP-1, the following relationship can be observed:

$$\frac{h_{salts}}{h_{oil}} = \left(\frac{2319}{1450}\right)^{0.4} \cdot \left(\frac{0.0002}{0.00637}\right)^{0.4} \cdot \left(\frac{0.52}{0.1}\right)^{0.6} = 0.81$$

In this case, molten salts lead to slightly lower convection coefficient because their higher density does not influence the coefficient anymore.

As the study fluids operate at different temperatures and the temperature influences the properties, the following table shows the properties of the fluids at the average operating temperature (350 °C for the thermal oil, since it operates in temperature ranges between the 300 °C and 400 °C, and 400 °C for the molten salts, considering an operating temperature between 290 °C and 500 °C).

***Table 36**:Values of thermal properties at 350 °C for thermal oil and 400 °C for molten salts.*

	Therminol VP-1 (at 350°C)	Solar Salt (at 400°C)	Hitec (at 400°C)	HitecXL (at 400°C)
Melting point [°C]	13	220	142	120
T max [°C]	400	600	535	500
Density, ρ [kg.m^{-3}]	761	1838.78	1794.86	1913.34
Viscosity, μ [Pa.s]	0.000177	0.00182	0.00188	0.00253
Specific heat, Cp [J.kg^{-1}.K^{-1}]	2454	1511	1550	1400
Conductivity, k [W.m^{-1}.K^{-1}]	0.086	0.52	0.48	0.52

• For the third approach, the same conditions as the second one was taken into consideration, considering only the influence that the temperature has on the properties of the fluids, i.e., considering the values presented in the table above.

Repeating the calculation with the properties of Hitec XL and Therminol VP-1:

$$\frac{h_{salts}}{h_{oil}} = \left(\frac{Cp_{oil}}{Cp_{salts}}\right)^{0.4} \cdot \left(\frac{\mu_{oil}}{\mu_{salts}}\right)^{0.4} \cdot \left(\frac{k_{salts}}{k_{oil}}\right)^{0.6}$$

In the end, for the working conditions of each fluid, the convection coefficient is higher for the salt

$$\frac{h_{salts}}{h_{oil}} = \left(\frac{2454}{1400}\right)^{0.4} \cdot \left(\frac{0.000177}{0.00253}\right)^{0.4} \cdot \left(\frac{0.52}{0.086}\right)^{0.6} = 1.27$$

It therefore shows that if salts are used at their operating temperature instead of the ones of the oil, they lead to slightly higher convection coefficient for a same temperature difference.

By observing the results of the second and third approaches, it is possible to observe in a simplified way the influence that the viscosity has on the heat transfer coefficient (h).

• Finally, in the fourth approach, the ΔT of operation of each fluid was taken into account.

$$\frac{h_{salts}}{h_{oil}} = \frac{0.023 \cdot \left(\frac{P \cdot D}{Cp_{salts} \cdot \mu_{salts} \cdot S \cdot \Delta T_{salts}}\right)^{0.8} \cdot \left(\frac{\mu_{salts} \cdot Cp_{salts}}{k_{salts}}\right)^{0.4} \cdot \frac{k_{salts}}{D}}{0.023 \cdot \left(\frac{P \cdot D}{Cp_{oil} \cdot \mu_{oil} \cdot S \cdot \Delta T_{oil}}\right)^{0.8} \cdot \left(\frac{\mu_{oil} \cdot Cp_{oil}}{k_{oil}}\right)^{0.4} \cdot \frac{k_{oil}}{D}}$$

The simplified equation is the following:

$$\frac{h_{salts}}{h_{oil}} = \left(\frac{Cp_{oil}}{Cp_{salts}}\right)^{0.4} \cdot \left(\frac{\mu_{oil}}{\mu_{salts}}\right)^{0.4} \cdot \left(\frac{\Delta T_{oil}}{\Delta T_{salts}}\right)^{0.8} \cdot \left(\frac{k_{salts}}{k_{oil}}\right)^{0.6}$$

In this last equation it is verified that in relation to the third approach the value of the heat transfer coefficient of the salts (h_{salts}) will decrease in relation to thermal oil (h_{oil}) due to the fact that the salts work with temperature intervals (ΔT) higher.

Doing the calculations with the properties values of Hitec XL and Therminol VP-1:

$$\frac{h_{salts}}{h_{oil}} = \left(\frac{2454}{1400}\right)^{0.4} \cdot \left(\frac{0.000177}{0.00253}\right)^{0.4} \cdot \left(\frac{100}{210}\right)^{0.8} \cdot \left(\frac{0.52}{0.086}\right)^{0.6} = 0.70$$

Finally, since salts induce a higher temperature difference between inlet and outlet of the solar field, their operating mass flow is lower than for the oil, resulting in lower convection coefficient. Nevertheless, as already explained, the value of h is still sufficiently high for normal operation of the receiver tubes.

Appendix 2: Collector file

Table 37: *Collectors data file.*

Name	HelioTrough
Description	HelioTrough Collectors
Reflective Aperture Area [m^2]	1157.67
Aperture width total structure [m^2]	6.77
Length of Collector Assembly [m^2]	171
Number of modules per assembly	9
Average surface to focus path length [m]	1.71
Piping distance between assemblies [m]	0.5
IAM F0	1
IAM F1	-0.040107
IAM F2	-0.00206265
IAM F3	0
Tracking error	0.998
Geometry effects	0.98
Mirror Reflectance	0.9436
Dirt on Mirror	0.97
General optical error	0.99

Appendix 3: Receiver specifications (Rioglass PTR 70-5G)

***Table 38**:Receiver data file.*

Absorber tube inner diameter [m]	0.066
Absorber tube outer diameter [m]	0.070
Glass envelope inner diameter [m]	0.119
Glass envelope outer diameter [m]	0.125
Absorber flow plug diameter	0
Inner surface roughness [m]	0.000045
Absorber flow pattern (0=tube 1=annular)	0
Absorber material type (0=304L 1=216L 2=321H 3=B42Copper)	2
Var 1 Absorber absorptance	0.95
Var 1 Absorber emittance	[400|0.095],[550|0.14]
Var 1 Envelope absorptance	0.0225
Var 1 Envelope emittance	0.90
Var 1 Envelope transmittance	0.96
Var 1 Is broken glass	0
Var 1 Annulus gas type (0=air 1=argon 2=hydrogen)	0
Var 1 Annulus pressure	0.0001
Var 1 Estimated avg heat loss [$W.m^{-1}$]	236
Var 1 Bellows shadowing	0.96
Var 1 Dirt on receiver	0.98
Var 2 Absorber absorptance	0.963
Var 2 Absorber emittance	0.65
Var 2 Envelope absorptance	0.02
Var 2 Envelope emittance	0.86
Var 2 Envelope transmittance	0.964
Var 2 Is broken glass	0
Var 2 Annulus gas type (0=air 1=argon 2=hydrogen)	0
Var 2 Annulus pressure	750
Var 2 Estimated avg heat loss [$W.m^{-1}$]	1100
Var 2 Bellows shadowing	0.935
Var 2 Dirt on receiver	0.98
Var 3 Absorber absorptance	0.80
Var 3 Absorber emittance	0.65
Var 3 Envelope absorptance	0
Var 3 Envelope emittance	1
Var 3 Envelope transmittance	1
Var 3 Is broken glass	1
Var 3 Annulus gas type (0=air 1=argon 2=hydrogen)	0
Var 3 Annulus pressure [Pa]	750
Var 3 Estimated avg heat loss [$W.m^{-1}$]	1500
Var 3 Bellows shadowing	0.96
Var 1 Dirt on receiver	1

Where Var 1 corresponds to 90% of intact receivers, Var 2 corresponds to 5% of the receivers with broken glasses and Var 3 to 5% of the receivers with lost vacuum.

Appendix 4: Inputs of SAM

***Table 39**: Manual inputs of the SAM.*

System Design	Heat Sink Power [MW_t]	1.8
	Hours of storage at design point [h]	2.44
	Loop inlet HTF temperature [°C]	290
	Loop outlet HTF temperature [°C]	500

Solar Field	Solar Field Parameters	Row spacing [m]	18.9
		Piping thermal loss coefficient [$W.m^{-1}.K^{-1}$]	0.68
		Wind stow speed [$m.s^{-1}$]	14
		Length of piping through heat sink [m]	207.6
	Heat Transfer Fluid	Field HTF Fluid	Hitec XL
		Freeze protection temperature [°C]	170
		Min single loop flow rate [$kg.s^{-1}$]	4
		Max single loop flow rate [$kg.s^{-1}$]	12
		Header design min flow velocity [$m.s^{-1}$]	0.4
		Header design max flow velocity [$m.s^{-1}$]	1.1

Storage System	Tank height [m]	5
	Tank fluid minimum height [m]	0.7
	Parallel tank pairs	1
	Wetted loss coefficient [$W.m^{-2}.K^{-1}$]	0.163
	Initial hot HTF percent	0
	Cold tank heater temperature set point [°C]	200
	Cold tank heater capacity [MWe]	0.02
	Hot tank heater temperature set point [°C]	300
	Hot tank heater capacity [MWe]	0.02

Appendix 5: Air properties

***Table 40**: Air properties at different temperatures. [40]*

Temperature [°C]	Specific heat [$J.kg^{-1}.K^{-1}$]	Coefficient of expansion (10^{-3}) [K^{-1}]	Thermal Conductivity [$W.m^{-1}.K^{-1}$]	Density [$kg.m^{-3}$]	Number of Prandtl	Dynamic Viscosity (10^{-6}) [Pa s]
0	1.006	3.67	0.0243	1.293	0.71	17.23
10	1.006	3.53	0.0248	1.247	0.71	17.72
20	1.006	3.43	0.0257	1.205	0.71	18.2
30	1.006	3.3	0.0263	1.165	0.71	18.68
40	1.007	3.2	0.0271	1.127	0.71	19.15
50	1.007	3.09	0.0278	1.093	0.71	19.61
60	1.008	3	0.0285	1.059	0.71	20.06
70	1.009	2.91	0.0292	1.029	0.71	20.51
80	1.01	2.83	0.0299	1	0.71	20.95
90	1.01	2.75	0.0306	0.972	0.71	21.38
100	1.011	2.68	0.0314	0.946	0.7	21.81
110	1.012	2.61	0.032	0.921	0.7	22.23
120	1.013	2.55	0.0328	0.898	0.7	22.65
140	1.013	2.43	0.0343	0.854	0.69	23.53
160	1.017	2.32	0.0358	0.815	0.69	24.33
180	1.022	2.21	0.0372	0.779	0.69	25.15
200	1.026	2.11	0.0386	0.746	0.68	25.83
250	1.034	1.91	0.0421	0.675	0.68	27.79
300	1.047	1.75	0.0454	0.616	0.68	29.48
350	1.055	1.61	0.0485	0.566	0.68	31.16
400	1.068	1.49	0.0515	0.524	0.68	32.77

Appendix 6: Hitec XL molten salt properties

***Table 41**: Hitec XL molten salt properties at different temperatures.*

T [°C]	Specific Heat [kJ.kg^{-1}.K^{-1}]	Density [kg.m^{-3}]	Viscosity [Pa.s]	Kinematic viscosity [m^2.s]	Thermal conductivity [W.m^{-1}.K^{-1}]	Enthalpy [kJ.kg^{-1}]
150	1.494	2116	0.06561	0.000031	0.519	227.3
168.4	1.489	2101	0.04444	0.0000212	0.519	254.8
186.8	1.483	2086	0.03134	0.000015	0.519	282.2
205.3	1.477	2070	0.02284	0.000011	0.519	309.4
223.7	1.472	2055	0.01711	0.00000832	0.519	336.6
242.1	1.466	2040	0.01311	0.00000643	0.519	363.6
260.5	1.46	2025	0.01024	0.00000506	0.519	390.6
278.9	1.454	2009	0.00814	0.00000405	0.519	417.4
297.4	1.448	1994	0.006564	0.00000329	0.519	444.2
315.8	1.442	1979	0.005363	0.00000271	0.519	470.8
334.2	1.436	1964	0.004431	0.00000226	0.519	497.3
352.6	1.429	1949	0.0037	0.0000019	0.519	523.7
371.1	1.423	1933	0.003117	0.00000161	0.519	549.9
389.5	1.417	1918	0.002648	0.00000138	0.519	576.1
407.9	1.41	1903	0.002267	0.00000119	0.519	602.1
426.3	1.403	1888	0.001954	0.00000104	0.519	628.0
444.7	1.397	1872	0.001695	0.000000905	0.519	653.8
463.2	1.39	1857	0.001479	0.000000796	0.519	679.5
481.6	1.383	1842	0.001297	0.000000704	0.519	705.0
500	1.376	1827	0.001143	0.000000626	0.519	730.5
700	1.376	1827	0.001143	0.000000626	0.519	730.5

Appendix 7: Values used for cycle efficiencies of conventional power plant

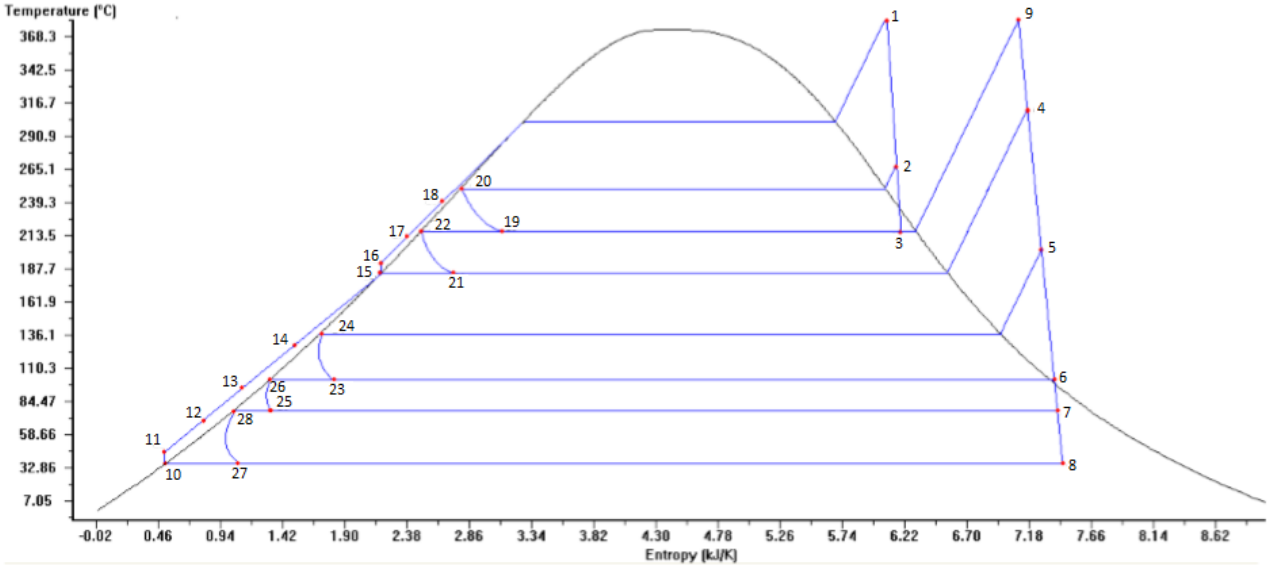

***Figure 38**:Complete cycle of a conventional power plant.*

***Table 42**:Values of pressure, temperature, mass flow and enthalpy for each point [39].*

Point	Pressure [bars]	Temperature [°C]	Mass flow [$kg.s^{-1}$]	Enthalpy [$kJ.kg^{-1}$]
1	105	380	57.4	3019
2	42.3	265.3	5.4	2841
3	21	214.9	3.38	2722
4	11	311.3	2.82	3072
5	4	205.2	3.21	2871
6	1	99.63	2.34	2647
7	0.4	75.88	2.42	2520
8	0.06	36.17	37.84	2294
9	19	380	48.62	3205
10	0.06	36.17	45.81	151.4
11	11	36.23	45.81	152.7
12	11	66.96	45.81	281.2
13	11	97.23	45.81	408.2
14	11	134.7	45.81	566.9
15	11	175.6	57.4	744
16	120	177.4	57.4	757.6
17	120	205.4	57.4	880.9
18	120	241.3	57.4	1044
19	21	214.9	5.4	1103
20	42.3	253.7	5.4	1103
21	11	184.1	8.78	920
22	21	214.9	8.78	920
23	1	99.63	3.21	604.9
24	4	143.6	3.21	604.9
25	0.4	75.88	5.55	417.5
26	1	99.63	5.55	417.5
27	0.06	36.17	7.97	317.6
28	0.4	75.88	7.97	317.6

Appendix 8: Values used for basic cycle efficiency calculation with MS

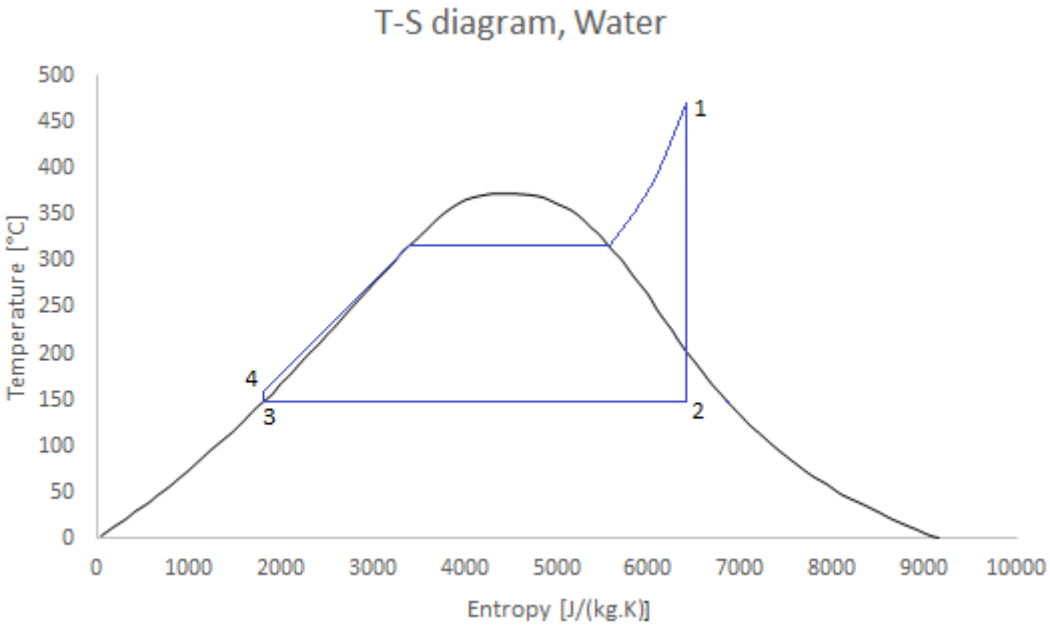

***Figure 39**: Diagram T-S with basic Rankine cycle.*

***Table 43**:Values of pression, temperature, mass flow and enthalpy for each point.*

Point	Pressure [Bars]	Temperature [°C]	Mass flow [$kg.s^{-1}$]	Enthalpy [$kJ.kg^{-1}$]
1	135	490	36.25	3300
2	10	180	36.25	2750.17
3	10	180	36.25	763.18
4	135	182.99	36.25	775.68

$$\eta_{cycle} = \frac{W_{turbine} - W_{pump}}{W_{heat}} = \frac{(h_1 - h_2) - (h_4 - h_3)}{(h_1 - h_4)} = 0.2129$$

Appendix 9: Values used for cycle with reheating efficiency calculation

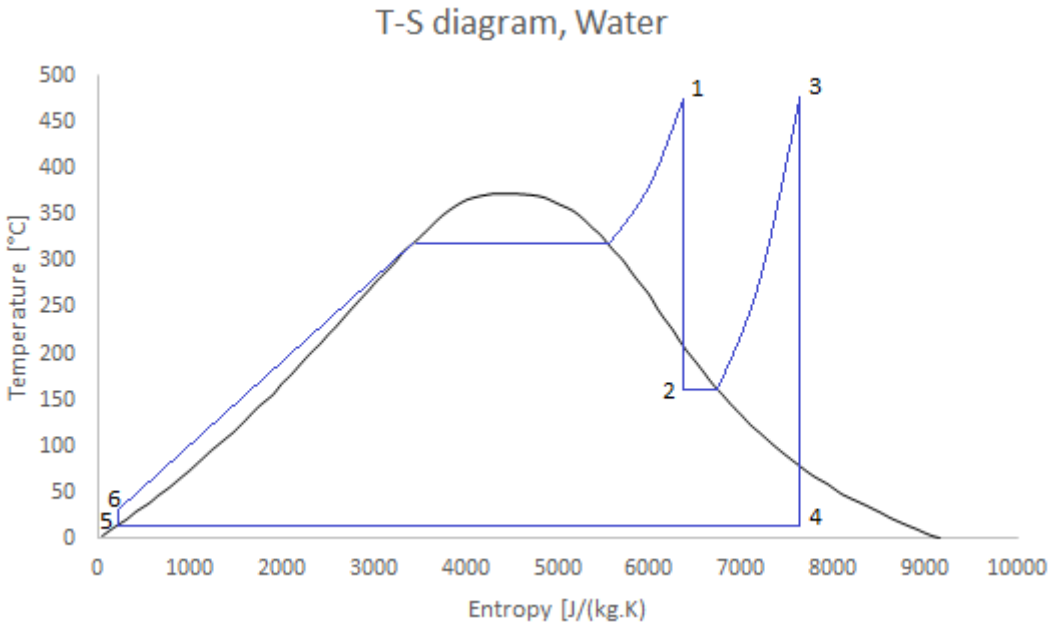

***Figure 40**: Rankine cycle with reheating.*

***Table 44**: Values of pressure, temperature, mass flow and enthalpy for each point.*

Point	Pressure [Bars]	Temperature [°C]	Mass flow [kg.s^{-1}]	Enthalpy [kJ.kg^{-1}]
1	135	490	26.36	3300
2	10	180	26.36	2750.17
3	8	490	26.36	3458.71
4	0.06	36.17	26.36	2530.09
5	0.06	36.17	26.36	151.27
6	135	39.40	26.36	164.76

$$\eta_{cycle} = \frac{W_{turbine\,1} + W_{turbine\,2} - W_{pump}}{W_{heat\,1} + W_{heat\,2}}$$

$$= \frac{(h_1 - h_2) + (h_3 - h_4) - (h_6 - h_5)}{(h_1 - h_6) + (h_3 - h_2)} = 0.3811$$

Appendix 10: Values used for efficiency calculation of cycle with reheating and 1 bleeding at 290 °C

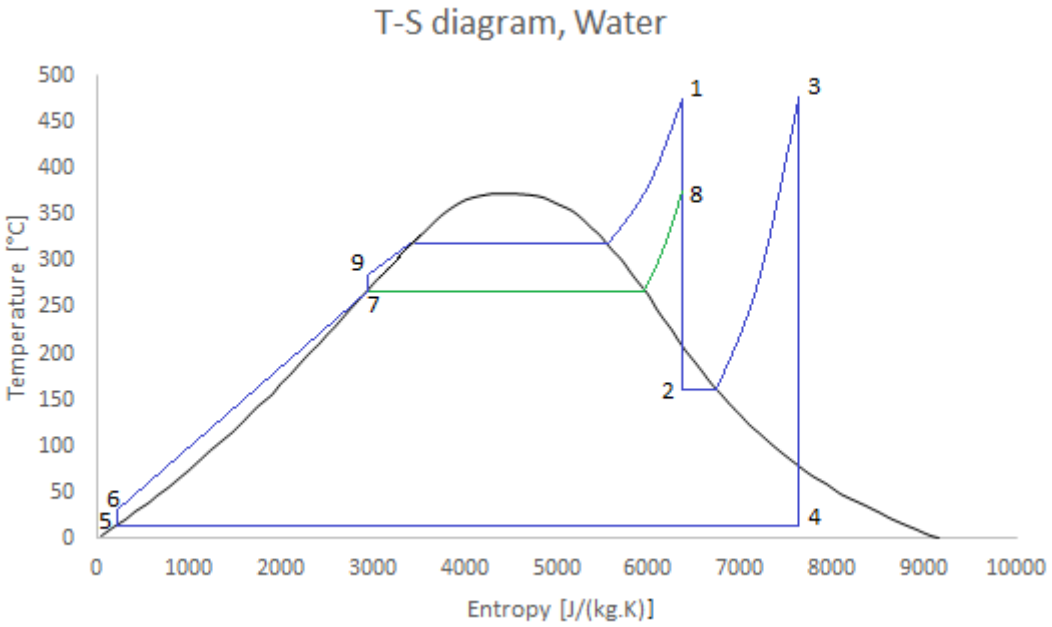

***Figure 41**: Rankine cycle with reheating and 1 bleeding at 290 °C.*

***Table 45**:Values of pressure, temperature, mass flow and enthalpy for each point.*

Point	Pressure [Bars]	Temperature [°C]	Mass flow [kg.s^{-1}]	Enthalpy [kJ.kg^{-1}]
1	135	490	36.82	3300
2	10	180	22.79	2750.17
3	8	490	22.79	3458.71
4	0.06	36.17	22.79	2530.09
5	0.06	36.17	22.79	151.27
6	74.36	37.95	22.79	158.70
7	74.36	290	36.82	1289.64
8	74.36	392	14.03	3127.10
9	135	291.45	36.82	1295.70

$$\eta_{cycle}$$

$$= \frac{m_1(h_1 - h_8) + m_2(h_8 - h_2) + m_3(h_3 - h_4) - m_5(h_6 - h_5) - m_7(h_9 - h_7)}{m_1(h_1 - h_9) + m_3(h_3 - h_2)}$$

$$= 0.3972$$

Appendix 11: Values used for efficiency calculation of cycle with reheating and 2 bleedings at 100 °C and 290 °C

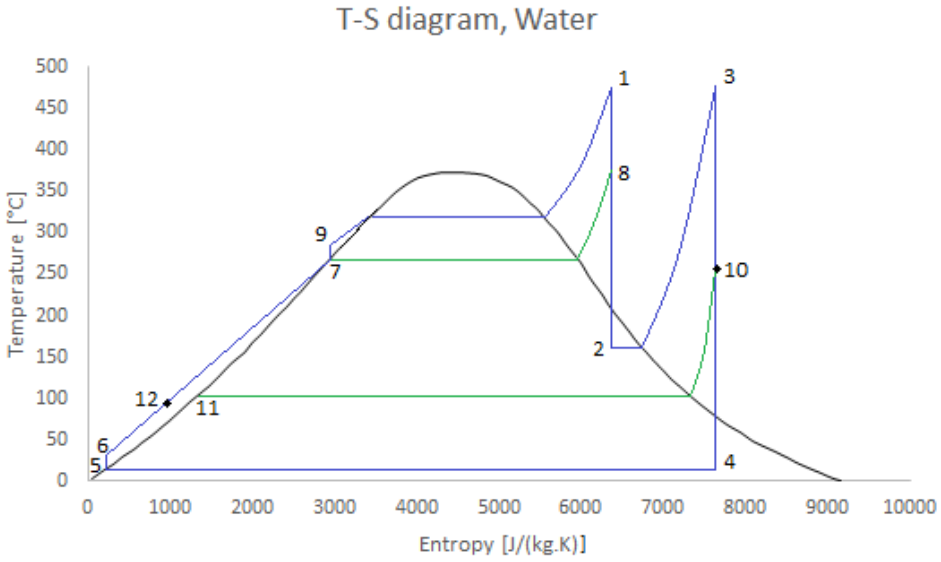

***Figure 42**:Rankine cycle with 2 bleedings at 100 °C and 290 °C.*

***Table 46**:Values of pressure, temperature, mass flow and enthalpy for each point.*

Point	Pressure [bars]	Temperature [°C]	Mass flow [kg.s^{-1}]	Enthalpy [kJ.kg^{-1}]
1	135	490	48.92	3300
2	10	180	32.87	2750.17
3	8	490	32.87	3458.71
4	0.06	12.58	29.88	2530.09
5	0.06	12.58	32.87	151.27
6	74.36	14.36	32.87	158.70
7	74.36	290	48.92	1289.64
8	74.36	392	16.05	3127.10
9	135	291.45	48.92	1295.70
10	1.01	202.46	2.99	2879.74
11	1.01	100	2.99	419.71
12	74.36	93.79	32.87	392.13

$$\eta_{cycle} = \frac{m_1(h_1 - h_8) + m_2(h_8 - h_2) + m_3(h_3 - h_{10}) + m_4(h_{10} - h_4) - m_5(h_6 - h_5) - m_7(h_9 - h_7)}{m_1(h_1 - h_9) + m_3(h_3 - h_2)}$$

$$= 0.4102$$

Appendix 12: Values used for efficiency calculation of cycle with reheating and 1 bleeding at 200 °C

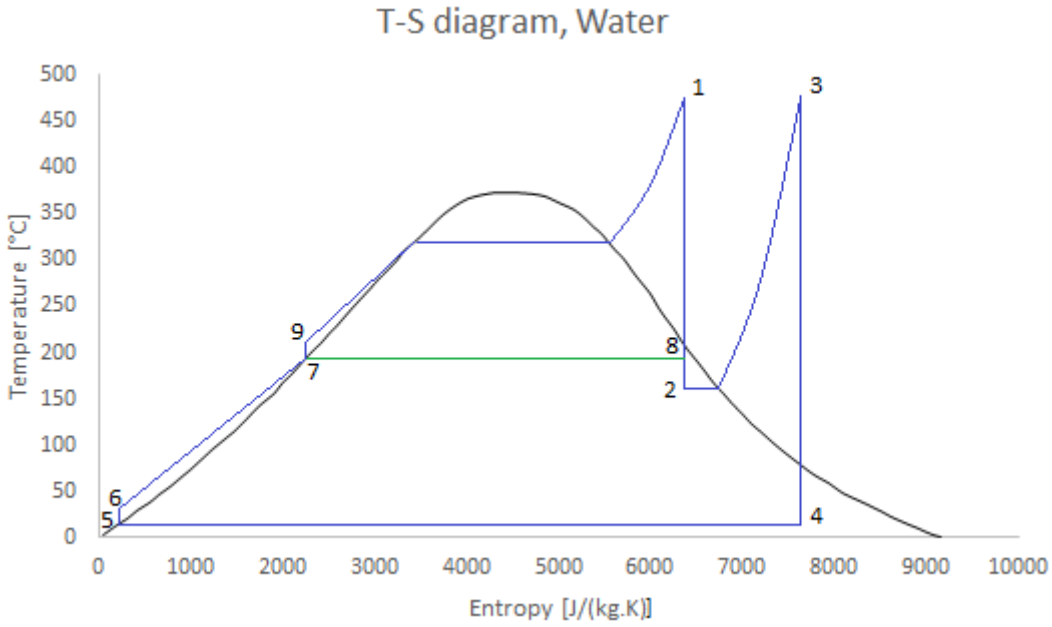

***Figure 43**: Rankine cycle with reheating and 1 bleeding at 200 °C.*

***Table 47**:Values of pressure, temperature, mass flow and enthalpy for each point.*

Point	Pressure [bars]	Temperature [°C]	Mass flow [kg.s^{-1}]	Enthalpy [kJ.kg^{-1}]
1	135	490	40.80	3300
2	10	180	29.88	2750.17
3	8	490	29.88	3458.71
4	0.06	36.17	29.88	2530.09
5	0.06	36.17	29.88	151.27
6	15.54	36.54	29.88	152.82
7	15.54	200	40.80	852.74
8	15.54	200	10.93	2766.60
9	135	202.86	40.80	864.69

$$\eta_{cycle} = \frac{m_1(h_1 - h_8) + m_2(h_8 - h_2) + m_3(h_3 - h_4) - m_5(h_6 - h_5) - m_7(h_9 - h_7)}{m_1(h_1 - h_9) + m_3(h_3 - h_2)}$$
$$= 0.4104$$

Appendix 13: Values used for efficiency calculation of cycle with reheating and 2 bleedings at 100 °C and 200 °C

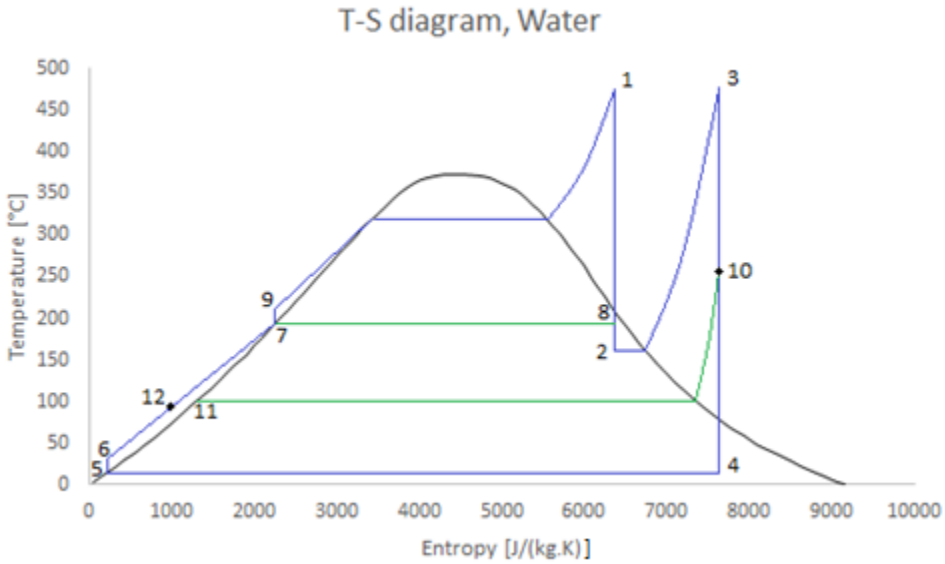

***Figure 44**: Rankine cycle with 2 bleedings at 100 °C and 200 °C.*

***Table 48**:Values of pressure, temperature, mass flow and enthalpy for each point.*

Point	Pressure [bars]	Temperature [°C]	Mass flow [kg.s^{-1}]	Enthalpy [kJ.kg^{-1}]
1	135	490	39.66	3300
2	10	180	31.96	2750.17
3	8	490	31.96	3458.71
4	0.06	36.17	28.99	2530.09
5	0.06	36.17	31.96	151.27
6	15.54	36.54	31.96	152.82
7	15.54	200	39.66	852.74
8	15.54	200	7.70	2766.6
9	135	202.86	39.66	864.69
10	1.01	202.46	2.97	2879.74
11	1.01	100	2.97	419.71
12	15.54	93.65	31.96	391.56

$$\eta_{cycle} = \frac{m_1(h_1 - h_8) + m_2(h_8 - h_2) + m_3(h_3 - h_{10}) + m_4(h_{10} - h_4) - m_5(h_6 - h_5) - m_7(h_9 - h_7)}{m_1(h_1 - h_9) + m_3(h_3 - h_2)}$$

$$= 0.4176$$

Appendix 14: Values used for efficiency calculation of complete cycle

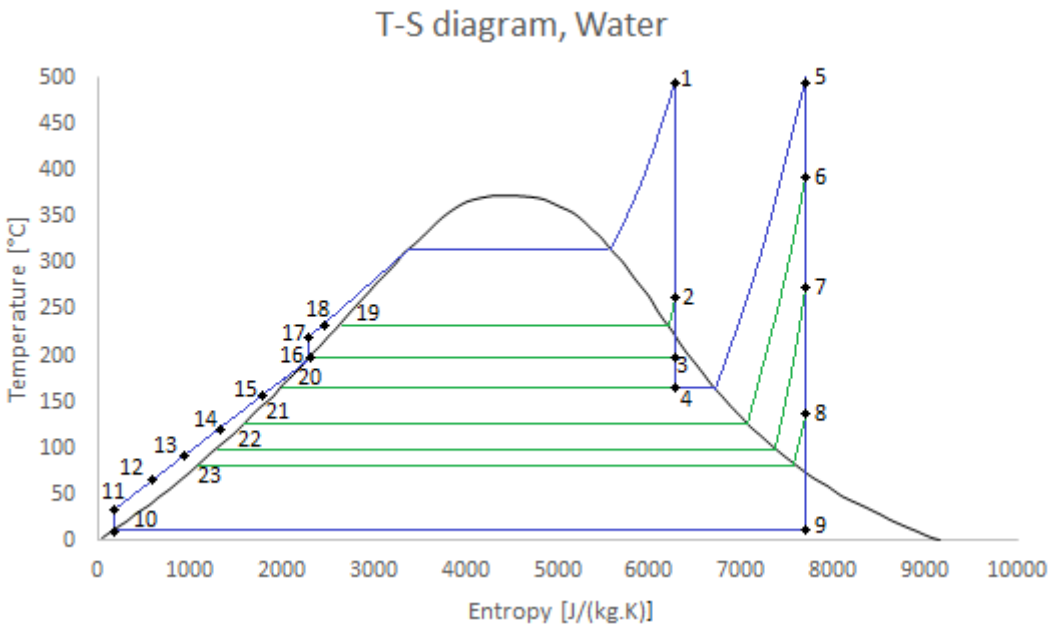

Figure 45: Complete cycle of direct storage with molten salts plant.

***Table 49**: Values of pressure, temperature, mass flow and enthalpy for each point.*

Point	Pressure(bars)	Temperature [°C]	Mass flow [$kg.s^{-1}$]	Enthalpy [$kJ.kg^{-1}$]
1	135	490	40.05	3300
2	27.95	257.32	2.16	2886.80
3	15.54	200	3.42	2766.60
4	10	180	2.18	2750.17
5	8	490	32.29	3458.71
6	2.7	324.73	1.51	3120.09
7	1.01	202.46	1.69	2879.74
8	0.31	84	1.40	2655.15
9	0.06	36.17	27.70	2530.09
10	0.06	36.17	34.47	151.27
11	15.54	36.54	34.05	152.82
12	15.54	66.65	34.05	268.04
13	15.54	96.67	34.05	402.34
14	15.54	126.67	34.05	528.62
15	15.54	156.67	34.05	654.10
16	15.54	200	40.05	852.74
17	135	202.86	40.05	864.69
18	135	227.29	40.05	966.81
19	27.95	230	2.16	990.77
20	10	180	2.18	763.18
21	2.7	130	3.68	546.28
22	1.01	100	5.38	419.71
23	0.31	70	6.77	293.89